IDŐJÁRÁS

QUARTERLY JOURNAL
OF THE HUNGARIAN METEOROLOGICAL SERVICE

CONTENTS

****

http://www.met.hu/Journal-Idojaras.php

VOL. 116 * NO. 2 * APRIL – JUNE 2012

IDŐJÁRÁS

Quarterly Journal of the Hungarian Meteorological Service

Editorial Office: Kitaibel P.u. 1, H-1024 Budapest, Hungary
P.O. Box 38, H-1525 Budapest, Hungary
E-mail: journal.idojaras@met.hu
Fax: (36-1) 346-4669

Indexed and abstracted in Science Citation Index Expanded™ and Journal Citation Reports/Science Edition
Covered in the abstract and citation database SCOPUS®

Subscription by

mail: IDŐJÁRÁS, P.O. Box 38, H-1525 Budapest, Hungary
E-mail: journal.idojaras@met.hu

IDŐJÁRÁS

Quarterly Journal of the Hungarian Meteorological Service
Vol. 116, No. 2, April–June 2012, pp. 77-91

Convective systems and periods with large precipitation in Hungary

Ákos Horváth[1*], **András Tamás Seres**[2], and **Péter Németh**[3]

[1]*Hungarian Meteorological Service,*
Vitorlás u. 17, H-8600 Siófok, Hungary,
E-mail: horvath.a@met.hu

[2]*Hungarian Defence Forces Geoinformation Service,*
Szilágyi E. fasor 7-9, H-1024 Budapest, Hungary
E-mail: seres.andrastamas@upcmail.hu

[3]*Hungarian Meteorological Service,*
Kitaibel P. u. 1, H-1024 Budapest, Hungary,
E-mail: nemeth.p@met.hu

**Corresponding author*

(Manuscript received in final form January 10, 2012)

Abstract—This paper presents a study describing the synoptic scale meteorological conditions and the mesoscale structures of phenomena which can cause large amounts of convective precipitation and often flash floods in Hungary. This examination is based on radar observations, 24-hour rain gauge precipitation measurements, model analyses and forecasts in the six-year period of 2003–2010. For the investigated precipitation period, an objective procedure was applied to decide whether convection had determining role in producing of precipitation. The procedure used radar based precipitation measurements and ECMWF precipitation forecasts. ECMWF analyses and forecasts were also applied to determine the representative synoptic scale weather patterns. Based on observed radar image structures and movements of radar echoes, the mesoscale structures were identified. Studies show that most of the cases can be classified into three main clusters: events with (1) convective chains (squall lines) in the warm sector of a cyclone; (2) convective lines with related cold front; and (3) convective lines in occluded cyclones. These most common types are demonstrated by case studies. This study may help to recognize weather conditions and patterns that are responsible for flash flood events in the Carpathian Basin.

Key-words: radar, large precipitation, convection, flash flood, Hungary.

1. Introduction and background

Climate research revealed that a number of extremely rainy days had significantly grown in the last quarter of the 20th century in Hungary (*Bartholy* and *Pongrácz*, 2005), and the chance of flash floods had increased, too. The aim of this study is to describe the meteorological conditions and the structures of phenomena which can cause flash floods. This examination is based on Hungarian radar observations, rain gauge measurements, and numerical model analyses.

Investigation of flash floods has a long history, especially in the United States. One of the most severe flash floods happened in the Big Thomson Canyon (USA) in 1976, where 143 people were killed (*Caracena et. al.*, 1979). Intensive research in connecting with these phenomena started after this tragedy. Several examinations investigated flash floods and their hydrological aspects (for example run-off simulations) in the USA and Europe (*Maddox*, 1979; *Hansen et al.*, 1982; *Browning,* 1986; *Doswell et al.*, 1996; *Warner et al.,* 2000; *Yates et al.*, 2000; *Davis*, 2001; *Rigo* and *Liasat* ,2002; *Blöschl et al.,* 2008; *Déqué* and *Somot*, 2008).

Marshall and *Palmer* (1948) introduced the so-called Z-R relation between radar reflectivity and precipitation intensity, which is still used with little modifications for precipitation estimation.

The main advantage of radars is that the time and spatial resolution of data are much higher than that of the ground observations. However, radar measurements may have many errors and precipitation data are provided indirectly (*Lombardo* and *Baldini*, 2010). In the last few decades, radar precipitation measurements were used for meteorological and hydrological modeling and forecasts (*Kessler* and *Wilk*, 1968; *Wilson* and *Brandes,* 1979; *Mimikou* and *Baltas*, 1996; *Smith et al.,* 2007; *Rossa et al.,* 2010).

In Hungary, the mesometeorological research started at the beginning of the 1960s. Early studies dealt with the structure and dynamics of convective systems and used data obtained by synoptic scale measurements and observations (*Bodolai*, 1954; *Götz* and *Bodolainé*, 1963a, 1963b, *Bodolainé et al.,* 1967). From the early 1980s, researches started to use remote sensing (radar, satellite, later lightning) data (*Bodolainé*, 1980; *Kapovits*, 1986; *Boncz et al.,* 1987; *Bodolainé* and *Tänczer,* 1991). The examination of weather situations with heavy precipitation, focusing on extreme floods became more common (*Bodolainé,* 1983; *Bodolainé* and *Homokiné*, 1984; *Bonta* and *Takács*, 1988, 1989, 1990; *Takács et al.*, 2000; *Geresdi et. al*, 2004). Floods of river Tisza in 1998 and 2001 were described by *Homokiné* (1999, 2001) from a synoptic meteorological point of view. Nowadays, flash floods can be detected by satellite observations (*Kerényi* and *Putsay*, 2005), and case studies using nowcasting models appeared, too (*Horváth* and *Geresdi,* 2003; *Horváth et al.*, 2007).

Mesoscale convective complexes (MCCs) are circular mesoscale convective systems which produce large amount of precipitation. These phenomena were firstly described by *Maddox* (1980), and in Hungary by *Bodolainé* and *Tänczer* (2003). MCC-s are very rare in Hungary.

In Hungary, *linear mesoscale convective systems* are more common than circular ones. Convective systems have two main parts: the strongest, mature (thunderstorm) cells which have the highest radar echoes, and the weaker, stratiform zone which consists of dissipating cells with less intense radar echoes. These systems were classified into three main clusters by *Parker* and *Johnson* (2000): the *TS (trailing stratiform),* the *PS (parallel stratiform)*, and the *LS (leading stratiform)* types. In the TS and LS systems, the heaviest thunderstorms move (almost) perpendicular to the convergence (instability) line, and the weaker, stratiform parts move behind (trailing) or ahead (leading) of the thunderstorm zone. In this paper TS and LS systems are referred to as *convective chains* or *squall lines*. In the PS types *(convective lines)*, the strongest cells move (almost) parallel to the convergence line. In this study it was found that the TS and PS systems were common, while LS was very rare in Hungary. All of these systems can produce large precipitation. In Hungary, many squall lines come from southwest, and these phenomena are called *Slovenian instability lines* (*Bodolainé et al.,* 1967).

In this paper, the most significant synoptic patterns and mesoscale precipitation structures responsible for large precipitation are coupled to each other, and large precipitation cases are classified into ascertained types.

2. Methodology

The investigation focused on 24-hour periods (from 06 UTC to 06 UTC next day) from 2003 to 2010. In our work, the following data were applied: daily, 24-hour (from 06 UTC to 06 UTC next day) precipitation amounts provided by the Hungarian rain gauge measurement network, composite radar images (resolution is 2 × 2 km in space and 15 minutes in time), 24-hour precipitation estimated by radars, and ECMWF (European Centre for Medium-Range Weather Forecast) analysis or 36-hour forecasts (resolution is 30 × 30 km in space and 3 hours in time). Note that the calculations were based on an area covered by the HMS's (Hungarian Meteorological Service) radar system which is much greater than Hungary (245 116 km^2 vs. 93 030 km^2).

A 24-hour period was considered as a *convective period with large precipitation*, when the following conditions were satisfied:

(1) Two or more stations of the Hungarian rain gauge measurement network reported at least 50 mm precipitation.

(2) At least 60% of the forecasted precipitation was convective in the ECMWF model forecast during the period.

(3) There were one or more pixels (2×2 km areas) with at least 50 mm precipitation measured by radar.

(4) At least 60% of the radar cells with large precipitation had strong echo (intensity ≥ 40 dBz).

To check the realization of the second condition, the ECMWF convective precipitation and the total precipitation were compared for the whole domain at every grid point for the entire precipitation period.

To test the third and fourth conditions, a radar based precipitation estimation procedure, named TREC, was applied. Using this procedure, it was possible not only to estimate the amount of precipitation in all radar pixels but estimate the rate of intensive convective rainfall, separately. A short description of TREC is given in the Appendix.

In the next step, the most significant mesoscale structures of the precipitation period were examined. The *TITAN-method* (Thunderstorm Identification Tracking Analysis and Nowcasting, *Dixon* and *Weiner*, 1993; *Horváth et al.*, 2008) was applied to detect the existence of intensive convective echoes in an objective way. It is important to emphasize that the heavy precipitation falls both from the strong cells (intensity > 40 dBz) and from the weaker trailed or associated stratiform zone. Considering the structure based on movement, the convective precipitation systems were divided into three main clusters:

A. disorganized or weakly organized convective patches (mainly thunderstorms),

B. convective lines (LS systems, mainly thunderstorm lines), where movements of individual cells along the line are more significant than the replacement of the line, and

C. convective chains or squall lines (TS systems) where cells move perpendicular to the thunderstorm line.

The appearance of convective precipitation systems was also classified from a synoptic aspect. For this investigation ECMWF analyses were used. The model fields were visualized by the HAWK-2 (Hungarian Advanced WorKstation) application. Three main synoptic classes were found:

(1) cold front (both slow and fast),

(2) convergence-line of cyclone or cyclone cloud band, and

(3) sporadic cells in weak pressure depression with featureless distributions of values about the mean-sea-level pressure.

The first type is associated with a cold front, it refers to mostly pre-frontal, frontal, rarely post-frontal synoptic situations. The second cluster contains the precipitation zones which form along the convergence-lines of an (occluded) cyclone. The third type represents those situations, when on the ground there is weak pressure gradient with an upper cold and low trough.

Except for one case, all 24-hour periods were classified into these clusters, and combined categories were created as follows:

A1: cold front with sporadic thunderstorms;

A2: sporadic thunderstorms with a convergence line in a cyclone;

A3: sporadic thunderstorms in a weak depression;

B1: convective lines related to a cold front;

B2: convective lines along the convergence zones of a cyclone;

B3: convective lines in weak depression;

C1: squall lines related to a cold front;

C2: squall lines in a cyclone;

C3: weak squall lines in a depression.

If more than one convective system were detected in a 24-hour period, the most significant was considered.

3. Results

Altogether 56 convective periods with large precipitation were found between 2003 and 2010. As it was expected, most of the convective periods appeared between May and September. Concerning their distribution in time the maximum was in 2010 (*Fig. 1*) and in June (*Fig. 2*). Note that one period was found in March.

In the eight-year period, the most frequent combined types were C1 (squall lines related to a cold front), B2 (convective lines along the convergence zones of a cyclone), and B1 (convective lines related to a cold front). The fourth pattern was A3 (low pressure gradient field with disorganized thunderstorms), followed by C2 (squall lines in cyclone). Frequencies of the other types are only 0 or 1 (*Fig. 3*). Note that periods with squall lines (C1 and C2 types) or situations with cold fronts (A1, B1, C1 patterns) appeared more often than the lines (B1 and B2 patterns) or cyclonic situations (B2, C2 combinations). One situation (May 26, 2003) could not be clustered into this classification. On this day, strong squall lines formed and moved from east to west in the central and western parts of Hungary.

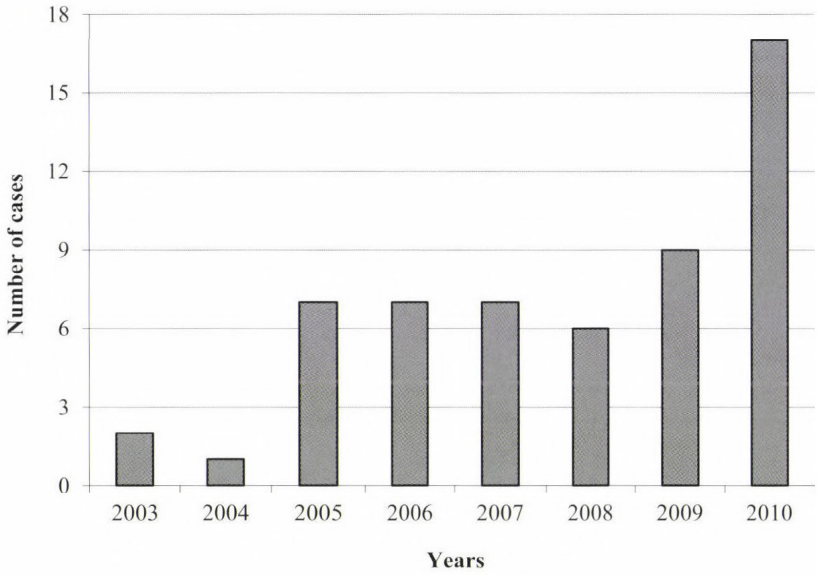

Fig. 1. Frequency distribution of 24-hour periods with large precipitation by year.

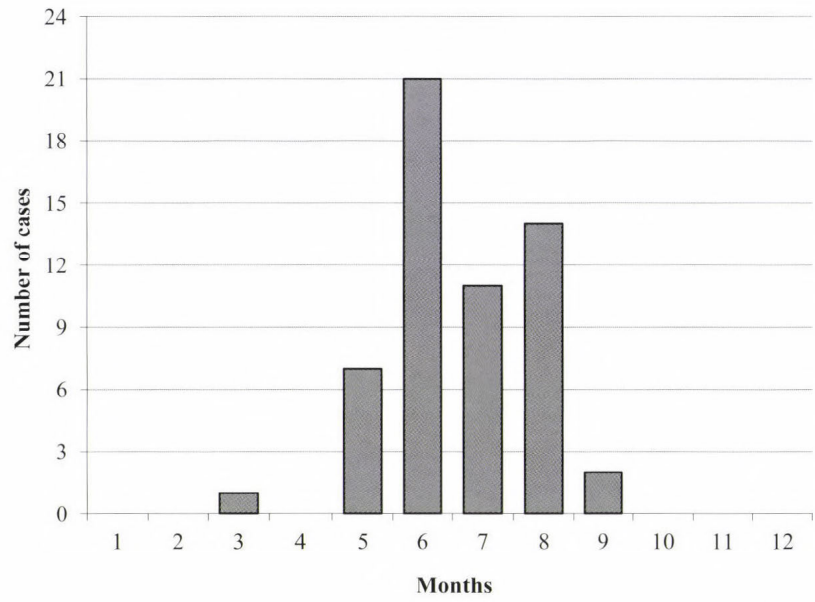

Fig. 2. Frequency distribution of 24-hour periods with large precipitation by month.

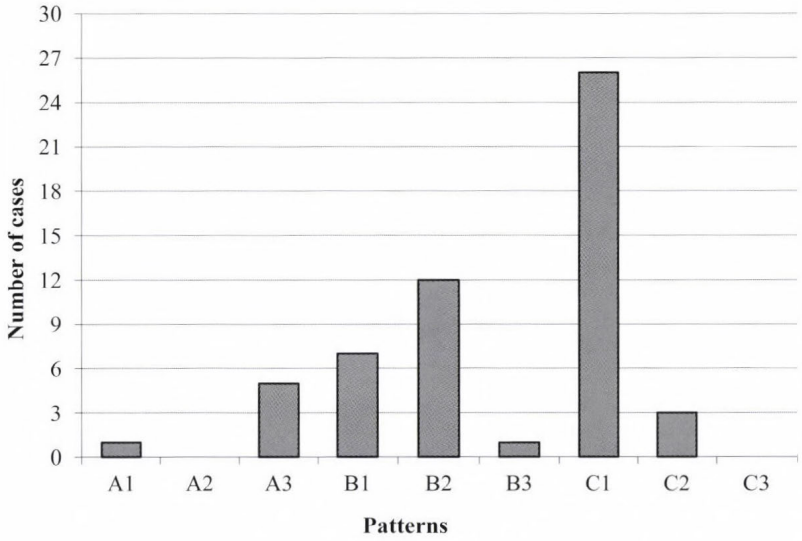

Fig. 3. Frequency distribution of 24-hour periods with large precipitation by combined patterns.

Considering all case studies, it was found that in average, the amount of radar estimated precipitation was larger than 50 mm only on 0.23% of the entire area (that means 564 km^2 of 245 116 km^2). In the large precipitation areas, 18% of the precipitation arose from echoes with reflectivity $\geq$40 dBz (this was the so-called *convective part*). Meanwhile, nearly at about 50% of all cases, the rate of convective precipitation was higher than 60% in large precipitation areas. It was also found that there was at least one strong echo (intensity $\geq$40 dBz) in about 92% of areas with large precipitation. Average characteristics of the most frequent five types as well as the average values for all the seven types are shown in *Table 1.*

3.1. C1 type (Squall line related to cold front)

On August 20, 2007, a cold front reached Hungary from north-west (*Fig. 4*). Thunderstorms developed in front of the cold front, and formed an extended squall line. Behind the intensive cells, a massive stratiform zone was forming. In advance of the squall line, in the prefrontal zone (in the Great Plain), isolated convective systems developed. In the western part of Hungary (Transdanubia), large amounts of precipitation fell both from the intensive cells and from the trailed stratiform regions of the squall line, while in south-east the precipitation fell mainly from the most intensive parts. There was strong contrast in temperature at 850 hPa level, while at 700 hPa wet airmasses were advected. In the mid-troposphere region (at 500 hPa), Hungary was situated in front of a cold low. There was strong, southerly wind, and the cold advection was just

beginning from south-west in the afternoon. This case can be considered as a type of large precipitation with intensive, fast moving thunderstorms.

Table 1. Average characteristics of the most frequent patterns and for all cases. Rows mean:
Note: the last column shows the average values for all (seven) cases.

	A3	B1	B2	C1	C2	All
1	0.04	0.20	0.14	0.30	0.37	0.23
2	6.57	26.21	7.45	26.75	26.32	17.92
3	45.34	52.50	43.02	57.08	54.03	50.34
4	90.87	91.88	85.66	97.40	95.59	91.94

1 Ratio of areas with large precipitation (where the calculated 24-hour amount is above 50 mm). Total area: 245116 km^2.

2 Rate (in percentage) of convective (calculated only from echoes above 40 dBz) and total precipitation in areas with large precipitation.

3 On areas with large precipitation ratio of pixels where the convective part reached at least 60 % of the total amount.

4 On areas with large precipitation percentage of pixels where at least one strong echo (intensity $\leq$ 40 dBz) appeared.

Case studies also show that for types C1 or C2, greater amount of the large precipitation originated from strong echoes, and the convective activity was heavier having more cells with large precipitation as compared to other types.

Short case studies of the three most frequent combinations are described below.

3.2. B2 combination (Convective lines along the convergence zones of cyclone)

On August 11–12, 2007, a shallow, occluded cyclone could be analyzed on surface weather maps *(Fig. 5)*. In the upper levels, the synoptic scale vorticity was more significant, especially at 500 hPa, where a cut-off low zone could be detected. The relative humidity analyses on the 700 hPa level marked the wet convergence lines (so-called cyclone arms). One of these convective lines is shown in the radar image. The higher reflectivity echoes, surrounded by less intensive but still convective-derived areas, move almost in parallel to the curved convective line. This is a typical PS system (convective line). The maxima of the 24-hour precipitation are organized almost in lines in Transdanubia. This situation is a good example of a decaying, occluded cyclone, which can stay in the region of the Carpathian Basin for several days. In the upper levels, the cold, cut-off low and the stronger (but not jet-stream) winds guarantee the convective instability. The convergence lines ('arms') of the cyclone collect the humidity, and developing thunderstorms propagate slowly along these lines, producing large amounts of precipitation. This case can be considered as a type of large precipitation with less intensive thunderstorms.

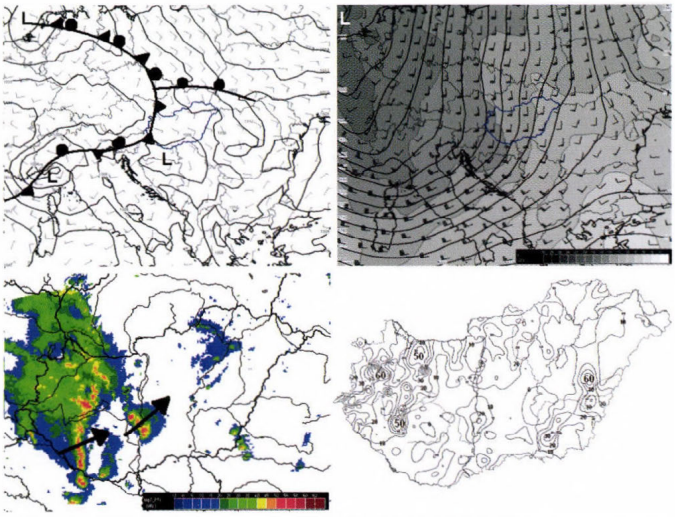

Fig. 4. Top: ECMWF analyses for August 20, 2007, 12:00 UTC.
Top left: MSL pressure (isobars by 2 hPa) wind field at the 925 hPa level and fronts. *Top right*: geopotential heights (lines by 20 gpm), temperature (monochrome shades by 2 °C) and wind field at 500 hPa level. *Bottom left*: composite radar image on August 20, 2007, 14:45 UTC. The arrows show the motion of the most intensive cells. *Bottom right*: Spatial distribution of 24-hour precipitation from August 20, 2007, 06:00 UTC to August 21, 2007, 06:00 UTC.

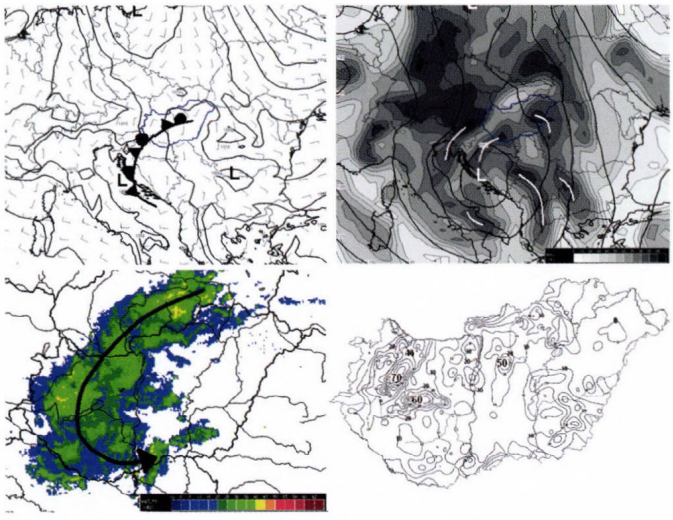

Fig. 5. Top: ECMWF analyses for August 11, 2007, 12:00 UTC.
Top left: MSL pressure (isobars by 2 hPa) at the 925 hPa level wind field and fronts. *Top right*: geopotential heights (lines by 20 gpm), 700 hPa humidity (monochrome shades) and wind. Convergence lines are drawn by white, curved lines. *Bottom left*: mosaic radar image on August 12, 2007, 03:30 UTC. The arrow marks the convective line. *Bottom right*: spatial distribution of 24-hour precipitation from August 11, 2007, 06:00 UTC to August 12, 2007, 06:00 UTC.

3.3. B1 type (Convective lines with cold front)

On July 14, 2008, a cold front was located over Hungary (*Fig. 6*). The front came from north-west and was moving slowly to south-east. Heavy thunderstorms developed ahead of it; some of them were long-living supercells. The most intensive storms were moving along lines from south-west to north-east, almost parallel to the front-line (*Csonka* and *Kolláth*, 2008). At the 500 hPa level, on the prefrontal side of the cold low (situated west of Hungary), cold advection could be observed, while on lower levels, the colder air reached only the north-western parts of Hungary. Strong upper winds generated significant shear, while at 700 hPa, from south-west humid airmasses were approaching. The maxima of 24-hour precipitation marked the path of the strongest cells. This case can be considered as the type of relative slow moving, sometimes extremely strong severe thunderstorms with supercells.

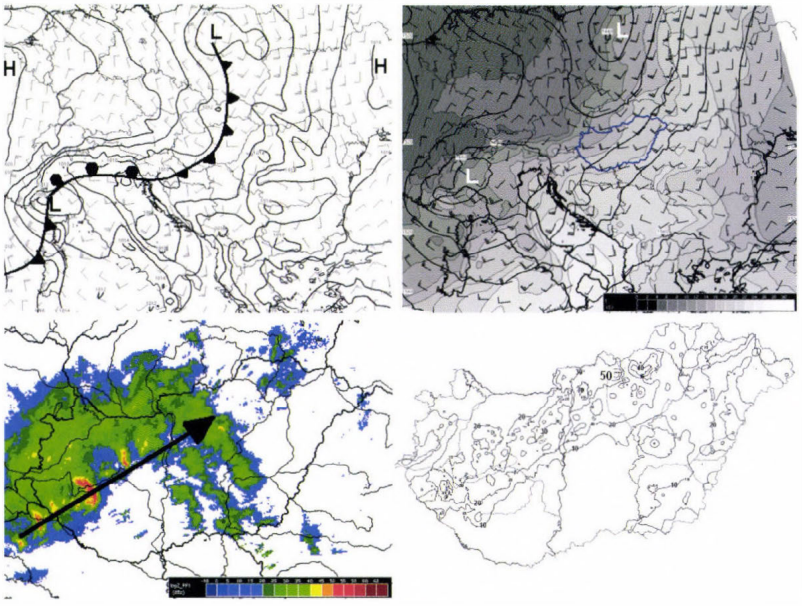

Fig. 6. Top : ECMWF analyses for July 14, 2008, 00:00 UTC
Top left: MSL pressure (isobars by 2 hPa) and the wind fields at the 925 hPa level and the front lines. *Top right*: geopotential heights (lines by 20 m), temperature (monochrome shades by 2 °C) and wind field of the 850 hPa level. *Bottom left*: composite radar images on July 14, 2008, 06:00 UTC. The arrow indicates the tracks of the most intensive storms. *Bottom right*: spatial distribution of 24-hour precipitation from July 14, 2008, 06:00 UTC to July 15, 2008, 06:00 UTC.

4. Conclusions

This paper presents the results of a study of large amount precipitation events in Hungary for the eight-year period of 2003–2010. The aim of this study was to describe these phenomena (which may cause flash flood) and to cluster them from synoptic and mesoscale points of view. Following this objective, 24-hour precipitation data, composite radar images, radar precipitation measurements, and ECMWF analyses and forecasts were applied. Nine combined patterns were created by considering mesometeorological, phenomenological, and synoptic points of view. The most frequent three types were demonstrated with case studies.

The main results of the research are as follows:

- 56 convective periods with large precipitation were found, and 55 were classified into 7 combined clusters.
- Most of the periods appeared in summer, the maxima were in June and in 2010.
- The most frequent combined types were squall lines with cold front (C1), convective lines along the convergence zones of a cyclone (B2), and convective lines with cold front (B1).
- Periods of convective squall lines with cold fronts appeared more often than convective lines in cyclonic situations.
- In each period, pixels with large precipitation (the calculated 24-hour amount is above 50 mm) appeared in about 0.23% of the total area (which is 564 km^2) on the average.
- Considering the large precipitation areas, the average ratio of convective precipitation (calculated only from strong echoes with reflectivity higher than 40 dBz) was approximately 18% in each period, but in about 50% of these cases the convective part was at least 60%.
- Periods with squall lines have higher convective activities and more cells with large precipitation than periods with lines or disorganized/weakly organized convective patches, because greater part of the large precipitation was produced by strong echoes.

In the future, this examination will be extended by focusing on regions endangered by flash floods involving more hydrological aspects.

Acknowledgements—This research was supported by the Jedlik Ányos Program 2005, identification number: OM-00103/2005.

Appendix

Calculation of motion vectors and accumulated precipitation using time series of radar reflectivity

HMS radar network collects data in 15-minute cycles, which can result in significant under-sampling in both space and time. A typical 12-hour accumulation precipitation field based on HMS radar network observation is shown in *Fig. 7*. The under-sampling strongly depends on the velocity of the radar cells, and can result in serious underestimation of the surface accumulated precipitation in the case of the fast moving squall lines.

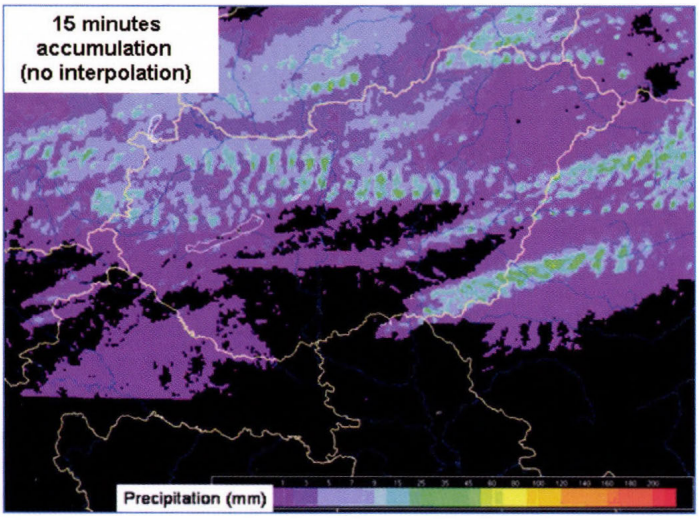

Fig. 7. 12-hour accumulated precipitation calculated by radar images with 15-minute time resolution.

The error caused by the under-sampling was reduced by using correlation tracking method (TREC, Tracking Radar Echoes by Correlation). During the TREC procedure, the radar grid was divided into so-called macro grids, and the calculation of motion vectors was based on maximum correlations for the macro grids. After quality control to filter out noisy vectors on macro grids, fine resolution motion vectors were interpolated for all grid points of the original radar grid. Once a motion vector field belonging to radar images at times T2 and T1 is available, interpolation of the radar reflectivity can be done at any time between T1 and T2. Echoes from T1 are moved forward and echoes from T2 moved backward by motion vectors, and the reflectivity of a given pixel is

interpolated between the forward and backward moving reflectivity values as shown in *Fig. 8.*

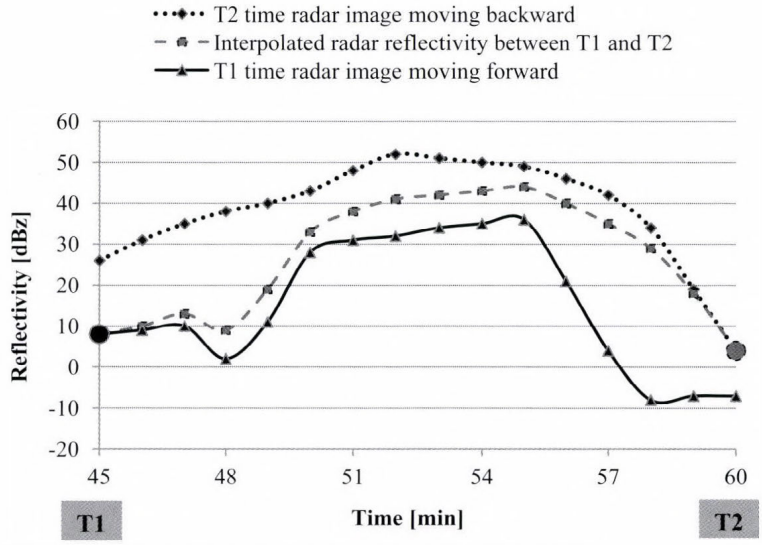

Fig. 8. Interpolation of radar reflectivity using motion vectors.

The application of the TREC method offers a more realistic accumulated precipitation field (*Fig. 9*). The 12-hour precipitation field in *Fig. 9* is calculated from 15-minute sampling cycle data. The optimal interpolation time step for precipitation calculation was found to be 1 minute.

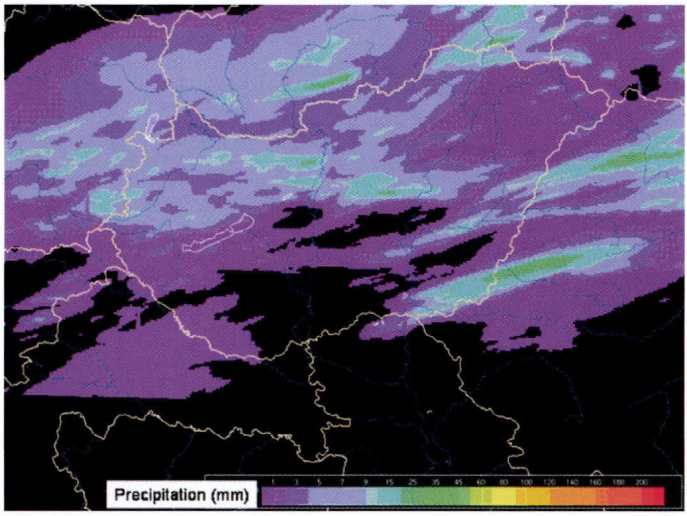

Fig. 9. 12-hour accumulated precipitation calculated by 1 minute interpolated radar images.

References

Bartholy, J. and *Pongrácz, R.*, 2005: Tendencies of extreme climate indices based on daily precipitation in the Carpathian Basin for the 20th century. *Időjárás 109*, 1–20.

Blöschl, G., Reszler, C. and *Komma, J.*, 2008: A spatially distributed flash flood forecasting model. *Environ. Modell. Softw. 23*, 464–478.

Bodolai, I., 1954: *Aerological and synoptical conditions of forming convective thunderstorms* (in Hungarian). Az OMI Kisebb Kiadványai 27, OMSZ, Budapest, 80 pp.

Bodolainé, J.E, 1980: *Using of radar measurements in short-range forecasting of precipitation* (in Hungarian) Az OMSZ Kisebb Kiadványai 48, OMSZ, Budapest, 79 pp.

Bodolainé, J.E., 1983: *Synoptical conditions of flood waves in the catchment of the Danube and Tisza* (in Hungarian). Az OMSZ Hivatalos Kiadányai 56, OMSZ, Budapest, 126 pp.

Bodolainé, J.E, Bodolai, I. and *Böjti, B.*, 1967: Macrosynoptical conditions for the formation of Slovenian squall lines and some properties of cold fronts with thunderstorm. *Időjárás 67*, 129–143.

Bodolainé, J.E. and *Homokiné, U.K.*, 1984: *Quantitative precipitation forecasts using the orographic precipitation enhancement* (in Hungarian). Az OMSZ Kisebb Kiadványai 57, OMSZ, Budapest, 45 pp.

Bodolainé, J.E. and *Tänczer, T.*, 1991: Instability line in a regional cyclone (in Hungarian). *Időjárás 95*, 178–195.

Bodolainé, J.E. and *Tänczer, T.*, 2003: *Mesoscale convective complexes producing flash floodwaves* (in Hungarian). Budapest, OMSZ, 184 pp.

Boncz, J., Kapovits, A., Pintér, F. and *Tänczer, T.*, 1987: A method for the complex analysis of synoptic weather radar and satellite data. *Időjárás 91*, 11–22.

Bonta, I. and *Takács, Á.*, 1988: *Construct of warning system for heavy rainfall in Hungary* (in Hungarian). Az OMSZ Kisebb Kiadványai 63, OMSZ, Budapest, 31 pp.

Browning, K.A., 1986: Conceptual Models of Precipitation Systems. *Weather Forecast. 1*, 23–41.

Caracena, F., Maddox, A.R., Hoxit, R.L., and *Chappell, C.F.*, 1979: Mesoanalysis of the Big Thompson Storm. *Mon. Weather Rev. 107*, 1–17.

Csonka, T. and *Kolláth, K.*, 2008: 'Transpannon monster", long-lived supercells on July 14, 2008 (in Hungarian). Published on the Internet: http://owww.met.hu/pages/bogacs20080714.php

Davis, R.S., 2001: Flash Flood Forecast and Detection Methods. In *Meteorological Monographs 28*, (ed: Doswell, C.A.), AMS, 481–525.

Déqué, M. and *Somot, S.*, 2008: Analysis of heavy precipitation for France using high resolution ALADIN RCM simulation. *Időjárás 112*, 179–190.

Dixon, M. and *Wiener, G.*, 1993. TITAN: Thunderstorm Identification, Tracking, Analysis and Nowcasting – A radar-based methodology. *J. Atmos. Ocean. Tech. 10*, 785–797.

Doswell, C.A. III, Brooks, H.E. and *Maddox, R.A.*, 1996: Flash flood forecasting: An ingredients-based methodology. *Weather Forecast. 11*, 560–581.

Geresdi, I., Horváth, Á., and *Mátyus, Á.*, 2004: Nowcasting of the precipitation type, Part II.: Forecast of thunderstorms and hailstone size. *Időjárás 108*, 33–50.

Götz, G. and *Bodolainé, J.E.*, 1963a: About mesosysnoptical forms (in Hungarian). *Időjárás 67*, 46–53.

Götz, G. and *Bodolainé, J.E.*, 1963b: Structures and analyses of instability lines (in Hungarian). Az OMI Kisebb Kiadványai 33, OMSZ, Budapest, 79 pp.

Hansen, E.M., Schreiner, L.C. and *Miller, J.F.*, 1982: *Application of probable maximum precipitation estimates – United States East of the 105th meridian.* Hydrometeorological Report 52, National Weather Service, NOAA, US Department of Commerce, Washington, DC., 168 pp.

Homokiné, U.K., 1999: Flood of River Tisza at autumn (in Hungarian). *Légkör 64(1)*, 2–6.

Homokiné, U. K., 2001: Flood in March in Transcarpathia (in Hungarian). *Légkör 66(2)*, 2–5.

Horváth, Á., Ács, F. and *Seres, A.T.*, 2008: Thunderstorm climatology analyses in Hungary using radar observations. *Időjárás 112*, 1–13.

Horváth, Á. and *Geresdi, I.* 2003: Severe Storms and Nowcasting in the Carpathian Basin. *Atmos. Res. 67–68*, 319–332.

Horváth, Á., Geresdi, I., Németh, P. and *Dombai, F.*,2007: The Constitution Day storm in Budapest: Case study of the August 20, 2006 severe storm. *Időjárás 111*, 41–63.

Kapovits, A., 1986: Hydrological aspect of using radar precipitation measurements (in Hungarian). *Vízügyi Közlemények 68.*, 486–499.

Kerényi, J. and *Putsay, M.*, 2005: Extreme flood monitoring in Romania and Hungary using Earth Observation Data, *Időjárás 109*, 205–216.

Kessler, E. and K.E. Wilk, 1968: Radar measurements of precipitation for hydrological purposes. Report 5, International Hydro. Decade. WMO, Geneva

Lombardo, F. and *Baldini, L.*: 2010: *Study on the rainfall dependence structure using radar and rain gauge data.* International Workshop Advances in Statistical hydrology, May 23–25 2010, Taormina, Italy

Maddox, R.A., 1979: A methodology for forecasting heavy convective precipitation and flash flooding. *National Weather Digest: Flood 4*(4), 30–42.

Maddox, R.A., 1980: Mesoscale convective complexes. *B. Am. Meteorol. Soc. 61*, 1374–1387.

Marshall, J.S. and *Palmer, W.M.*, 1948: The distribution of raindrops with size. *J. Meteorol. 5*, 165–166.

Mimikou, M.A. and *Baltas, E.A.*, 1996: Flood Forecasting Based on Radar Rainfall Measurements. *J.Water Res. Plan. Manage.* 122, 151–156.

Parker, M.D. and *Johnson, R. H.*, 2000: Organizational Modes of Midlatitude Mesoscale Convective Systems. *Month. Wea. Rev. 128*, 3413–3436.

Parker, M.D. and *Johnson, R.H.*, 2004: Structures and Dynamics of Quasi-2D Mesoscale Convective Systems. *J. Atmos. Sci. 61*, 545–567.

Rigo, T. and *Liasat, M.C.*, 2002: Analysis of convective structures that produce heavy rainfall events in Catalonia (NE of Spain), using meteorological radar. *Proc. ERAD*, 45–48.

Rossa, A.M., Cenzon, G., and *Monai, M.*, 2010: Quantitative comparison of radar QPE to rain gauges for the 26 September 2007 Venice Mestre flood. *Nat. Hazards Earth Syst. Sci. 10*, 371–378.

Smith, J.A., Baeck, M.L., Meierdiercks, K.L., Miller, A.J., and *Krajewski, W.F.*, 2007: Radar rainfall estimation for flash flood forecasting in small urban watersheds. *Adv. Water Res. 30*, 2087–2097.

Takács, Á., Girz, C., Tollerud, E., and *Kertész, S.*, 2000: New methods for severe precipitation warning for Hungary. *Időjárás 104*, 1–67.

Warner, T.T, Brandes, E.A, Sun, J., Yates, D.N., and *Mueller, C.K.*, 2000: Prediction of a flash flood in complex terrain. Part I: A comparison of rainfall estimates from radar, and very short range rainfall simulations from a dynamic model and an automated algorithmic system. *J. Appl. Meteorol. 39*, 797–814.

Wilson, J.W., and *Brandes, E.A, 1979*: Radar measurement of rainfall – a summary. *B. Am. Meteorol. Soc. 60*, 1048–1058.

Yates, D.N., Warner, T.T., and *Leavesley, G.H.*, 2000: Prediction of a flash flood in complex terrain. Part II: A comparison of flood discharge simulations using rainfall input from radar, a dynamic model, and an automated algorithmic system. *J. Appl. Meteor. 39*, 815–825.

IDŐJÁRÁS

Quarterly Journal of the Hungarian Meteorological Service
Vol. 116, No. 2, April–June 2012, pp. 93-107

Application of a novel photoacoustic instrument for ammonia concentration and flux monitoring above agricultural landscape – results of a field measurement campaign in Choryń, Poland

Andrea Pogány[1*], Tamás Weidinger[2], Zoltán Bozóki[3], Árpád Mohácsi[3], Jerzy Bieńkowski[4], Damian Józefczyk[4], Attila Eredics[5], Árpád Bordás[2], András Zénó Gyöngyösi[2], László Horváth[6], and **Gábor Szabó[1]**

[1]*Department of Optics and Quantum Electronics, University of Szeged, Dóm tér 9, 6720 Szeged, Hungary, E-mails: andrea@titan.physx.u-szeged.hu, gszabo@physx.u-szeged.hu*

[2]*Department of Meteorology, Eötvös Loránd University, Pázmány P. sétány 1/A, 1117 Budapest, Hungary, E-mails: weidi@ludens.elte.hu, zeno@nimbus.elte.hu, bordas.arpad@gmail.com*

[3]*Research Group on Laser Physics of the Hungarian Academy of Sciences, Dóm tér 9, 6720 Szeged, Hungary, E-mails: zbozoki@physx.u-szeged.hu, mohacsi@titan.physx.u-szeged.hu*

[4]*Institute for Agricultural and Forest Environment, PAS, Bukowska st. 19, Poznań, Poland, E-mail: bienkowjerzy@poczta.onet.pl*

[5]*Institute of Environmental and Earth Sciences, Faculty of Forestry, University of West Hungary, Cházár A. tér 1, 9400 Sopron, Hungary, E-mail: aeredics@yahoo.com*

[6]*Hungarian Meteorological Service, P.O. Box 39 H-1675, Budapest, Hungary; E-mail: horvath.l@met.hu*

[*]*Corresponding author*

(Manuscript received in final form January 19, 2012)

Abstract—A one-week field measurement campaign has been carried out on a winter wheat field nearby a cattle farm in Poland. The aim of the campaign was to demonstrate applicability of a recently developed photoacoustic ammonia monitoring instrument for environmental research purposes. The photoacoustic instrument was operated with three sampling lines, and a wet-chemical AMANDA instrument with one sampling inlet was used as a reference for ammonia concentration monitoring. In addition to the ammonia measurements, several meteorological parameters were measured with a micro-meteorological station. The campaign was started with instrument intercomparison when all inlets of the ammonia monitoring instruments were placed at the same point. Good agreement has been found between concentration data measured by the three channels of the photoacoustic instrument and the AMANDA, which proves reliability of the instruments. In the second part of the campaign, plume detection and flux measurement were carried out. During this period the photoacoustic instrument was placed 130 m east, the AMANDA instrument was placed 46 m northeast from the farm; and the photoacoustic instrument operated in gradient configuration, i.e., with the three sampling inlets placed at three different heights above canopy level. Background concentration was found to be around 2 $\mu g m^{-3}$, which is typical for agricultural landscapes. Concentrations up to 60 $\mu g m^{-3}$ were observed in case of wind blowing from the direction of the farm, and difference between concentrations measured at the two different locations around the farm varied according to wind direction, indicating changing position of the ammonia plume around the farm. Concentration gradients measured by the photoacoustic instrument during the campaign showed strong diurnal variation according to atmospheric stability. Ammonia fluxes calculated from the measured gradients were in the range of 0 to –90 $ng m^{-2} s^{-1}$, in good agreement with expectations.

Key-words: ammonia, photoacoustic spectroscopy, surface-atmosphere exchange flux, plume detection, agriculture

1. Introduction

Measuring ambient concentration and surface-atmosphere exchange of ammonia is an important problem in environmental science (*Sutton et al.,* 2009a). Ambient concentration of ammonia varies within a wide range: background concentration is typically a few $\mu g m^{-3}$, while concentrations up to several ten $mg m^{-3}$ might occur near emission sources. The most important emission source of ammonia is agriculture, and environmental impacts include acidification, eutrophication, and formation of secondary aerosol particles. During the past decades, ammonia as an air pollutant has been gaining increasing attention. Reasons for this increasing interest are increasing emission of ammonia as a result of increasing agricultural production, as well as success of previous environmental regulations on industrial air pollutants (e.g., sulfur-dioxide and nitrogen oxides). Furthermore, reduced sulfur-dioxide level decreases the rate of co-deposition of sulfur-dioxide and ammonia as well as the rate of conversion of gaseous NH_3 to ammonium (hydrogen) sulphate particles resulting in higher ambient ammonia concentration (*Flechard et al.*, 1999; *Fowler et al.*, 2001; *Erisman et al.*, 2001a). As environmental impacts of ammonia became clear, importance of regulations concerning emission of ammonia as well as

monitoring and modeling tasks were recognized (*Galloway et al.,* 2002; *Sutton et al.,* 2009b).

The first international agreement regulating ammonia emission was the Gothenburg Protocol of the UN Convention on Long Range Transboundary Air Pollution in Europe in 1999 (*Erisman et al.,* 2003). The Protocol determined emission ceilings for each participating country and required the annual reporting of national ammonia emissions. Therefore, measuring ammonia emissions became an important issue.

Since the most important source of ammonia is the agriculture, it originates mainly from areal sources, such as fertilized agricultural fields and animal farms, as a result of which quantifying emission (or deposition) of ammonia requires the application of micrometeorological methods or models.

Ammonia concentrations measured at different distances and directions from a concentrated source, such as an animal farm can be used to study the ammonia plume formed around the source. Plume detection together with dispersion modeling can be used to establish and verify emission factors and, thereby, estimate the amount of ammonia emitted by the source (*Faulkner et al.,* 2007; *Staebler et al.,* 2009; *Loubet et al.,* 2010).

Micrometeorological flux calculation methods are used to quantify ammonia emission from fertilized fields (*Milford et al.,* 2001, 2009; *Spirig et al.,* 2009), or deposition to areas surrounding point sources (*Fowler et al.,* 1998). Although, several instruments have been developed for ammonia concentration measurement (*Erisman et al.,* 2001b; *von Bobrutzki et al.,* 2010), their applicability for routine monitoring tasks, and especially for flux measurement is not trivial, due to high requirements regarding ease of operation, accuracy, and time resolution. At this time, gradient measurement using wet-chemical instruments (e.g., AMANDA instruments) is believed to be the most reliable, although it is a rather laborious method for measuring ammonia concentration and flux. The first wet-chemical ammonia analyzers were developed in the 1990s (*Wyers et al.,* 1993) and became the most widely used instruments for environmental ammonia monitoring by now. Wet-chemical instruments ensure detection limit around 0.1 $\mu g m^{-3}$ with time resolution of a few minutes and simultaneous concentration measurement at up to three channels. The gradient technique requires simultaneous concentration measurements at different heights above canopy. This technique has been used for quantifying trace gas fluxes since the 1930s (*Thornthwaite* and *Holzman*, 1939), as a result of which necessary correction algorithms and limitations of the applicability of the method are well established. Differences in concentrations measured at different heights within a few meters above canopy are typically 5–20% of the ambient concentration, which means a required precision of a few tenth $\mu g m^{-3}$ in case of elevated concentration in agricultural landscapes. Time resolution is not critical, measurement of 30–60 min concentration averages is appropriate for gradient measurements.

Previously, we have developed a novel photoacoustic instrument for environmental ammonia monitoring (*Pogány et al.*, 2009, 2010). In this paper we report the field application of this instrument near a cattle farm in an agricultural landscape and demonstrate that the instrument is suitable for on-line, automatic measurement of both ammonia concentration and flux around point sources; therefore, it is a useful tool for quantifying ammonia load caused by concentrated sources.

2. *Experimental*

2.1. Description of the field and instrumentation

The field campaign has been carried out near Choryń, Poland (52°02'N, 16°46'W, 80 m asl.), in an agricultural landscape with total area of 15,000 ha. The campaign lasted for one week in autumn, between 21 and 28, October 2008. Aerial photograph of the field is shown in *Fig 1.*

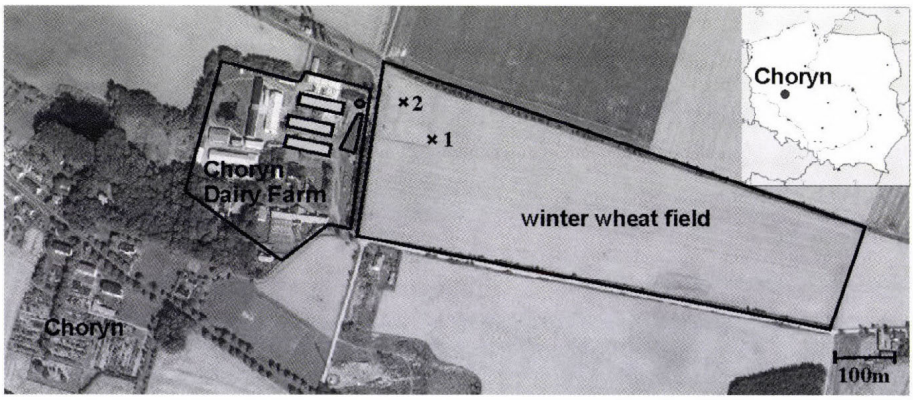

Fig. 1. Aerial photograph of the measurement sites. Light gray rectangles indicate farm buildings, dark grey frames indicate manure stack and slurry tank. Crosses show measurement sites 1 and 2, where the different instruments were installed (see in the text).

The Choryń Dairy Farm consists of three main buildings with 425 animals. Manure from the buildings is transported to an uncovered farmyard manure stack, while liquid fraction of cattle manure is stored in an uncovered slurry tank, both in a close vicinity of the farm buildings. Two measurement sites have been established in a winter wheat field with total area of 18 ha, at 130 m (site 1) and 46 m (site 2) distances from the cattle farm, as it is shown in *Fig. 1.*

A diode laser based photoacoustic instrument was used for measuring concentration and vertical concentration gradient of ammonia. Our previous results have proven that diode laser based photoacoustic spectroscopy is a reliable method for measuring gas concentration in field applications (*Bozóki et*

al., 2011), however, minimum detectable concentration with a simple diode laser based photoacoustic ammonia monitoring instrument (35 μgm^{-3}, *Huszár et al.,* 2008) is not sufficient for ambient ammonia concentration monitoring. Therefore, we supplemented the instrument with a pre-concentration unit, which resulted in an about 100-fold decrease in minimum detectable concentration (*Pogány et al.,* 2009). Furthermore, we have supplemented the instrument with two further sampling lines, which enables concentration measurement at three different sampling levels (*Pogány et al.,* 2010). Air sampling is carried out simultaneously through all sampling lines, while the subsequent concentration measurement is done one line after the other, using the same photoacoustic detector. The sampling lines are 3 m long Teflon tubes, with 8 mm inner diameter, and heated to ~50 °C to decrease adsorption of ammonia and water vapor in the sampling line. Teflon filters with 1 μm pore size in filter holders are placed at the inlets to prevent capture of aerosol particles in the pre-concentration units as well as to eliminate interference from ammonium containing particles. Vertical concentration gradient of ammonia can be measured by placing the three sampling inlets at three different heights above canopy, and ammonia flux can be calculated from the measured gradients. Time resolution of the instrument is 45 minutes that enables detection limit of 0.35 $\mu g m^{-3}$. Previously, the instrument was tested both for ammonia concentration (*von Bobrutzki et al.,* 2010) and flux (*Pogány et al.,* 2010) measurements.

An AMANDA system (Ammonia Measurement by ANnular Denuder sampling with on-line Analysis) purchased from ECN (Energy Research Centre of the Netherlands) was used as a reference instrument to measure ammonia concentration (*Wyers et al.,* 1993). The AMANDA instrument operated with one sampling inlet, 2 minutes time resolution and was calibrated daily with carefully prepared liquid samples.

Micrometeorological data were monitored by a meteorological station of four masts. Micrometeorological parameters for ammonia flux calculation were determined from data measured by an ultrasonic anemometer (METEK USA-1) placed at 2 m height on a separate mast. A microcomputer system was used for data acquisition at a rate of 10 Hz. Several further meteorological sensors were placed on the other three masts and in the soil; however, thorough analysis of all meteorological data is out of the scope of the current study. In this paper only a few data are shown to give an overview on the weather conditions during the experiment. The following meteorological data are shown in the present study: global radiation and net radiation (measured by Kipp & Zonen CNR1 net radiometer at 2 m height), air temperature and relative humidity (measured by a Vaisala HMP45 sensor from Campbell Scientific at 3.2 m height), soil temperature (measured by a 107-L thermistor from Campbell Scientific at 10 cm depth), wind speed and direction (measured by a Young wind monitor at 3.4 m height), and precipitation (measured by a Young tipping bucket rain gauge).

Data from the sensors were recorded by a Campbell CR23 datalogger every 10 minutes.

2.2. Measurement methods

The micrometeorological station and the photoacoustic instrument were operating throughout the whole campaign at site 1 (see *Fig. 1*). During the first part of the campaign as well as the last half day, the three inlets of the photoacoustic instrument were placed at the same height (1.2 m above canopy) to check precision of the instrument. Gradient measurements were carried out between 10 am on October 24 and 11 pm on October 27 at 0.5, 1.2, and 2.4 m heights above canopy.

During the first part of the campaign the AMANDA was also operating at site 1 and was moved to site 2 in the morning of October 25. The inlet of the AMANDA was placed at 1.2 m height at both sites.

Ammonia concentration data measured by the three channels of the photoacoustic instrument at the same height were compared, and precision of flux measurement was estimated on the basis of these data. Concentration data measured by the photoacoustic instrument and the AMANDA at the same site were also compared.

Ammonia concentrations measured by the two instruments at the two different sites were analyzed according to wind direction.

Ammonia fluxes were calculated from concentration data measured at three heights by the photoacoustic instrument using the gradient method (*Foken,* 2008), similarly to the method used in our previous work (*Pogány et al.,* 2010). In the followings, main steps of the applied flux calculation method are summarized.

Ammonia flux (F, in $\mu g\,m^{-2}\,s^{-1}$) was calculated as the product of friction velocity (u_*, in $m\,s^{-1}$) and dynamic concentration (c_*, in $\mu g\,m^{-3}$).

$$F = -u_* \cdot c_* . \tag{1}$$

Friction velocity was determined using the eddy covariance method, from vertical and horizontal wind velocity measured by the ultrasonic anemometer.

Dynamic concentration is calculated from concentrations measured at two different heights as:

$$c_* = \frac{\left[c(z_i) - c(z_j)\right]\kappa}{\ln\frac{z_i}{z_j} + \Psi(\zeta_i) - \Psi(\zeta_j)} , \tag{2}$$

where $c(z_i)$ and $c(z_j)$ are ammonia concentrations measured at z_i and z_j heights above canopy level, and □ is the von Kármán constant (0.4). □ is the universal function, i.e., a correction for atmospheric stability, and is a function of the dimensionless stability parameter ($\zeta = z / L$, where L is the Monin-Obukhov length). We used universal functions suggested by *Dyer* (1974), which is the most widely used correction in case of trace gas fluxes (*Weidinger et al.,* 2000).

Since we have measurement data from three heights, c_* was calculated for each sub-layer using concentrations measured at two heights (0.5–1.2 m, 1.2–2.4 m, and 0.5–2.4 m), and the average of the three values was used for ammonia flux calculation. For comparison, fluxes were also calculated for the individual sub-layers.

Raw data were filtered according to the following criteria. We did not calculate fluxes for periods with extraordinary stability, i.e., either $u < 0.8$ m s^{-1} or $|L| < 2.4$ m (corresponding to $|\zeta| > 1$ at 2.4 m height) due to limitations of the gradient method. Non-monotonic concentration profiles were also omitted from the calculations.

Precision of flux measurements was estimated by calculating "virtual ammonia flux" from concentration data measured at the same height. Virtual ammonia flux was calculated with the same method as real flux, supposing that the inlets are at 0.5, 1.2, and 2.4 m heights, however, they were at the same height. Average of the calculated virtual flux values should be zero, and standard deviation of the virtual ammonia flux gives the precision of flux measurements (*Pogány et al.,* 2010).

3. Results and discussion

3.1. Meteorological conditions

The weather during the campaign was cold with daily temperature maxima of 10–15 °C and minima around 0 °C. Relative humidity was high during the whole week, fog and dew formed during nighttime and one rain event occurred during the campaign, on October 22 (8.6 mm). Main micrometeorological parameters are shown in *Fig. 2*.

3.2. Instrument intercomparison

Fig. 3a shows the concentration readings of the three channels of the photoacoustic instrument for a one-day period, during which the inlets were placed at the same height. Difference of concentrations measured by the individual channels from the average concentration is depicted in *Fig. 3b*. Remarkably good agreement was found between the readings of the three channels.

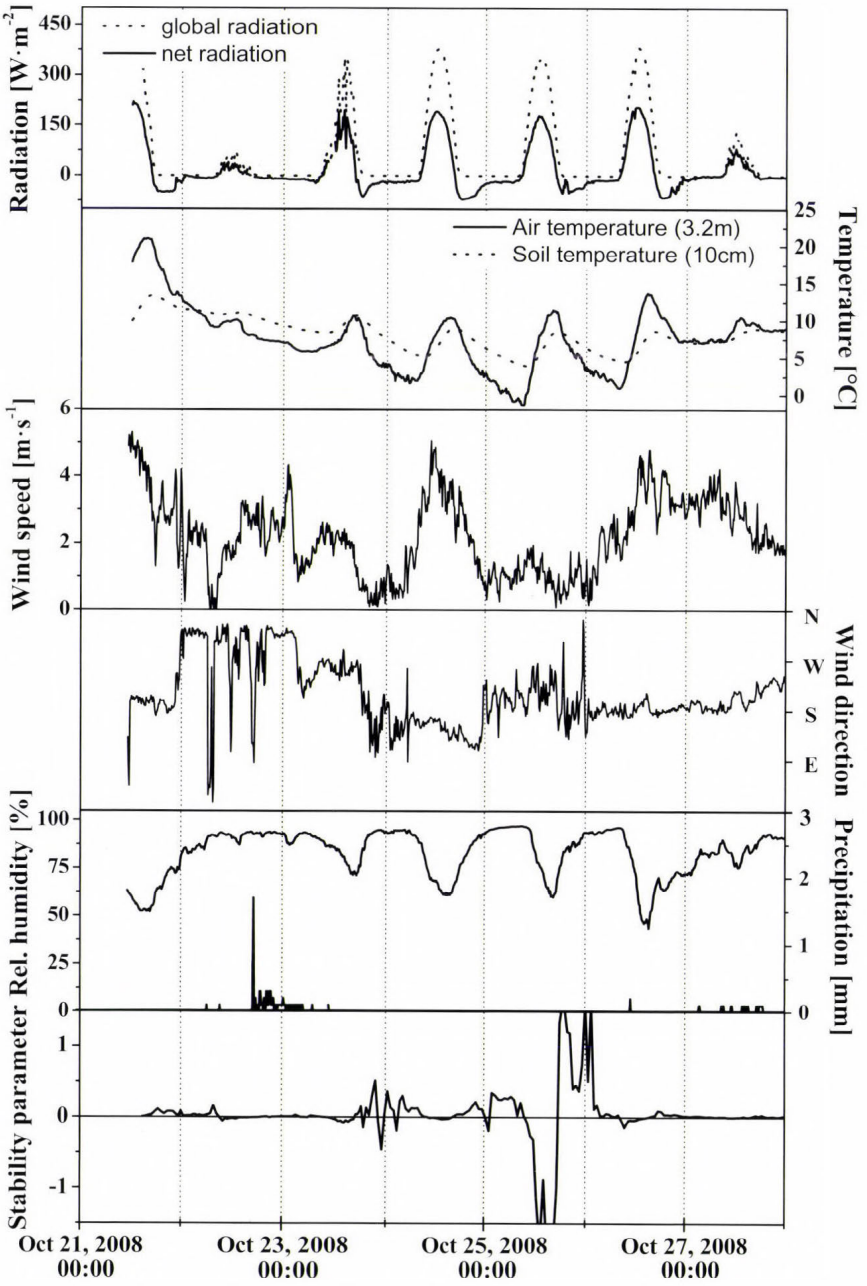

Fig. 2. Main meteorological parameters measured during the campaign (Note: ζ is calculated for 2.4 m height).

Average of the calculated virtual fluxes was found to be practically zero, i.e., smaller than the scatter of virtual flux, indicating that there is no systematic difference between the concentration readings of the three channels. Precision of flux measurements was found to be 15 $ng\,m^{-2}\,s^{-1}$, which is similar to the value determined during a similar flux measurement campaign with the same instrument (*Pogány et al.,* 2010). This value ensures precision better than 15% over fertilized agricultural fields, where typical ammonia fluxes range from 100 to several thousand $ng\,m^{-2}\,s^{-1}$.

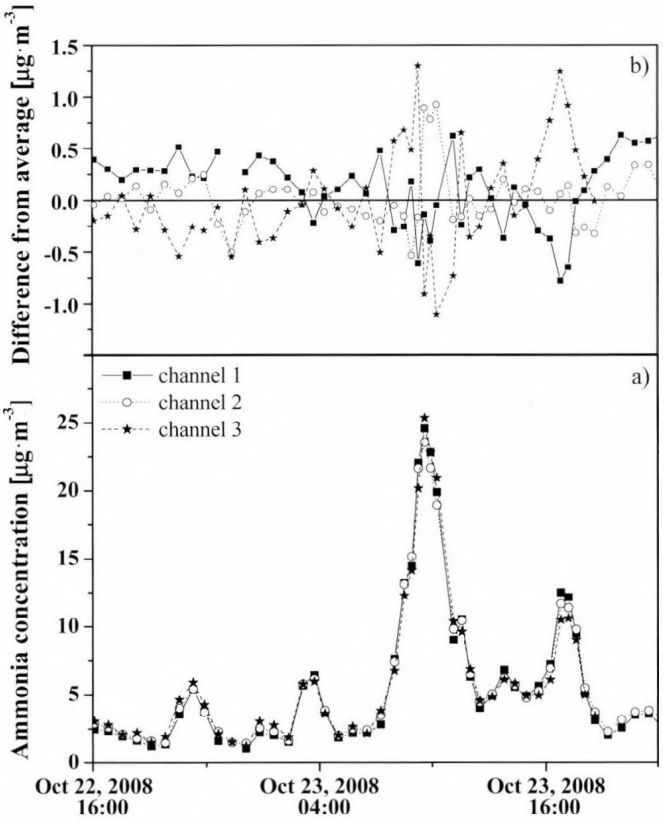

Fig. 3. Ammonia concentration measured at the same height by three channels of the photoacoustic instrument and deviation of the concentration reading of each channel from the average value.

Fig. 4 shows concentration data measured by the photoacoustic instrument and the AMANDA during the period when both instruments were operating at site 1. Closed symbols with solid line represent the average of the concentration readings of the three channels of the photoacoustic instrument, open symbols with dotted line represent concentration data measured by the AMANDA

averaged for the sampling periods of the photoacoustic instrument. The figure shows overall good agreement between the readings of the two instruments.

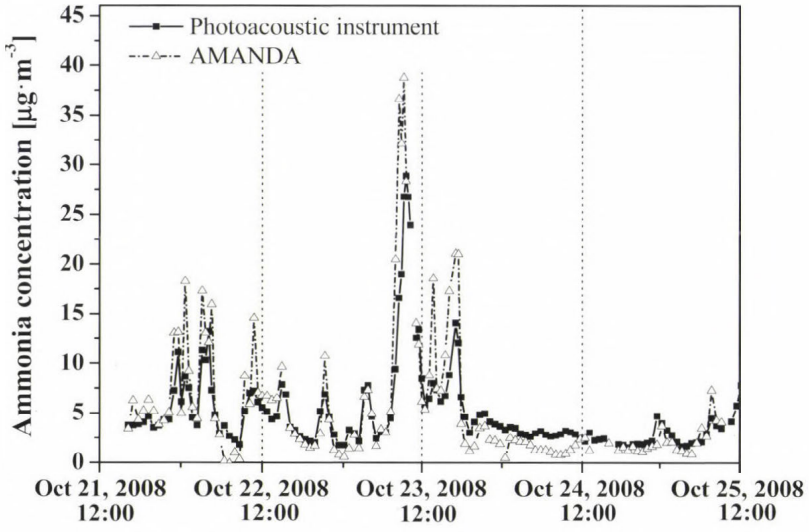

Fig. 4. Ammonia concentration measured by the photoacoustic instrument (closed squares and solid line) and by the AMANDA (open triangles and dotted line) at site 1 between October 21 and 25, 2008.

3.3. Plume detection

Fig. 5a shows ammonia concentration data measured by the photoacoustic instrument at site 1 and the AMANDA at site 2. *Fig. 5b* and *Fig. 5c* show wind direction and wind speed for the same period. During the first two days of the measurement, wind was not favorable for plume detection: on October 25, wind speed was very low, and afterwards southerly winds occurred, which caused the ammonia plume to form north of the farm, not in the direction of the instruments. During this period, only a few minor concentration peaks were observed indicating that the ammonia plume reached the AMANDA for a few short periods. Around midday on the October 27, wind direction changed to southwest and west, and differences in the measured concentration data clearly show the periods when only the AMANDA (October 27-28, southwesterly wind) or both instruments (in the morning October 28, westerly winds) were within the ammonia plume of the farm. Difference in the measured concentrations in case of westerly winds can be explained by the different distances of the two instruments from the farm.

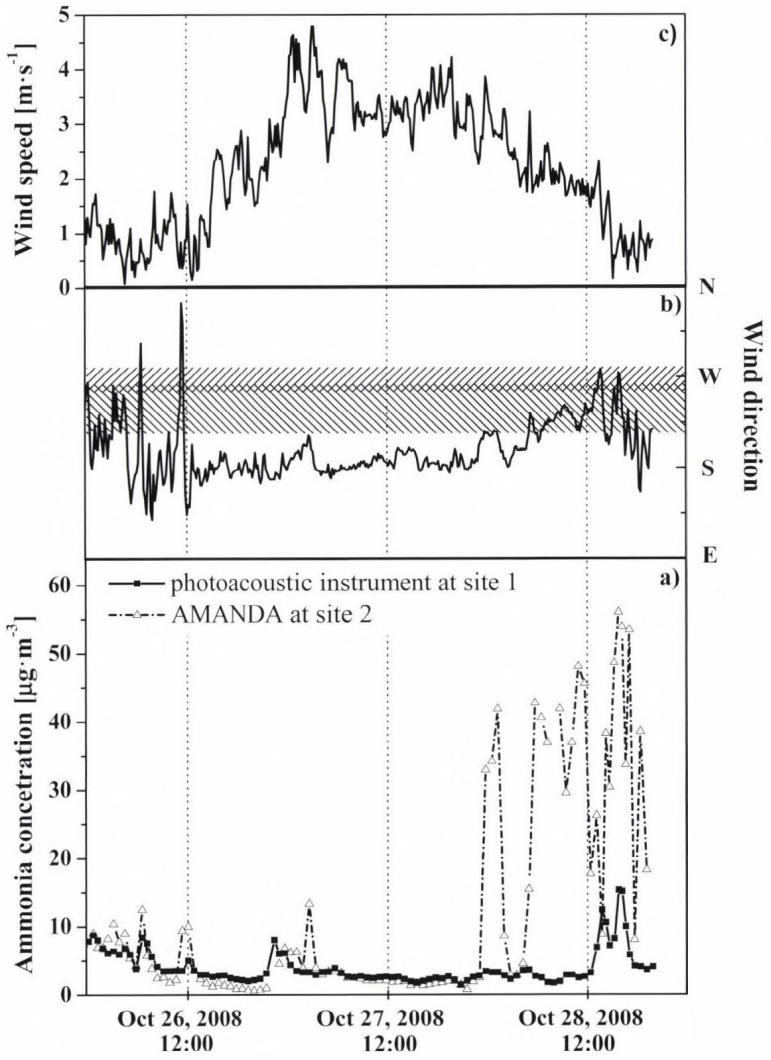

Fig 5. Ammonia concentration measured by the photoacoustic instrument at site 1 and by the AMANDA at site 2, together with wind direction and wind speed data. Shading indicates wind directions when the photoacoustic instrument (slope to the right) or the AMANDA (slope to the left) was within the ammonia plume of the cattle farm.

3.4. Flux measurements

Fig. 6 shows ammonia concentration data measured by the three channels of the photoacoustic instrument when the inlets were placed at three different heights.

Vertical gradient of ammonia shows very clear diurnal variation: differences between concentrations measured at the different heights were larger at night, and decreased to almost zero around midday both on the October 25 and 26, due to increased turbulence.

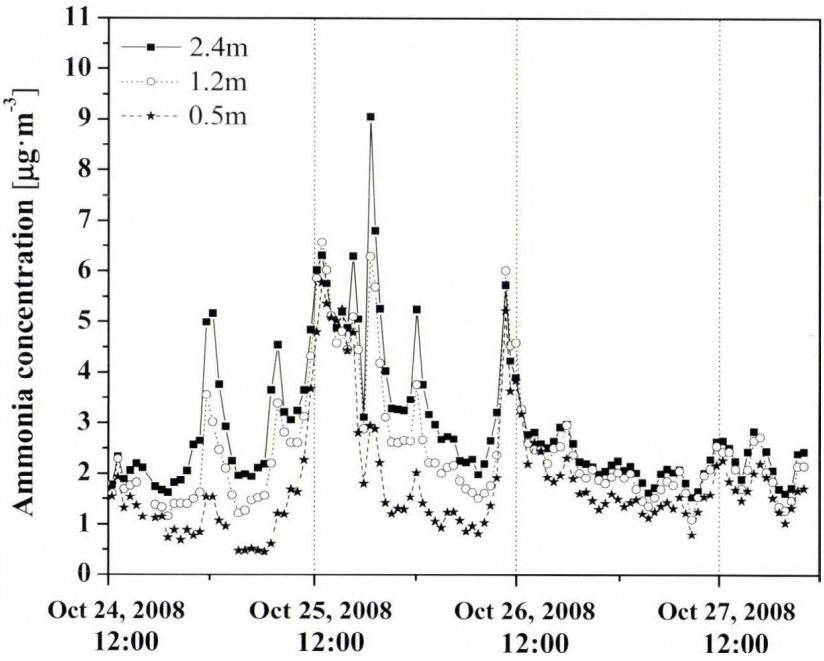

Fig. 6. Ammonia concentration measured by three channels of the photoacoustic instrument at 0.5, 1.2, and 2.4 m heights.

Fig. 7 shows the ammonia flux calculated from the concentration data depicted in *Fig. 6*. Altogether, 116 concentration gradient measurements were done with the sampling inlets placed at three different heights. 25 of these data were filtered out due to extreme stability conditions ($|\zeta|>1.5$, as it is shown in *Fig. 2*) or low wind speed on the October 25, while non-monotonic concentration profiles were the reason for omission in only 8 cases. Differences between fluxes calculated for the different sub-layers were in the 0–30 ng m^{-2} s^{-1} range.

The observed fluxes were negative in the range of 0 to -90 ng m^{-2} s^{-1} indicating ammonia deposition. Deposition of ammonia can be explained by elevated ammonia concentration caused by the farm, which exceeded the ammonia compensation point above the wheat field (*Asman,* 1998; *Fowler et al.,* 1998).

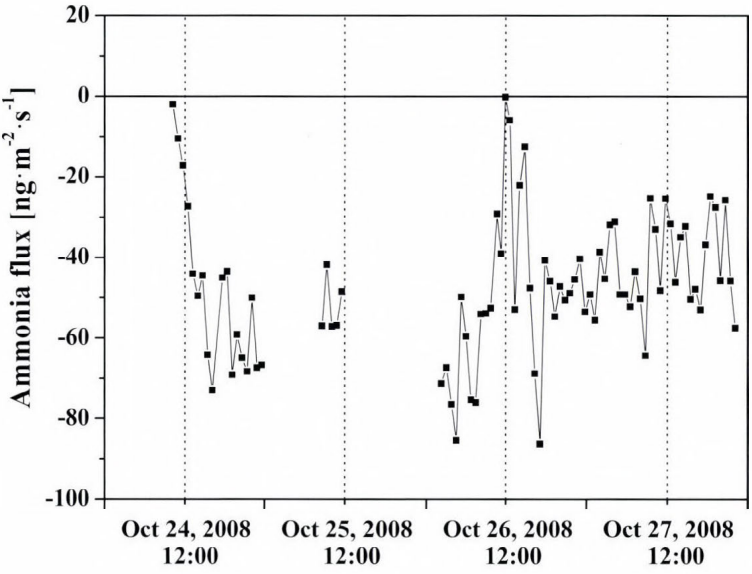

Fig. 7. Ammonia flux calculated from the concentration data shown in *Fig. 6.*

4. Conclusions

Results of the presented measurement campaign prove the applicability of our recently developed ammonia monitoring instrument in concentration and flux measurements over agricultural landscape. During the whole campaign, the photoacoustic instrument operated fully automatically and trouble-free, it required no maintenance, in contrast to the AMANDA instrument that requires frequent calibration and supply of chemicals. This fact proves that the photoacoustic instrument has the necessary robustness and it is easy to operate even under field conditions, therefore, fulfills technical requirements of environmental monitoring. Precision and time resolution of the instrument is proved to be suitable for field applications as well.

As far as the environmental impact of the studied emission source is concerned, measured data were found to agree with results of similar experiments. Concentration as well as deposition flux measured at 130 m distance from the farm was found to be slightly higher than the background value, similarly to results of an experiment around a poultry farm reported by *Fowler et al.* (1998).

Acknowledgements—We thank the Hungarian National Office for Research and Technology (NKFP3-00021/2005, and TUDAS-1-2006-0037), the OTKA foundation (Research and Technology

Innovation Fund, project number: CNK 78549), the European Social Fund (TÁMOP 4.2.1./B-09/1/KMR-2010-0003), COST action ES0804, NiNE Short Visit Grant No. 2417, and the NitroEurope EU 6th Framework Program "Energy, Environment and Sustainable Development, Global Change, Climate and Biodiversity; The nitrogen cycle and its influence on the European greenhouse gas balance NITROEUROPE IP" (2006–2011, Contract 017841) for financial support.
We thank *Mark Sutton* for initiating Hungarian-Polish scientific collaboration within the NitroEurope program, *Krzysztof Janku* for his help in organizing the campaign and setting up the instruments, and *Zoltán Istenes* for his help in designing the data acquisition system.

References

Asman, W.A.H., 1998: Factors influencing local dry deposition of gases with special reference to ammonia. *Atmos. Environ. 32*, 415–421.

von Bobrutzki, K., Braban, C.F., Famulari, D., Jones, S.K., Blackall, T., Smith, T.E.L., Blom, M., Coe, H., Gallagher, M., Ghalaieny, M., McGillen, M.R., Percival, C.J., Whitehead, J.D., Ellis, R., Murphy, J., Mohácsi, A., Pogány, A., Junninen, H., Rantanen, S., Sutton, M.A. and *Nemitz, E.*, 2010: Field inter-comparison of eleven atmospheric ammonia measurement techniques. *Atmos. Meas. Tech. 3*, 91–112.

Bozóki, Z., Pogány, A. and *Szabó, G.*, 2011: Photoacoustic instruments for practical applications: present, potentials and future challenges. *Appl. Spectrosc. Rev. 46*, 1–37.

Dyer, A. J., 1974: A review of flux-profile relationships. *Bound-Lay. Meteorol. 7*, 363–372.

Erisman, J.W., Hensen, A., Fowler, D., Flechard, C., Grüner, A., Spindler, G., Duyzer, J., Westsrate, H., Römer, F., Vonk, A. and *Jaarsveld, H.*, 2001a: Dry deposition monitoring in Europe. *Water Air Soil Poll. Focus 1*, 17–27.

Erisman, J.W., Otjes, R., Hensen, A., Jongejan, P., van den Bulk, P., Khlystov, A., Möls, H. and *Slanina, S.*, 2001b: Instrument development and application in studies and monitoring of ambient ammonia. *Atmos. Environ. 35*, 1913–1922.

Erisman, J.W., Grennfelt, P. and Sutton, M., 2003: The European perspective on nitrogen emission and deposition. Environ. Int.29, 311–325.

Faulkner, W.B., Powell, J.J., Lange, J.M., Shaw, B.W., Lacey, R.E. and *Parnell, C.B.*, 2007: Comparison of Dispersion Models for Ammonia Emissions from a Ground-Level Area Source. *Trans. ASABE. 50*, 2189–2197.

Foken, T., 2008: *Micrometeorology*. Springer Verlag ISBN 978-3-540 74666-9 308 pp.

Flechard, C.R., Fowler, D., Sutton, M.A. and *Cape, J.N.*, 1999: A dynamic chemical model of bi-directional ammonia exchange between semi-natural vegetation and the atmosphere. *Q. J. Roy. Meteorol. Soc. 125*, 2611–2641.

Fowler, D., Pitcairn, C.E.R., Sutton, M.A., Flechard, C., Loubet, B., Coyle, M. and *Munro, R.C.*, 1998: The mass budget of atmospheric ammonia in woodland within 1 km of livestock buildings. *Environ. Poll. 102 (S1)*, 343–348.

Fowler, D., Sutton, M.A., Flechard, C.R., Cape, J.N., Storeton-West, R., Coyle, M. and *Smith, R.I.*, 2001: The control of SO_2 dry deposition on to natural surfaces and its effects on regional deposition. *Water Air Soil Poll. Focus 1*, 39–48.

Galloway, J., Cowling, E., Erisman, J.W., Wisniewsky, J. and *Jordan, C.*, 2002: *Optimizing nitrogen management in food and energy production and environmental protection: contributed papers from the 2nd International Nitrogen Conference*, 14-18 October 2001, Potomac, Maryland, *USA*, Taylor & Francis, ISBN 90 265 1927 3, 1013 pp.

Huszár, H., Pogány, A., Bozóki, Z., Mohácsi, Á., Horváth, L. and *Szabó, G.*, 2008: Ammonia monitoring at ppb level using photoacoustic spectroscopy for environmental application. *Sensor. Actuator. B 134*, 1027–1033.

Loubet, B., Génermont, S., Ferrara, R., Bedos, C., Decuq, C., Personne, E., Fanucci, O., Durand, B., Rana, G. and *Cellier, P.*, 2010: An inverse model to estimate ammonia emissions from fields. *Eur. J. Soil Sci. Special Issue: Nitrogen and greenhouse gas exchange 61*, 793–805.

Milford, C., Theobald, M. R., Nemitz, E. and *Sutton, M. A.*, 2001: Dynamics of ammonia exchange in

response to cutting and fertilizing in an intensively-managed grassland. *Water Air Soil Poll. Focus 1,* 167–176.

Milford, C., Theobald, M.R., Nemitz, E. , Hargreaves, K.J., Horvath, L., Rásó, J., Dämmgen, U., Neftel, A., Jones, S.K., Hensen, A., Loubet, B., Cellier, P. and *Sutton, M.A.,* 2009: Ammonia fluxes in relation to cutting and fertilization of an intensively managed grassland derived from an inter-comparison of gradient measurements. *Biogeosciences 6,* 819–834.

Pogány, A., Mohácsi, Á., Varga, A., Bozóki, Z., Galbács, Z., Horváth, L. and *Szabó, G.,* 2009: A compact ammonia detector with sub-ppb accuracy using near-infrared photoacoustic spectroscopy and preconcentration sampling. *Environ. Sci. Tech. 43*, 826–830.

Pogány, A., Mohácsi, Á., Jones, S. K., Nemitz, E., Varga, A., Bozóki, Z., Galbács, Z., Weidinger, T., Horváth, L. and *Szabó, G.,* 2010: Evaluation of a diode laser based photoacoustic instrument combined with preconcentration sampling for measuring surface-atmosphere exchange of ammonia with the aerodynamic gradient method. *Atmos. Environ. 44,* 1490–1496.

Spirig, C., Flechard, C. R., Ammann, C. and *Neftel, A.,* 2009: The annual ammonia budget of fertilized cut grassland – Part 1: Micrometeorological flux measurements and emissions after slurry application. *Biogeosci. Discuss. 6,* 9583–9625.

Staebler, R.M., McGinn, S.M., Crenna, B.P., Flesch, T.K., Hayden, K.L. and *Li, S.-M.,* 2009: Three-dimensional characterization of the ammonia plume from a beef cattle feedlot. *Atmos. Environ. 43,* 6091–6099.

Sutton, M.A., Erisman, J.W, Dentener, F. and *Möller, D.,* 2009a: Ammonia in the environment: From ancient times to the present. *Environ. Poll. 156,* 583–604.

Sutton M.A., Reis, S. and *Baker, S.M.H.,* 2009b*: Atmospheric ammonia. Detecting emission changes and environmental impacts.* Springer Science, ISBN 978-1-40-20-9120-9. 461 pp.

Thornthwaite, C.W. and *Holzman, B.,* 1939: The determination of evaporation from land and water surfaces. *Month. Weather Rev. 67,* 4–11.

Weidinger, T., Pinto, J. and *Horváth, L.,* 2000: Effects of uncertainties in universal functions, roughness length, and displacement height on the calculation of surface layer fluxes. *Meteorol. Z. 9,* 139–154.

Wyers, G.P., Otjes, R.P. and *Slanina, J.,* 1993: A continuous flow denuder for the measurement of ambient concentration and surface-exchange fluxes of ammonia. *Atmos. Environ. 27A,* 2085–2090.

IDŐJÁRÁS

Quarterly Journal of the Hungarian Meteorological Service
Vol. 116, No. 2, April–June 2012, pp. 109-122

Microclimate simulation of climate change impacts in a maize canopy

Tímea Kocsis* and **Angéla Anda**

Department of Meteorology and Water Management,
University of Pannonia Georgikon Faculty,
P.O. Box 71, Keszthely H-8361, Hungary

Corresponding author; E-mail: timea.kocsis@gmail.com

(Manuscript received in final form January 5, 2012)

Abstract—Effects of possible climate modification on maize plant features have been evaluated by using the simulation model of *Goudriaan* for local climatic conditions and locally measured plant characteristics. Moderate climate modifications were hypothesized. According to the purpose of detecting local impacts of climate change, researches were made on the microclimate of maize canopies. In the energy transport of the plant stand, no shift has been experienced to the direction of the latent heat as it was expected because of the effect of warming up and decrease of precipitation. The changes of stomatal resistance and inside canopy air temperature suggested that the natural water supply will probably not cover the water demand of the plant, if the climate change is more intensive, therefore farmers must prepare to irrigated cultivation and to apply different agro-technical methods to save the water supplies of the ground.

Key-words: climate change, microclimate simulation model, maize, Keszthely, Hungary

1. Introduction

Climate change and variability may have an impact on the occurrence of food security hazards at various stages of the food chain, from primary production through to consumption (*Tirado et al.,* 2010). Worldwide agriculture has to face major changes in land use in the coming decades, and agriculture needs to meet rising claim with less resource while satisfying quality and environmental demands (*Stein* and *Goudriaan,* 2000). Agriculture is one of the fields that are highly affected by climate change also in Hungary (*Jolánkai,* 2010), therefore, researches in this field and developing adaptation strategies are very important. Prognostics of the impacts of climatic changes for the Carpathian Basin

(Hungary) in air temperature and precipitation in the range of 0.5–4°C global change were described by *Mika* (2002). The main statement of the scenarios is that the local weather would get warmer (1–5°C) and drier ((–40) – (–66) mm) in the first some decades of the global warming (*Mika,* 2002). *Bartholy et al.* (2004) estimated the regional effects of climate change at Lake Balaton – Sió Canal catchment area (where the experimental site of the researches is situated) by a stochastic-dynamic downscaling model using the ECHAM/GCM outputs. *Bartholy et al.* (2004) predict a decrease of 25–35% of precipitation amount in the summer half-year and 0–10% decline in the winter half-year at a climate corresponding to double CO_2 level. These statements were enhanced by *Bartholy et al.* (2008), *Szépszó* and *Horányi* (2008), and by the *Hungarian Meteorological Service* (2010) according to further regional climate model simulations.

Crop simulation models are often used to predict the impact of global atmospheric changes on food production (*Ewert et al.,* 2002). Plant canopies' role and their capability of modifying local microclimate has come into focus in the issue of adaptations to climate change. *Easterling et al.* (1997) provided an approximation of the potential for strategically positioned shelterbelt systems to reduce climate change-related stress on maize in the USA. *Guilioni et al.* (2000) examined the influence of temperature on plant's development rates and worked out a model that uses meteorological data to estimate the temperature of a maize apex. *Goudriaan* and *Zadoks* (1995) analyzed the combined effects of pests and diseases under changing climate by using modeling tools, because climatic change not only affects the potential yield levels, but it may also modify the effects of pests and diseases.

Fodor and *Pásztor* (2010) used the 4M crop simulation model to quantify some indices of the agro-ecological potential of Hungary and its future development under climate change. Their results indicate that the Hungarian agriculture cannot avoid the effects of climate change, and these effects will be mostly negative. The yields of the spring crop as maize, sunflower, etc. will decrease, while higher yields might be expected for the autumn crops. *Gaál* (2007) analyzed the modification of the climatic conditions of maize production in Hungary using HadCM3 and B2 SRES scenario for the periods of 2011–2020 and 2031–2040. The results concluded that with higher temperature, maize hybrids of 2–3 FAO group of longer vegetation period could be cultivated, but the limiting factor will be the precipitation.

Dióssy and *Anda* (2008) focused the attention on the impacts of drastic climate change on the energy consumers of maize canopy in Hungary. The energy distribution for sensible and latent heat fluxes of the applied scenarios were not significantly modified (*Dióssy* and *Anda*, 2009; *Anda* and *Dióssy,* 2010). *Dióssy* (2008) reports the effect of global warming on the inside air temperature of maize canopies. According to the degree of warming up, the air temperature in the canopy increased.

At the Agrometeorological Research Station of Keszthely, observations of the microclimate have been made for several decades. As field experiments are time consuming and expensive, another method is the use of crop growing models that can quantify the effects of management practices and environmental circumstances on crop growth and productivity (*Knörzer et al.,* 2011). At Keszthely for more than one decade, information was gained by using simulation model about crop microclimate that could rarely be registered earlier. Numerical models are often used to simulate the complex energy and mass transfer processes in soil-plant-atmosphere system (*Sauer* and *Norman*, 1995). In this study, the Crop Micrometeorological Simulation Model (CMSM) constructed by *Goudriaan* (1977) was applied. Using the earlier data of Keszthely station, and the downscaled information for the country and the watershed area of Lake Balaton, the aim was to simulate the impacts of some expected climatic conditions on the microclimate and the physiological processes of the maize stand.

2. Material and methods

2.1. The selected site and origin of input data

The inputs, both meteorological and plant features used in the simulations were collected at Keszthely Agrometeorological Research Station (46°44'N, 17°14' E, 114.2 m). The required above-canopy meteorological parameters are daily runs of air temperature, air humidity, wind speed, net radiation and/or incoming global radiation (*Stigter et al.,* 1977). Meteorological data were measured by a QLC-50 automatic climate station by 10 sec sampling time that was established in 1996. Hourly meteorological data were formed for the requirements of the model. Our sample day was an average day in July, when the plants were fully developed. The reference level of the model inputs was taken into account by calculated aerodynamic depths for every stage of plant development (*Goudriaan,* 1977). The roughness length and zero-plane displacement for maize was adapted from *Monteith* (1973). Wind speed was estimated at a reference level using combination of friction velocity and the logarithmic wind speed profile above the canopy (*Goudriaan,* 1977). In case of the wind speed, measurements were made at 10 meters above the ground.

Test plant, the mid-season maize hybrid Norma (FAO 450) has been sown and cultivated since the 1970s at a plant density of 7 plants m^{-2} on plots of 0.7 ha. The inputs of the model were site and plant specific parameters (plant height, leaf density in three layers), different soil characteristics (soil moisture content and physical properties), and hourly meteorological data from local measurements which were transformed from the standard observation level of 2 m above soil surface to the reference level required by the model (*Anda* and *Kocsis,* 2008). The height of reference level depends on actual plant development.

In the past 40 growing seasons, the leaf area and its density were measured in the field on the same 10 sample plants weekly, using an LI-3000A portable planimeter. The soil moisture content in the upper 1 m was also measured in the field gravimetrically every 10 days at 10 cm intervals. The actual soil water content was expressed in terms of soil water potential. The physical properties of the local Ramann type brown forest soil were determined at the beginning of the investigations.

2.2. The applied Crop Micrometeorological Simulation Model (CMSM)

Goudriaan's (1977) simulation model and its improved version (*Goudriaan* and *Van Laar,* 1994) follow the division of the radiation inside the canopy and its utilization in different energy-intensive processes (*Anda* and *Lőke,* 2003). The theoretical background of the Crop Micrometeorological Simulation Model (CMSM) is the physics of the energy-transfer and transport processes. CMSM is based on the traditions of model-developing work of Wageningen group (*Van Ittersum et al.,* 2003).

The productivity of crops is directly related to their capture of resources (water, light) and the efficiency with which they convert these physical resources into biological materials (*Yi et al.,* 2010). One part of the radiation energy that reaches the plants reflects, the second part penetrates into the stock, and the third part is fixed by the plant stand (*Jones,* 1983; *Anda* and *Lőke,* 2003). As the vertical structure of the plant stand is not homogeneous, the height of the plant is usually divided into different number of layers, the characteristics of which can be regarded as more or less homogeneous (multi-layer model). The resistances between air layers in the canopy are not neglected, and gradients in air properties inside the canopy are also taken into account (*Goudriaan,* 1989). The number of the layers can be influenced by the characteristics of the canopy, the aim, and the element to be examined (*Goudriaan,* 1977; *Anda et al.,* 2002). CMSM is a static model according to the air conditions and dynamic for the soil and plant data (*Hunkár,* 1990; *Páll et al.,* 1998; *Hunkár,* 2002). Exchange processes at the soil surface are important from a modeling perspective in that the soil surface is the interface between the soil and atmospheric systems (*Sauer* and *Norman,* 1995).

Within the parameters calculated by the model, sensible and latent heat fluxes, air temperature inside the canopy, plant temperature, stomatal resistance, and intensity of the photosynthesis were involved into our simulation examinations. The sensible and latent heat fluxues were described as *Bowen ratio* (β) that is the proportion of the sensible and latent heat fluxes. These parameters were presented on the border of the upper third of plant height in the study. This is the place of cob formation, where the intensity of physiological processes is the highest.

Model results were analyzed by *paired t-test* using *STATA 5.0* (1996) statistical program package in order to prove the significant deviations.

Scenarios were set up to simulate the effects of climate change on the maize stand. Carbon-dioxide concentration was raised of the intercellular spaces in accordance with the changes of the carbon-dioxide concentration of the atmosphere on the basis of the data of the literature (*Jackson et al.,* 1994).

In each layer there are energy sources and sinks. The intensity and direction of the source and loss of the different forms of energy must be determined. On the basis of detailed calculations, the model creates profiles for the meteorological elements inside the canopy.

The theory of the CMSM is the calculation of the radiation distribution among different environmental processes. The sensible heat flux (H_i) [J m^{-2}] in the *i*th layer is (*Goudriaan* and *Van Laar,* 1994):

$$H_i = \frac{(T_{L,i} - T_{a,i})\rho c_p}{r_{H,i}}, \tag{1}$$

where
ρc_p is the volumetric heat capacity of the air [J m^{-3} K^{-1}],
$T_{L,i}$ is the temperature of the plant [°C],
$T_{a,i}$ is the air temperature [°C], and
$r_{H,i}$ is the resistance against heat transmission [s m^{-1}].

The latent heat flux (λE_i) [J m^{-2}] in the *i*th layer can be calculated as follows (*Goudriaan* and *Van Laar,* 1994):

$$\lambda E_i = \frac{(e_{s,T_{L,i}} - e_{a,i})\rho c_p}{r_{V,i}\gamma}, \tag{2}$$

where
γ is the psychometric constant [mbar K^{-1}]
$e_{s,T_{L,i}}$ is the saturation water vapor pressure at actual plant temperature [mbar]
$e_{a,i}$ is the vapor pressure of the air [mbar]
$r_{V,i}$ is the resistance against the entrance of moisture into the layer [s m^{-1}].

Basis of the assumption of leaf resistance simulation is that mass transport processes – both water vapor and carbon-dioxide – occur via stomata, so that the ratio between their resistances is equal to the ratio between their diffusivities. In case of maize a linear relationship exists between net CO_2 assimilation and inverse leaf resistance at constant CO_2 concentration of substomatal cavity. This connection served to simulate the leaf resistance, since net CO_2 assimilation can be deducted precisely from the absorbed short wave radiation (*Goudriaan,* 1977). Exceeding the saturation point of CO_2 assimilation (200 J m^{-2} s^{-1} for sunny maize leaves), the leaf resistance approaches its minimum value (*Stigter*

et al., 1977). Rate of net CO_2 assimilation (F_n) [kg CO_2 m^{-2} s^{-1}] was found by an empirical representation of measured curves (*Van Laar* and *Penning de Vries,* 1972, *Goudriaan,* 1977):

$$F_n = (F_m - F_d)[1 - exp(-R_v \varepsilon / F_m)] + F_d, \quad (3)$$

where

F_m is the maximum rate of net CO_2 assimilation [kg CO_2 m^{-2} s^{-1}],
F_d is the net CO_2 assimilation in the dark respiration [kg CO_2 m^{-2} s^{-1}],
R_v is the absorbed visible radiation (per leaf area) [J m^{-2} s^{-1}], and
ε is the slope of the curve of F_n–R_v at low light intensities [kg CO_2 J^{-1}], or efficiency ($17.2 \cdot 10^{-9}$ kg CO_2 J^{-1} light in maize).

At calculation of F_m the influence of leaf age and ambient CO_2 concentration were simplified and their average values were applied. Dependence of leaf temperature was considered as a dependence on ambient air temperature. Dark respiration was at about –0.1 of F_m (*Goudriaan*, 1977). From the net CO_2 assimilation calculated by Eq. (3) the leaf resistance is calculated with:

$$F_n = \frac{1.83 \cdot 10^{-6}(C_e - C_r)}{1.66 r_{leaf} + 1.32 r_H}, \quad (4)$$

where

r_H is resistance against heat transmission [s m^{-1}],
1.66 is the ratio between diffusivities (for CO_2 and H_2O),
$1.83 \cdot 10^{-6}$ converts CO_2 concentration into kg CO_2 m^{-3} from ppmv at 20°C,
C_e is the external CO_2 concentration [ppmv],
C_r is assumed as 'regulatory' CO_2 concentration [ppmv], and
1.32 originates from calculation of boundary layer resistance for CO_2,

or

$$r_{leaf} = \frac{1.83 \cdot 10^{-6}(C_e - C_r)}{1.66 F_n} - 0.783\, r_H \quad [\text{s m}^{-1}], \quad (5)$$

where 0.783 is an empirical constant given in *Goudriaan* (1977).

After calculation of the sensible and latent heat, the estimation of the crop temperature in the *i*th layer ($T_{L,i}$) [°C] was as follows (*Goudriaan,* 1977):

$$T_{L,i} = T_{a,i} + (H_i - H_{i-1}) \frac{r_{H,i}}{\rho c_p}, \quad (6)$$

where

ρc_p is the volumetric heat capacity of the air [J m^{-3} K^{-1}],
$T_{a,I}$ is the air temperature [°C], and
$r_{H,I}$ is the resistance against heat transmission [s m^{-1}].

There is an analogy in calculation of canopy inside air temperature and crop temperature. When i=1, $T_{a,i-1}$ is the temperature from the reference level. The zero level (if i=1, i–1 is the level zero) is the place of the reference height.

Validation of the model outputs (crop temperature, leaf resistance, some elements of microclimate, photosynthesis) were carried out locally (*Anda* and *Lőke,* 2002, 2005; *Lőke*, 2004, *Anda et al.*, 1997) using RMSD (*Willmott,* 1982) and the model does not need further adaptation.

2.3. The applied scenarios

For the reason of climate change impact simulation in case of maize, scenarios that represent moderate climatic variations (compared to the model runs carried out by *Dióssy* and *Anda,* 2008) for Hungary were established. By most of the publications regarding local climate modifications, precipitation decrease is to be continued in the future. 25–35% decrease is expected in case of modelling doubled CO_2 concentration together with air temperature increase (1.3–2°C in summer) for Lake Balaton – Sió Canal catchment area, on the western part of Hungary, where Keszthely is situated (*Bartholy et al.,* 2004). The inputs of plant architecture, the size of the assimilatory surface and its density were chosen from the local measurements of the past four decades by using the principle of analogy. Plant data (LAI) of those seasons were used, when the air temperature and soil water content were similar in July as in the scenarios, respectively. In Scenario 1, continuous linear changes were supposed to be on the basis of the meteorological data of July between 1977 and 2006 at Keszthely. CO_2 concentration rise that should be pared to 0.6 °C temperature rise was 440 ppmv (*Mika,* 2007). In Scenarios 2 and 3, the atmospheric CO_2 concentration was increased to 760 ppmv (*Table 1*) with higher rise of the air temperature and decrease of the soil moisture.

Table 1. The applied scenarios

Scenario	Air temperature	Soil moisture	CO_2	LAI
Control	average in July	average soil moisture	380 ppmv	3.0
Scenario 1	+ 0.6 °C	– 10%	440 ppmv	2.8
Scenario 2	+ 1.3 °C	– 25%	760 ppmv	2.3
Scenario 3	+ 2.0 °C	– 35%	760 ppmv	2.0

3. Results

The incoming radiation, that is absorbed in a given crop layer after reflecting from the canopy or proceeding towards the soil, becomes the energy source of the heating processes (sensible heat flux), and evapotranspiration (latent energy flux). If there is no water restriction, evapotranspiration is the main energy consumer of the plant stand. The diurnal mean *Bowen ratio* is shown in *Fig. 1*, and the statistical analysis showed that significant deviation cannot be observed from the control run in any of the scenarios (*Table 2*).

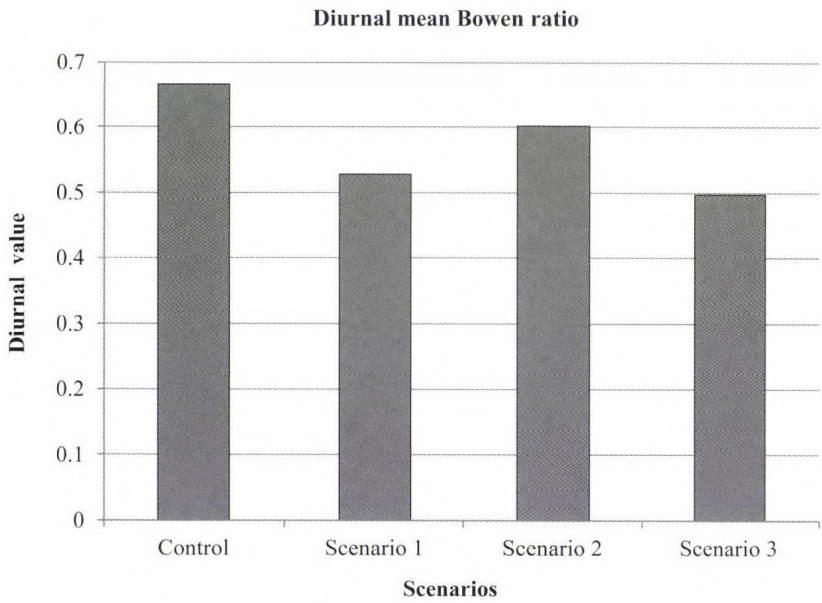

Fig. 1. Diurnal mean Bowen ratio.

Table 2. Results of the statistical analysis in case of the Bowen ratio

	Paired t-test	
	Mean (1–24 hours)	**p value**
Control	0.66	–
Scenario 1	0.53	0.21
Scenario 2	0.60	0.65
Scenario 3	0.50	0.13

The intensity of the photosynthesis and transpiration are influenced by the concentration of CO_2 because of its effect on the stomatal resistance. In order to get a higher yield, the plant must reach a balance between the as high as possible CO_2 amount that is needed for the photosynthesis, and gets into the leaves through the openings of the stomata, and the level of the amount of water that leaves the foliage which must be as low as possible in our climate. The two opposing processes are connected by the pores.

The stomatas can be regarded as closed when the stomatal resistance surpasses 2000 s m^{-1}. The stomatal resistance of the maize surpassed this value at night (between 8 pm and 7 am). On a daily average (between 8 am and 7 pm) the resistance rose by 16.76%, 61.55% and 69.1% in Scenarious 1, 2, and 3, respectively comparing them to the control run (*Fig. 2*). On the basis of statistical examinations, these deviations indicate significant changes.

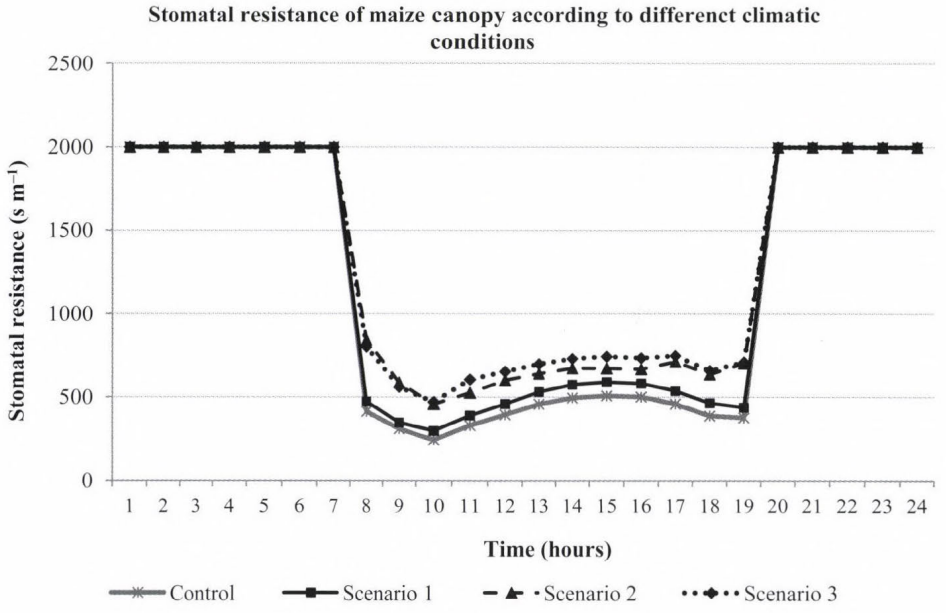

Fig. 2. Stomatal resistance of maize canopy according to different climatic conditions.

In the course of the production of organic matter, the process of photosynthesis uses carbon-dioxide from the surrounding air and water from the soil. The final benefit of the process is the difference between the amount of the organic matter created in the process of assimilation and used amount of

assimilates in the course of respiration (mainly at night). The intensity of the respiration (between 8 pm and 6 am) did not seem to be sensitive to climate change. The intensity of the photosynthesis, in the average of the values of day time, slightly decreased in the 1st and 3rd scenarios (*Table 3*), which indicates that the available carbon-dioxide (440 ppmv and 760 ppmv) could not compensate the reduction of precipitation (that was represented by ground water potential decrease in the model runs) and although the water consumption became more economical because of the narrowed stomatas, the amount of carbon-dioxide that got into the foliage was also restricted. In the 2nd scenario the 760 ppmv carbon-dioxide concentration could compensate the effects of the restriction of water supply and the intensity of photosynthesis increased. While in the 1st and 2nd scenarios the change of the intensity of photosynthesis indicates a significant deviation comparing to the control, the 3rd scenario does not show a significant modification (*Table 4*).

Table 3. Deviations between the control run and the scenarios for photosynthetic intensity

	Mean deviation from the control run in daytime hours (8–19 hours)
Scenario 1.	–2.99%
Scenario 2.	4.48%
Scenario 3.	–7.31%

Table 4. Results of the statistical analysis in case of the photosynthetic intensity

	Paired t-test	
	Mean (1–24 hours)	**p value**
Control	5.55E–07	–
Scenario 1.	5.36E–07	0.0174*
Scenario 2.	5.98E–07	0.0093*
Scenario 3.	5.26E–07	0.1954

*Significant difference if p is lower than 0.05.

In the Scenarious 2 and 3, the 24-hour average value of the inside canopy air temperature surpassed the additional air temperature rise while the average rise in the Scenario 1 was lower than the input temperature rise. The results of the plant temperature showed a higher rise in all scenarios than the rise of the ambient air temperature. In case of the average values of the daytime rise, the average growth in the cob level canopy temperature of all the three scenarios is

lower than the added temperature rise. The reason for this phenomena can be the self-shade of plants by day, and the leaves gave a special protection against sunshine, therefore, the inside canopy air temperature was more moderate than the temperature rise around it. In the case of the plant temperature, the average rise is almost the same or a little lower than the input temperature rise. The plant could keep its own temperature close to the temperature of the air surrounding it. Despite the decrease of the water supply and warming, the plant did not seem to suffer of heat-stress. The changes in all scenarios (regarding both temperature characteristics) show significant deviations (*Table 5* and *6*).

Table 5. Results of the statistical analysis in case of the inside canopy air temperature

	Paired t-test	
	Mean (1–24 hours)	**p value**
Control	21.56	–
Scenario 1	22.05	1.72E-03*
Scenario 2	23.14	3.28E-07*
Scenario 3	23.63	1.44E-08*

*Significant difference if p is lower than 0.05.

Table 6. Results of the statistical analysis in case of the crop temperature

	Paired t-test	
	Mean (1–24 hours)	**p value**
Control	20.75	–
Scenario 1	21.49	4.41E-07*
Scenario 2	22.65	2.68E-08*
Scenario 3	23.21	5.31E-10*

*Significant difference if p is lower than 0.05.

From the changes of the stomatal resistance and temperature of the air inside the canopy, it can be concluded that the natural water supply will not cover the water demand of the plant with the manifestation of the climate change, therefore, farmers must prepare for irrigation and application of agro-technical methods to save the water supplies of the ground. However, at the beginning of the climate change, the maize plant at Keszthely is able to compensate the unfavorable conditions and does not suffer damage when the water supply is moderately less.

4. Conclusions

Examining the microclimate of maize canopies it can be concluded, that in the energy transport of the plant stand no shift can be experienced to the direction of the latent heat as the effect of warming up and the decrease of precipitation. The increase of the stomatal resistance can be detected, while the intensity of the photosynthesis first increases, but when we assume stronger climate change, it decreases. Examining the changes of microclimatic elements, it can be concluded that besides the climate, the architecture of the plant stand has an important role as well. From the changes of the stomatal resistance and inside canopy air temperature it can be concluded that the natural water supply will probably not cover the water demand of the plant, if the climate change is more intensive, therefore, farmers must prepare to irrigation and to use different agro-technical practices to keep the water stores of the soil if they want to avoid yield loss.

Acknowledgements—This work was derived from the PhD thesis of *Timea Kocsis* who owes special thanks to *Prof. János Mika* and *Dr. Zoltán Varga* for their support.

References

Anda, A. and *Dióssy, L.*, 2010: Simulation in maize-water relations: case study for continental climate (Hungary). *Ecohydrology 3*, 487–496.

Anda, A. and *Kocsis, T.*, 2008: Impacts of atmospheric CO_2 enrichment on some elements of microclimate and physiology of locally grown maize. *Appl. Ecol. Environ. Res. 6,* 85–94.

Anda, A. and *Lőke, Zs.*, 2002: Stomatal resistance investigations in maize. *Acta Biol. Szegediensis 46,* 181–183.

Anda, A. and *Lőke, Zs.*, 2003: Parameters determining the evaporation of maize, calculation of stomatal resistance, plant temperature and photosynthetic intensity by simulation model. *Növénytermelés 52*, 351–363. (in Hungarian)

Anda, A. and *Lőke, Zs.*, 2005: Microclimate simulation in maize with two watering levels. *Időjárás 109*, 21–39.

Anda, A., Lőke, Zs., and *Sz. Kirkovits, M.*, 2002: Simulation of some parameters of plant water relation in maize. *J. Cent. Eur. Agric. 3*, 95–103. (in Hungarian)

Anda, A., Páll, J. and *Lőke, Zs.* 1997: Measurement of mean stomatal resistance in maize. Időjárás 101: 275–288.

Bartholy, J., Pongrácz, R., Matyasovszky, I., and Schlanger, V., 2004: Climate tendencies occurred in the 20th century and projected for the 21st century in Hungary. *AGRO-21 Füzetek 33*, 3–18. (in Hungarian)

Bartholy, J., Pongrácz, R., Gelybó, Gy., and *Szabó, P.*, 2008: Analysis of expected climate change in the Carpathian Basin using the PRUDENCE results. *Időjárás 112,* 249–264.

Dióssy, L., 2008: The influence of global climate change on air and soil temperatures in maize canopy. *Időjárás 112*, 125–139.

Dióssy, L., and *Anda, A.*, 2008: Energy Based Approach of Local Influence of Global Climate Change

in Maize Stand. *Cereal Res. Commun. 36,* 591–600.
Dióssy, L., and *Anda, A.,* 2009: Consequences of climate change on some maize characteristics in Hungary. *Időjárás 113*, 145–156.
Easterling, W. E., Hays, C. J., Easterling, M. M., and *Brandle J. R.,* 1997: Modelling the effect of shelterbelts on maize productivity under climate change: An application of the EPIC model. *Agr. Ecosys. Environ. 61,* 163–176.
Ewert, F., Rodriguez, D., Jamieson, P., Semenov, M.A., Mitchell, R.A.C., Goudriaan, J., Porter, J.R., Kimball, B.A., Pinter, P.J., Manderscheid, R., Weigel, H.J., Fangmeier, A., Fereres, E., and *Villalobos, F.,* 2002: Effect of elevated CO_2 and drought on wheat: testing crop simulation models for different experimental and climatic conditions. *Agr., Ecosys. Environ. 93*, 249–266.
Fodor, N., and *Pásztor, I.,* 2010: The agro–ecological potential of Hungary and its prospective development due to climate change. *Appl. Ecol. Environ. Res. 8,* 177–190.
Gaál, M., 2007: The modification of the climatic conditions of maize production according to B2 scenario. *AGRO-21 Füzetek 51*, 48–56. (in Hungarian)
Goudriaan, J., 1977: *Crop micrometeorology: a simulation study.* Simulation monographs, Pudoc, Wageningen.
Goudriaan, J., 1989: Simulation of micrometeorology of crops, some methods and their problems, and a few results. *Agr. Forest Meteorol. 47,* 239–258.
Goudriaan, J., and *Van Laar, H.H.,* 1994: Modelling Potential Crop Growth Processes. In *Current issues in Production Ecology, Vol. 2.,* Kluwer Academic Publishers, Netherlands.
Goudriaan, J., and *Zadoks, J.C.,* 1995: Global climate change: modelling the potential responses of agro-ecosystems with special reference to crop protection. *Environ. Pollut. 87*, 215–224.
Guilioni, L., Cellier, P., Ruget, F., Nicoullaud, B., and *Bonhomme, R.,* 2000. A model to estimate the temperature of a maize apex from meteorological data. *Agr. Forest Meteorol. 100,* 213–230.
Hungarian Meteorological Service, 2010: *Climate modelling activity, results*, OMSZ. (in Hungarian)
Hunkár, M., 1990: Simulation of microclimate of maize canopy. *Időjárás 94,* 221–229. (in Hungarian)
Hunkár, M., 2002: Moisture supply and microclimate-interactions with productivity potential. *Phys. Chem. Earth 27,* 1113–1117.
Jackson, R.B., Sala, O.E., Field, C.B., and *Mooney, H.A.,* 1994: CO_2 alters water use, carbon gain, and yield for dominant species in a natural grassland. *Oecologia 98,* 257–262.
Jolánkai, M., 2010: Agriculture, soil management and climate change. *Climate change and Hungary: mitigating the hazard and preparing for the impacts* (The VAHAVA Report), 38–45.
Jones H.G., 1983: *Plants and microclimate.* Cambridge University Press, Cambridge
Knörzer, H., Grözinger, H., Graeff-Hönninger, S., Hartung, K., Piepho, H.-P., and *Claupein, W.,* 2011: Integrating a simple shading algorithm into CERES-wheat and CERES-maize with particular regard to a changing microclimate within a relay-intercropping system. *Field Crop. Res. 121*, 274–285.
Lőke, Zs. 2004: Measurement and modelling average photosynthesis of maize. *J. Cent. Eur. Agr. 5,* 281–288. (In Hungarian)
Mika, J., 2002. About global climate change: from the point of view of a meteorologist. *Fizikai Szemle 52*, 258–268. (In Hungarian)
Monteith, J.L., 1973. *Principles of Environmental Physics.* Edward Arnold, London.
Páll, J., Anda, A. and Hunkár, M., 1998. Modelling microclimate of maize canopies with different water supplies. *Acta Geograph. Geolog. Meteorol. Debrecina 34*, 41–60 (in Hungarian)
Sauer, T.J., Norman, J.M., 1995: Simulated canopy microclimate using estimated below-canopy soil surface transfer coefficients. *Agr. Forest Meteorol. 75,* 135–160.
STATA 5.0, 1996: Stata Corporation LP Texas, USA. www.stata.com
Stein, A., Goudriaan, J., 2000: Spatial statistics for production ecology. *Agr. Ecosys. Environ. 81*, 1–3.
Stigter, C.J., Goudriaan, J., Bottemanne, F.A., Birnie, J., Lengkeek, J.G., and *Sibma, L.,* 1977: Experimental evaluation of a crop climate simulation model for Indian corn (Zea mays L.). *Agr. Meteorol. 18*, 163–186.
Szépszó, G. and *Horányi, A.,* 2008: Transient simulation of the REMO regional climate model and its evaluation over Hungary. *Időjárás 112,* 203–232.
Tirado, M.C., Clarke, R., Jaykus, L.A., McQuatters-Gollop, A., and *Frank, J.M.,* 2010: Climate change and food safety: A review. Food *Res. Int. 43,* 1745–1765.

Van Ittersum, M.K., Leffelaar, P.A., Van Keulen, H., Kropff, M.J., Bastiaans, L., and *Goudriaan, J.*, 2003: On approaches and applications of the Wageningen crop models. *Eur. J. Agron. 18*, 201–234.

Van Laar, H.H. and *Penning de Vries, F.W.T.* 1972: CO_2 assimilation light responce curves of leaves, some experimental data. *Vels. Inst. biol. scheik. Onderz. LandbGewassen* 62, Wageningen.

Willmott, C.J., 1982: Some comments on the evaluation of model performance. *Bull. Am. Meteorol. Soc.*, 1309–1313.

Yi, L., Shenjiao, Y., Shiqing, L., Xinping, C., and *Fang, C.*, 2010: Growth and development of maize (*Zea mays* L.) in response to different field water management practices: Resource capture and use efficiency. *Agr. Forest Meteorol. 150*, 606–613.

IDŐJÁRÁS

Quarterly Journal of the Hungarian Meteorological Service
Vol. 116, No. 2, April–June 2012, pp. 123-143

Assessing effect of time scale on the solar radiation sunshine duration relationship

Ji-Long Chen[1,2] and **Guo-Sheng Li**[1*]

[1]*Institute of Geographic Sciences and Natural Resources Research, Chinese Academy of Sciences, 100101 Beijing, China*

[2] *Graduate University of Chinese Academy of Sciences, 100039 Beijing, China*

[*]*Corresponding author; E-mail: ligscas@163.com*

(Manuscript received in final form September 12, 2011)

Abstract—Solar radiation is the principal and fundamental energy for many physical, chemical, and biological processes. Estimation of solar radiation from sunshine duration is common employed when no direct observation of solar radiation is available. Particularly, the *Ångström-Prescott* (A-P) model is widely used for its simplicity. This paper investigates the effect of time scale on the A-P parameters and the estimation accuracy using the data of 13 sites in Northeastern China. The results show that the A-P model can not be applied at annual, but less than seasonal time scale. Time scale effects the spatial variation of a and b parameters of the calibration curve, it has greater effect on parameter a than on b; while greater effect on temporal variation of b than that of a, and the differences of the parameters caused by time scales are generally large, however, the large differences of parameters do not result in significant difference of the estimation accuracy. Therefore, parameters at different time scales are interchangeable, the parameters calibrated at larger time scales can be applied to smaller time scales, and vice versa.

Key-words: solar radiation, estimation, *Ångström-Prescott* model, parameter, time scales

1. Introduction

Solar radiation is the principal and fundamental energy for many physical, chemical, and biological processes, and it is also an essential and important variable to many simulation models, such as agriculture, environment, hydrology, and ecology. However, in many cases, it is not readily available due to the cost and difficulty of maintenance and calibration of the measurement

equipment (*Hunt et al.*, 1998). Only a few meteorological stations measure solar radiation. For example, in USA, less than 1% of meteorological stations are recording solar radiation (*NCDC*, 1995; *Thorton* and *Running*, 1999). In China, more than 2000 stations have records of meteorological data, only 122 stations are recording solar radiation. The ratio of stations recording solar radiation to those recording temperature is about 1:500 around the world (*Thorton* and *Running*, 1999). Therefore, developing method to estimate solar radiation has been the focus of many studies.

Major methods including satellite-derived (*Frulla et al.*, 1988; *Pinker et al.*, 1995; *Olseth* and *Skartveit*, 2001; *Şenkal*, 2010), stochastic algorithm (*Richardson*, 1981; *Wilks* and *Wilby*, 1999; *Hansen*, 1999), empirical relationships (*Ångström*, 1924; *Prescott*, 1940; *Hargreaves*, 1981; *Bristow* and *Campbell*, 1984; *Hargreaves et al.*, 1985), interpolation (*Hay* and *Suckling*, 1979; *Rivington et al.*, 2006), and learning machine method (*Tymvios et al.*, 2005; *Cao et al.*, 2006; *Lam et al.*, 2008; *Jiang*, 2009; *Chen et al.*, 2011) have been developed for the purpose. Among them, the empirical relationship using other commonly measured meteorological data, such as sunshine duration, maximum and minimum temperatures, is attractive for its simplicity, efficiency, and lower data requirement. It is generally recognized that the sunshine-based methods outperform other meteorological variables models (*Iziomon* and *Mayer*, 2002; *Podestá et al.*, 2004; *Trnka et al.*, 2005), particularly the well-known *Ångström-Prescott* (A-P) model, proposed by *Ångström* (1924) and further modified by *Prescott* (1940), was widely used in different locations of the world (*Ångström*, 1924; *Prescott*, 1940; *Almorox* and *Hontoria*, 2004; *Liu et al.*, 2009). Several modifications to the A-P model have been proposed since it was developed (*Newland*, 1988; *Akinoglu* and *Ecevit*, 1990; *Ertekin* and *Yaldiz*, 2000). However, various comparative studies demonstrated that the modifications could not give significant improvement (*Iziomon* and *Mayer*, 2002; *Yorukoglu* and *Celik*, 2006; *Liu et al.*, 2009). As the result, the simple A-P model was preferred due to its greater simplicity and wider application.

A number of literatures focused on the studies of A-P model at monthly time scale (*Iziomon* and *Mayer*, 2002; *Almorox* and *Hontoria*, 2004; *Zhou et al.*, 2005), because the A-P model was initially developed using the monthly data; moreover, the author emphasized that the A-P model should be calibrated using the monthly data rather than the daily data (*Ångström*, 1956). Some literatures reported the studies at daily time scale (*Yorukoglu* and *Celik*, 2006), even at annual time scale (*Chen et al.*, 2006; *Liu et al.*, 2009), and showed that the parameters can be quite different in different places. Some of them noticed that the parameters changed with time scales (*Benson et al.*, 1984; *Ögelman et al.*, 1984), but they did not conclude the effect of the time scale. *Gueymard et al.* (1995) illustrated that the averaging time (time scale) is a critical factor in empirical and statistical models, stressed the importance of studying its effect,

and believed that the optimum averaging period for smoothing the data without significant loss of information remains unanswered. The effect of the time scale on relationship between solar radiation and sunshine duration remains unknown. Therefore, more investigation is necessary and important to clarify the effect of time scale on relationship between solar radiation and sunshine duration. The objectives of the current study are Eq.(1) to determine the A-P parameters at five time scales, namely, daily, half-monthly, monthly, seasonal and annual time scales (hereafter referred to as TS1, TS2, TS3, TS4, and TS5, respectively) in Northeastern China; Eq.(2) to investigate the effect of time scale on A-P parameters and estimation accuracy.

2. *Materials and method*

2.1. A-P model and calibration

The A-P model was proposed by *Ångström* (1924) and further modified by *Prescott* (1940). The original form of this model is:

$$\frac{Rs}{Ra} = a\frac{H}{Ho} + b \quad , \tag{1}$$

where Rs is daily actual global radiation [MJ m^{-2} d^{-1}], Ra is daily extra-terrestrial solar radiation [MJ m^{-2} d^{-1}], H is daily actual sunshine duration [h], Ho is daily potential sunshine duration [h], a and b are empirical parameters which are calibrated from regression analysis between H/Ho and Rs/Ra using the calibration data. The extra-terrestrial solar radiation and potential sunshine duration are calculated using the equations detailed by *Allen et al.* (1998).

$$Ra = 37.6d\left(\omega \sin\varphi \sin\delta + \cos\varphi \cos\delta \sin\omega\right), \tag{2}$$

$$d = 1 + 0.033\cos\left(\frac{2\pi}{365}n\right), \tag{3}$$

$$\delta = 0.4093\sin\left(\frac{2\pi}{365}n - 1.39\right), \tag{4}$$

$$\omega = \arccos\left(-\tan\varphi \tan\delta\right), \tag{5}$$

$$Ho = 24\omega / \pi \ , \tag{6}$$

where d is the correction of incoming solar radiation due to the changing distance between the Sun and the Earth, ω is the sunset hour angle [rad], φ is the latitude [rad], δ is the solar declination angle [rad], n is the number of the day of year starting from the first day of January.

2.2. Study area and site description

The current study focuses on Northeastern China (*Fig.1*), consisting of the three provinces of Liaoning, Jilin, and Heilongjiang and the four eastern prefectures of Inner Mongolia: Hulunbeier, Xinan, Tongliao, and Chifeng. The climate of the region has extreme seasonal contrasts, ranging from humid, almost tropical heat in the summer to windy, dry, and cold winter. The heartland of the region is the Northeast China Plain. It lies between the Greater and Lesser Khinggan and Changbai mountains, covering an area of 350 000 km^2. It is the main area of maize, millet and soybeans production in China, and hence the eco-environmental models and crop growth simulation are widely studied. However, only 13 meteorological stations provide solar radiation record. Moreover, no literature reported study on the solar radiation estimation for this region, and the information on the A-P model is limited.

A total of 13 stations with long-term available records of solar radiation are used in the present study (*Fig.1*). The mapping of stations roughly range from 38° to 52° latitude North, from 116° to 130° longitude East, and from 49 to 610 m altitude. *Table 1* shows the temporal period and the geographical information of the meteorological stations.

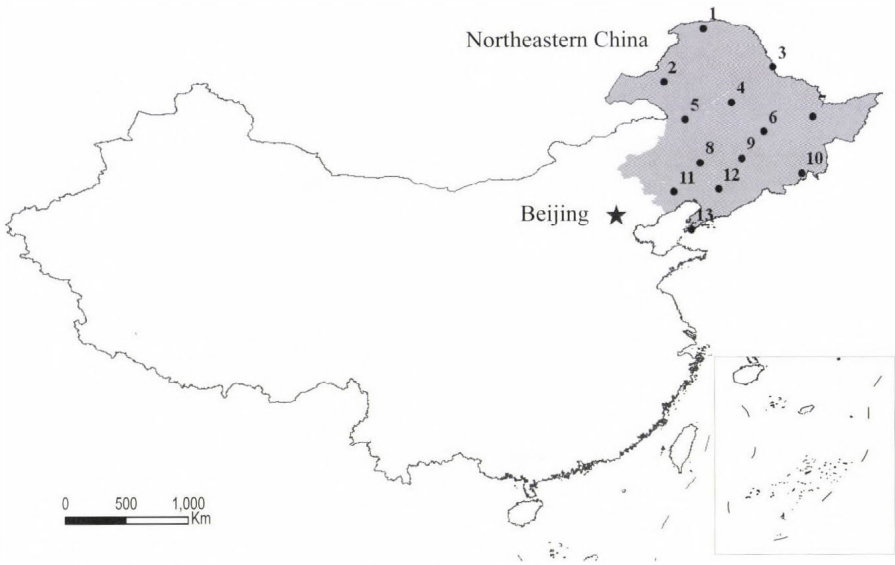

Fig.1. Location of the studied meteorological stations in Northeastern China (stations are numbered in compliance with *Table 1*).

2.3. Data collection and check

Daily actual global radiation and sunshine duration data of the study sites are used in the present study. The data were obtained from the National Meteorological Information Center (NMIC), China Meteorological Administration (CMA). The period of records ranges from 13 to 40 years covering the period between 1970 and 2009 (*Table 1*). Preliminary quality control tests were conducted by the suppliers. We further check the data according to the following criteria:

(a) For the daily data, records with missing data which were replaced by 32766, daily actual global radiation larger than the daily extra-terrestrial solar radiation, and actual sunshine duration larger than daily potential sunshine duration were removed from the data set.

(b) For half-month, we define days 1–15 as the first half month and day 16 through the end of the month as the latter half month. The half-monthly data is the average value of each day in the whole half-month. A half-month with more than 3 days of missing or faulty data in the same half-month was discarded.

(c) The monthly data is the average value of each day in the whole month. A month with more than 5 days of missing or faulty data in the same month was discarded.

(d) For season, we define March to May as spring, June to August as summer, September to November as autumn, December to February in the next year as winter. A season with more than 15 days of missing or faulty data in the same season, or 8 days of those in the same month was discarded.

(e) A year with more than 30 days of missing or faulty data, or 15 days of those in the same month, or 2 months with more than 10 days of missing or faulty data in the same month was discarded.

Two data sets are created for each time scale. About 75% of the total records are used for calibrating the parameters of A-P model, and the remainder for evaluating the model (*Table 1*). The investigation is operated at five time scales or averaging period, namely, daily (TS1), half-monthly (TS2), monthly (TS3), seasonal (TS4), and annual (TS5) time scales.

Table 1. Detailed information of the studied 13 stations in Northeastern China

Station ID	Station name	Latitude (N)	Longitude (E)	Altitude (m)	Calibration period	Validation period
1	Mohe	52.97	122.52	433.00	1997–2006	2007–2009
2	Hailaer	49.22	119.75	610.20	1972–1977 1982–2000	2001–2009
3	Heihe	50.25	127.45	166.40	1970–1999	2000–2009
4	Fuyu	47.80	124.48	162.70	1993–2004	2005–2009
5	Suolun	46.60	121.22	499.70	1992–2004	2005–2009
6	Haerbing	45.75	126.77	142.30	1970–1999	2000–2009
7	Jiamushi	46.82	130.28	81.20	1970–1978 1983–2000	2001–2009
8	Tongliao	43.60	122.27	178.70	1970–1999	2000–2009
9	ChangChun	43.90	125.22	236.80	1970–1981 1983–1999	2000–2009
10	Yanji	42.87	129.50	257.30	1970–1999	2000–2009
11	Chaoyang	41.55	120.45	169.90	1970–1999	2000–2009
12	Shengyang	41.73	123.52	49.00	1970–1999	2000–2009
13	Dalian	38.90	121.63	91.50	1970–1999	2000–2009

2.4. Data description

Fig. 2 shows the distribution of the averaged daily solar radiation (*Fig. 2*(a)) and sunshine duration (*Fig. 2*(b)) of the 13 sites in Northeastern China. Solar radiation and sunshine duration range from 4.53 to 21.73 MJ m^{-2} (averaged 13.26 MJ m^{-2}) and from 4.36 to 9.38 h (averaged 7.15 h), respectively. They generally have a similar tendency, with the maximum in July, and minimum in December. Pearson coefficient between solar radiation and sunshine duration is 0.92 ($p < 0.01$). Larger deviations of solar radiation and sunshine duration occur in April-September, which may be attributed to the large day-to-day fluctuation of the weather variables. Solar radiation shows larger variation than sunshine duration, with the *CV* of 40.68% and 16.87% for them, respectively, where *CV* is the ratio of standard deviation to arithmetic mean.

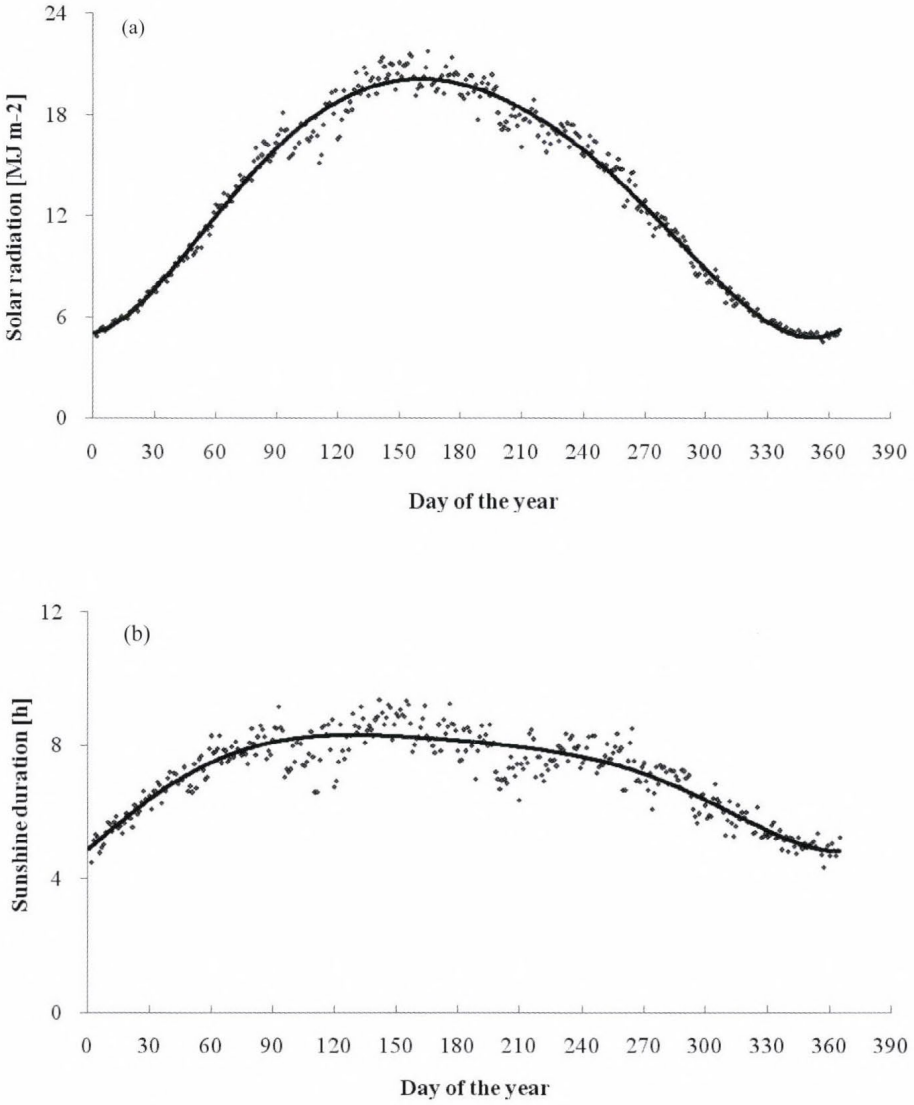

Fig.2. Distribution of the averaged daily solar radiation (a) and sunshine duration (b) of the 13 sites in Northeastern China.

2.5. Performance criteria

To assess the performance of the model, root mean square error (*RMSE*), relative root mean square error (*RRMSE*) [%] and coefficient of determination (R^2) are determined. R^2 is commonly calculated based on the calibration dataset

while *RMSE*, and *RRMSE* are based on the validation dataset. The metric R^2 varying from 0 to 1 is adopted to measure the fit of the model on calibration data, where the higher the value, better the fit. The *RMSE* provides information on the short term performance of the correlations by allowing a term by term comparison of the actual deviation between the estimated and measured values. The smaller the value, the better the model's performance. *RRMSE* is a dimensionless index allowing comparisons among a range of different model responses regardless of units. The value of *RRMSE* ranges from 0 to infinity. The smaller the *RRMSE*, the better is the model's performance. *RMSE* and *RRMSE* are calculated by the following equations:

$$RMSE = \sqrt{\frac{\sum_{i=1}^{n}(y_i - \hat{y}_i)^2}{n}}, \tag{7}$$

$$RRMSE = \frac{100}{\overline{y}}\sqrt{\frac{\sum_{i=1}^{n}(y_i - \hat{y}_i)^2}{n}}, \tag{8}$$

where n, y, $\hat{y}$, and $\overline{y}$ represent the number of testing data, the observed value, estimated value, and average value of the observation, respectively.

The metric *CV* calculated as ratio of standard deviation to arithmetic mean is adopted to measure the variation of the parameter. The higher the value, the larger the parameter's variation.

3. Results and discussion

3.1. Variations of A-P model parameters at five time scales

3.1.1. A-P model parameters calibrated at TS1

The calibrated parameters *a* and *b* at five time scales are summarized in *Table 2*. Using daily data (TS1), parameter *a* varies from 0.499 in Chaoyang to 0.606 in Heihe (averaged 0.545), *b* from 0.146 in Tongliao to 0.277 in Fuyu (averaged 0.196), and the sum of *a* and *b* (*a*+*b*) from 0.669 in Tongliao to 0.787 in Fuyu (averaged 0.741). Evidently, *a*+*b* are most stable with the *CV* of 4.89% followed by parameter a (*CV*=5.74%), while parameter *b* shows a larger variation with the *CV* of 21.44%.

Table 2. The parameters of A-P model calibrated at five time scales in the study area

Station	TS1				TS2				TS3			
	a	*b*	*a+b*	R^2	*a*	*b*	*a+b*	R^2	*a*	*b*	*a+b*	R^2
Mohe	0.538	0.241	0.779	0.757	0.600	0.206	0.806	0.567	0.627	0.190	0.817	0.483
Hailaer	0.518	0.252	0.770	0.725	0.518	0.252	0.770	0.522	0.517	0.253	0.769	0.445
Heihe	0.606	0.163	0.769	0.780	0.665	0.126	0.791	0.692	0.701	0.104	0.805	0.649
Fuyu	0.509	0.277	0.787	0.813	0.484	0.292	0.776	0.656	0.481	0.294	0.775	0.615
Suolun	0.551	0.232	0.783	0.743	0.483	0.276	0.759	0.473	0.463	0.288	0.752	0.404
Haerbing	0.532	0.192	0.724	0.721	0.484	0.220	0.705	0.524	0.439	0.247	0.686	0.403
Jiamushi	0.548	0.182	0.730	0.754	0.602	0.153	0.755	0.582	0.628	0.138	0.766	0.491
Tongliao	0.523	0.146	0.669	0.676	0.506	0.158	0.663	0.466	0.495	0.165	0.660	0.401
ChangChun	0.597	0.163	0.760	0.806	0.610	0.155	0.765	0.670	0.626	0.145	0.771	0.613
Yanji	0.550	0.183	0.733	0.788	0.473	0.223	0.697	0.540	0.447	0.237	0.684	0.455
Chaoyang	0.499	0.202	0.701	0.790	0.423	0.251	0.674	0.566	0.402	0.264	0.667	0.503
Shengyang	0.563	0.164	0.727	0.809	0.516	0.191	0.707	0.590	0.504	0.197	0.702	0.496
Dalian	0.556	0.152	0.708	0.720	0.499	0.188	0.687	0.555	0.503	0.186	0.690	0.480
Average	0.545	0.196	0.741	0.760	0.528	0.207	0.735	0.569	0.526	0.209	0.734	0.495
CV [%]	5.74	21.44	4.89	—	13.11	24.84	6.48	—	17.20	28.98	7.39	—

Table 2. (continued)

Station	TS4				TS5			
	a	*b*	*a+b*	R^2	*a*	*b*	*a+b*	R^2
Mohe	0.572	0.218	0.791	0.363	0.507	0.249	0.756	0.086
Hailaer	0.543	0.234	0.777	0.344	0.422	0.301	0.723	0.275
Heihe	0.725	0.088	0.813	0.587	0.973	-0.071	0.902	0.373
Fuyu	0.514	0.275	0.789	0.564	0.371	0.346	0.717	0.222
Suolun	0.452	0.296	0.748	0.355	0.028	0.554	0.582	0.001
Haerbing	0.370	0.286	0.656	0.364	0.040	0.475	0.515	0.001
Jiamushi	0.672	0.113	0.785	0.372	0.577	0.157	0.734	0.142
Tongliao	0.502	0.158	0.660	0.347	0.801	-0.050	0.751	0.187
ChangChun	0.654	0.127	0.781	0.533	0.284	0.340	0.624	0.055
Yanji	0.431	0.246	0.677	0.405	0.335	0.291	0.625	0.040
Chaoyang	0.371	0.284	0.655	0.443	-0.200	0.639	0.439	0.063
Shengyang	0.481	0.209	0.691	0.396	0.099	0.421	0.521	0.009
Dalian	0.436	0.228	0.664	0.393	0.294	0.317	0.611	0.027
Average	0.517	0.213	0.730	0.420	0.349	0.305	0.654	0.114
CV [%]	21.82	33.04	8.57	—	92.45	67.64	19.18	—

The values of R^2 vary from 0.676 to 0.813 (averaged 0.760). Although these values indicate that the simple linear equation gives goodness of fit on the calibration data set, other researchers have proposed several modifications by changing the order of *H/Ho*, such as, quadratic (*Akinoglu* and *Ecevit*, 1990), cubic (*Ertekin* and *Yaldiz*, 2000), and logarithmic models (*Ampratwum* and *Dorvlo*, 1999). In our work, we have used these functions to model the relation between *Rs/Ra* and *H/Ho*, however, they return quite similar values of R^2 to those of the simple linear A-P model within the same station. Several comparative studies also demonstrated that they returned almost identical values of R^2 and gave very similar accuracy (*Iziomon* and *Mayer*, 2002; *Almorox* and *Hontoria*, 2004; *Yorukoglu* and *Celik*, 2006). Therefore, there is no reason to choose a complex function to gain probably negligible accuracy at the cost of losing the simplicity and convenience of the simple A-P model. The goodness of fit also questions the restriction of A-P model calibration to monthly mean daily data (TS3) made by *Ångström* (1956).

3.1.2. A-P model parameters calibrated at TS2

There are many satellite imagine products data that scientists are using to study global change. Many products have been developed with Moderate Resolution Imaging Speetroradiometer (MODIS) data, these include 16-day composite images, such as the widely used MODIS Vegetation Index product. Together with these data, the 16-daily mean solar radiation is usually needed to parameterize or validate ecosystem process models and eco-environment simulation models. However, no literature has reported the study of A-P model at this time scales. In the present work, we calibrate the parameters and evaluate the performances of A-P model at half-monthly time scale (TS2), which differs little from the 16-day time scale, but does not result in significantly differences to the results. At this time scale, parameter a varies from 0.423 in Chaoyang to 0.665 in Heihe (averaged 0.528), b from 0.126 in Heihe to 0.292 in Fuyu (averaged 0.207), and $a+b$ from 0.663 in Tongliao to 0.806 in Mohe (averaged 0.735) (*Table 2*). The stability of the parameters is in order: $a+b$ (CV=6.48%) > a (CV=13.11%) > b (CV=24.84). R^2 varies from 0.466 to 0.692 (averaged 0.569). The values of R^2 indicate that A-P model gives goodness of fit, it therefore could be used to estimate solar radiation at this time scale.

3.1.3. A-P model parameters calibrated at TS3

Using the monthly mean daily data, parameter a varies from 0.402 in Chaoyang to 0.701 in Heihe (averaged 0.526), b from 0.104 in Heihe to 0.294 in Fuyu (averaged 0.209), and $a+b$ from 0.660 in Tongliao to 0.817 in Mohe (averaged 0.734), while R^2 varies from 0.401 to 0.649 (averaged 0.495). The A-P model was initially developed using the monthly mean daily data. More than 30 years later, the author stressed that the parameters of the model should be calibrated

from the monthly mean daily data rather than the daily data (*Ångström*, 1956). Consequently, a large amount of literatures reported the researches of the A-P model at TS3 (*Iziomon* and *Mayer*, 2002; *Almorox* and *Hontoria*, 2004; *Zhou et al.*, 2005). Another reason may be in that monthly mean daily data are more easily available than daily data. However, in the present work, better fits between Rs/Ra and H/H_0 are obtained at TS1 and TS2, as can be seen from *Table 2*, where the A-P model shows a 20.10%–83.80% (averaged 53.47%), and 6.54%–29.94% (averaged 14.97%) higher R^2 than those at TS3, respectively. Similar result was reported by *Tymvios et al.* (2005) who obtained higher R^2 of the A-P models established by using the daily data than that by monthly data of Athalassa. *Liu et al* (2009) also obtained a better fit between H/H_0 and Rs/Ra using daily data (TS1) than monthly mean daily data (TS3) of 29 stations in the Yellow River basin. These results again confirm our question of the restriction and suggest that it is unnecessary to restrict the A-P model calibration only to the monthly mean daily data.

3.1.4. A-P model parameters calibrated at TS4 and TS5

There is no any literature reported the study of A-P model using the seasonal mean daily (TS4) data. In the present work, the values of R^2 vary from 0.344 to 0.587(averaged 0.420), indicating that the A-P model retains goodness of fit and can be used at seasonal time scale. Parameter a vary from 0.370 in Haerbing to 0.725 in Heihe (averaged 0.517), b from 0.088 in Heihe to 0.296 in Suolun (averaged 0.213), and $a+b$ from 0.655 in Chaoyang to 0.813 in Heihe (averaged 0.730). Evidently, $a+b$ are much more stable (CV=8.57%) than parameter a (CV=21.82%) and b (CV=23.04%) individually.

The values of R^2 are very low at annual time scale (TS5), varying from 0.001 to 0.374 (averaged 0.114) is greater than 0.3only in Heihe (0.374), implying that the A-P model hardly explain the variation in solar radiation at TS5. The poor fit was also reported by *Chen et al.* (2006) who found that the fit was not improved by adding precipitation and air temperature data to the A-P equation. *Liu et al.* (2009) calibrated the A-P model using the hardly mean data from 13 sites in Yellow River basin. The returned R^2 varied from 0.02 to 0.61, it was greater than 0.5 at only two sites. Therefore, according to the analysis, the relation between solar radiation and sunshine duration can not be modeled by the A-P equation at hardly time scale, and the following discussion would be limited to the results fromTS1-TS4.

3.2. Analyses of effect of time scale on A-P model parameters

The spatial stability of parameters are dependent on time scale, as it can be seen from *Table 2*, where parameters at TS1 are the most stable with the CV of 5.74%, 21.44%, and 4.89% for a, b, and $a+b$, respectively, followed by those at

TS2 and TS3; while they show the largest spatial variations at TS4 with the *CV* of 21.82%, 33.04%, and 8.57%, respectively. Parameter *a* shows the largest differences of *CV* amongst different time scales, ranging from 4.09% between TS2 and TS3 to 16.08% between TS1 and TS4 (averaged 8.72%); while *a+b* shows small differences ranging from 0.91% between TS2 and TS3 to 3.68% between TS1 and TS4 (averaged 1.99%). These values indicate that time scale has greater effect on spatial variation of *a* than that of *b* and *a+b*.

There are significant correlations between the same parameters amongst different time scales, with the correlation coefficient $r>0.6$ and averaged r of 0.851 (*Table 3*). The most significant correlations are found between parameters at TS2 and TS3, with the r of 0.991 ($p<0.01$), 0.981 ($p<0.01$), and 0.991 ($p<0.01$) for *a*, *b*, and *a+b*, respectively. The correlations differ greatly among the parameters, *a+b* correlates most significantly amongst different time scales, with the $r>0.8$ ($p<0.01$) and averaged r of 0.917. These significant correlations indicate that the parameters at one time scale could be obtained from those at another time scale, and thus, the increase the availability of parameters without the need for calibration at all time scales.

Parameter *a* tends to decrease and *b* increase at larger time scales compared with those at smaller scale , as it can be seen in *Table 2*, where more than 61% of the stations have lower values of *a*, while higher *b* at larger time scales. The differences of the parameters caused by time scale are generally large, with 41% of the differences for *a* and 60% for *b* are greater than 10%. At some stations, this difference could be very large (e.g., Dalian, Chaoyang, Jamushi, Haerbing). Evidently, time scale has greater effect on temporal variation of *b* than that of *a*, with the differences ranging from 0.01% to 43.77% (averaged 9.99%) for *a* and from 0.09% to 61.74% (averaged 15.86%) for *b*. However, the differences of parameters *a* and *b* are always opposite as shown in *Fig. 3*, further confirming the stability of *a+b* with less variation at all spaces and time scales.

Table 3. Correlation efficient (r) between the parameters amongst different time scales

Time scale	Parameter	TS1			TS2			TS3			TS4		
		a	*b*	*a+b*	*a*	*b*	*a+b*	*a*	*b*	*a+b*	*a*	*b*	*a+b*
	a	1											
TS1	*b*	–0.544	1										
	a+b	0.234	0.689**	1									
	a	0.729**	–0.225	0.369	1								
TS2	*b*	–0.682*	0.807**	0.346	–0.726**	1							
	a+b	0.323	0.544	0.910**	0.670*	0.024	1						
	a	0.688**	–0.189	0.376	0.991**	–0.701**	0.684**	1					
TS3	*b*	–0.702**	0.702**	0.207	–0.821**	0.981**	–0.134	–0.813**	1				
	a+b	0.365	0.468	0.857**	0.737**	–0.076	0.991**	0.761**	–0.241	1			
	a	0.612*	–0.107	0.405	0.934**	–0.618*	0.692**	0.949**	–0.736**	0.762**	1		
TS4	*b*	–0.663*	0.601*	0.076	–0.850**	0.904**	–0.260	–0.849**	0.947**	–0.360	–0.868**	1	
	a+b	0.360	0.436	0.816**	0.732**	–0.100	0.957**	0.760**	–0.264	0.972**	0.830**	–0.444	1

* Significant at 0.05 significance level.
** Significant at 0.01 significance level.

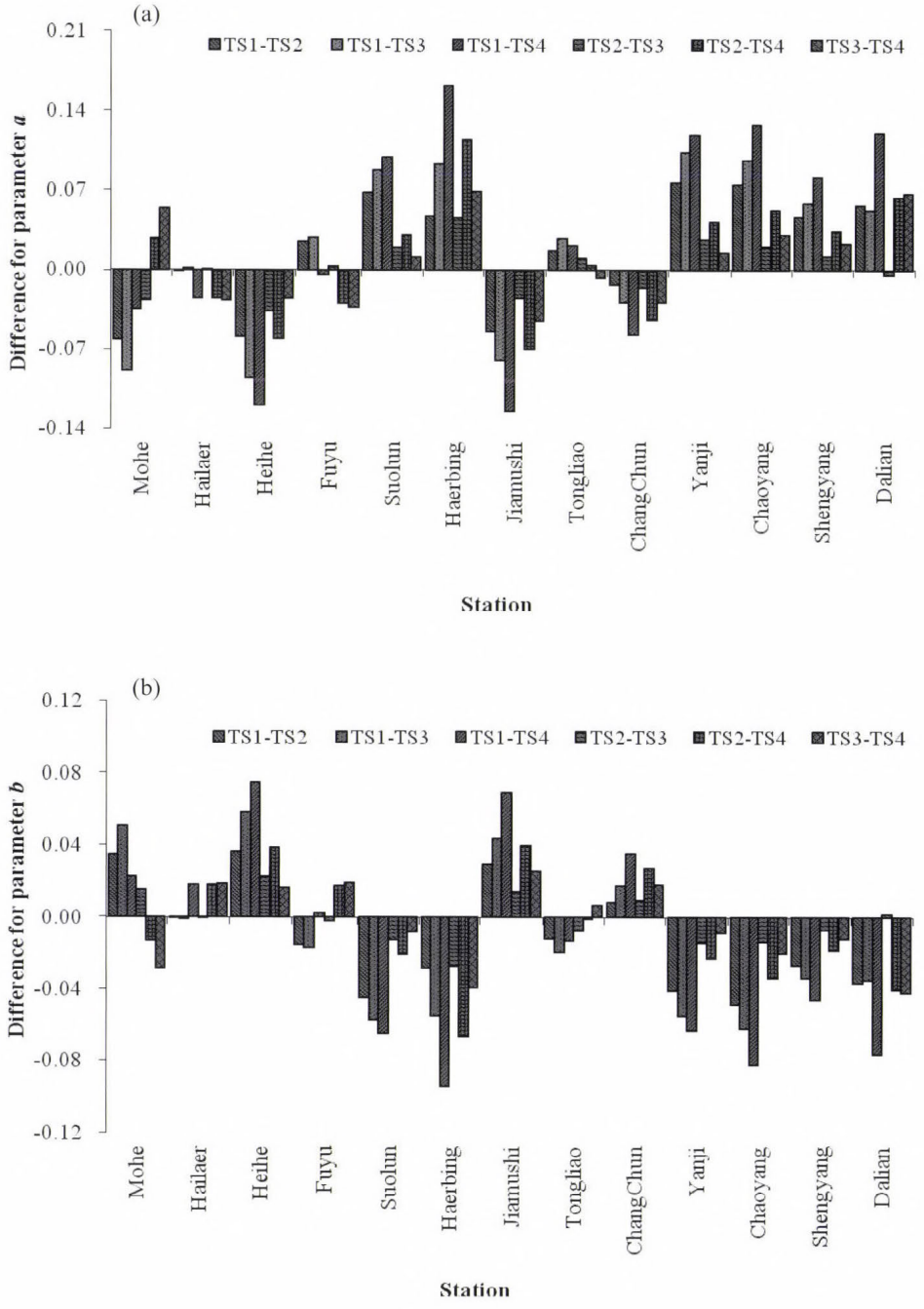

Fig.3. Difference of the parameter *a* (a) and *b* (b) among daily (TS1), half-monthly (TS2), monthly (TS3), and seasonal (TS4) time scales in the study area.

3.3. Comparison of the solar radiation estimation using parameters from different time scales

Conceptually, the calibrated parameters should only be used at the same time scale, namely, parameters calibrated from daily data should only be used to estimate daily solar radiation, while those calibrated at TS2, TS3, and TS4 should only be used at the corresponding time scales. It was also stated that the comparison in solar radiation at different scales can only be made possible when the estimation is in the same time scale. However, in many cases, no observation of meteorological data is available at some time scales, making the calibration difficult. To solve this problem, two possible alternatives may be considered, one is to use the values recommended by other authors who conducted the similar work. For example, *Ångström* suggested values of 0.2 and 0.5, and *Prescott* suggested 0.22 and 0.54 for the parameters a and b (*Prescott*, 1940), respectively; *Page* (1961) gave the corresponding values of 0.23 and 0.48, which was believed to be applicable anywhere in the world. However, lots of literatures reported the parameters for different places and showed that they varied from location to location, namely, they are site-dependent.

Another alternative is to directly use parameters calibrated at other time scales, for example, using the parameters at TS3 to estimate solar radiation at TS1, TS2, and TS4. This has never been done before but actually is of potential importance for practical applications, since monthly data are widely available. Therefore, in our work, an attempt is made to estimate solar radiation using the parameters calibrated at other different time scales, and the performances are summarized in *Tables 4–7*.

3.3.1. Estimating daily solar radiation using the parameters calibrated at all time scales

The A-P model gives good performances when using the parameters calibrated at TS1–TS4 to estimate the daily solar radiation, with the $RMSE < 2.7$ MJ m^{-2} (averaged 2.002 MJ m^{-2}) and $RRMSE < 20\%$ (averaged 15.01%) (*Table 4*). The estimation using parameters at TS1 is overall the best, with the lowest averaged *RMSE* of 1.949 MJ m^{-2} and *RRMSE* of 14.61%. However, it is noted that it is only slightly better than those using the parameters at TS2–TS4, with nearly identical averaged *RMSE* and *RMSE* of those at TS2–TS4 (*RMSE* of 1.978, 2.01, 2.068 MJ m^{-2}; *RRMSE* of 14.83%, 15.07%, 15.52%, respectively).

These values again prove that the A-P model can be used to estimate daily solar radiation with a good performance; furthermore, it implies that the parameters calibrated at TS2, TS3, and TS4 can replace those at TS1 in daily solar radiation estimation, suggesting that the parameters calibrated at larger time scale can be applied to smaller time scale.

Table 4. Root mean square error (*RMSE*) and relative root mean square error (*RRMSE*) of estimation daily solar radiation by A-P model using the parameters calibrated at all time scales.

Station	RMSE [MJ m^{-2}]				RRMSE [%]			
	TS1	TS2	TS3	TS4	TS1	TS2	TS3	TS4
Mohe	1.712	1.654	1.674	1.644	14.09	13.62	13.78	13.53
Hailaer	2.303	2.303	2.302	2.326	17.37	17.37	17.37	17.55
Heihe	1.636	1.809	1.969	2.019	12.70	14.04	15.29	15.67
Fuyu	1.871	1.917	1.923	1.867	13.30	13.62	13.67	13.27
Suolun	1.795	1.890	1.918	1.931	12.30	12.95	13.15	13.23
Haerbing	1.728	1.691	1.756	2.014	13.70	13.41	13.92	15.97
Jiamushi	1.489	1.575	1.592	1.671	11.85	12.53	12.66	13.29
Tongliao	2.615	2.591	2.579	2.611	18.41	18.24	18.16	18.39
ChangChun	1.906	1.920	1.946	2.020	14.26	14.37	14.56	15.11
Yanji	1.663	1.782	1.852	1.862	12.91	13.83	14.38	14.46
Chaoyang	2.516	2.549	2.591	2.678	18.43	18.67	18.98	19.62
Shengyang	2.240	2.176	2.174	2.195	16.80	16.32	16.30	16.46
Dalian	1.860	1.865	1.857	2.051	13.75	13.79	13.73	15.17
Average	1.949	1.978	2.010	2.068	14.61	14.83	15.07	15.52

3.1.2. Estimating half-monthly and monthly mean solar radiation using the parameters calibrated at all time scales

When estimating half-monthly and monthly mean solar radiation using the parameters calibrated at TS1–TS4, the A-P model also performs well, with the *RMSE* < 2.1 MJ m^{-2} (averaged 1.073 MJ m^{-2}) and *RRMSE* < 15% (averaged 8.01%) (*Table 5*), as well as *RMSE* < 2 MJ m^{-2} (averaged 0.990 J m^{-2}) and *RRMSE* < 14% (averaged 7.38%) (*Table 6*), respectively. The estimation of half-monthly solar radiation using parameters at TS2 is slightly better than that using parameters at TS1, TS3, and TS4, as it can been see from *Table 5*, where the differences for *RMSE* are less than 1%, and only in Jiamushi is greater than 0.1 MJ m^{-2}. Similar result is also found in the estimation of monthly solar radiation (*Table 6*), with the differences for *RMSE* and *RRMSE* less than 0.1 MJ m^{-2} and 1%, respectively.

These results indicate that the parameters calibrated at TS1, TS3, and TS4 can replace those at TS2 in half-monthly solar radiation estimation, and parameters calibrated at TS1, TS2, and TS4 can replace those at TS3 in monthly solar radiation estimation, not only suggesting that the parameters calibrated at a smaller time scale can be applied to larger time scales, but also again confirming that the parameters calibrated at a larger time scale can be applied to smaller time scales. Namely, the parameters at different time scales are interchangeable.

Table 5. Root mean square error (*RMSE*) and relative root mean square error (*RRMSE*) of estimation of half-monthly mean solar radiation by A-P model using the parameters calibrated at all time scales.

Station	RMSE [MJ m^{-2}]				RRMSE [%]			
	TS1	TS2	TS3	TS4	TS1	TS2	TS3	TS4
Mohe	0.822	0.751	0.737	0.736	6.77	6.18	6.07	6.06
Hailaer	1.577	1.577	1.576	1.606	11.90	11.90	11.89	12.12
Heihe	0.758	0.793	0.838	0.879	5.88	6.16	6.51	6.82
Fuyu	1.018	1.018	1.018	1.021	7.23	7.24	7.24	7.25
Suolun	0.881	0.946	0.978	1.004	6.04	6.49	6.71	6.88
Haerbing	0.799	0.748	0.740	0.804	6.34	5.93	5.87	6.38
Jiamushi	0.658	0.682	0.714	0.797	5.23	5.42	5.68	6.34
Tongliao	2.044	2.016	1.999	2.042	14.40	14.20	14.08	14.38
ChangChun	0.842	0.857	0.879	0.929	6.30	6.41	6.58	6.95
Yanji	0.702	0.698	0.726	0.748	5.45	5.42	5.64	5.81
Chaoyang	1.786	1.727	1.721	1.719	13.08	12.65	12.60	12.59
Shengyang	1.259	1.163	1.144	1.131	9.44	8.72	8.58	8.48
Dalian	0.813	0.783	0.778	0.831	6.01	5.80	5.75	6.15
Average	1.074	1.058	1.065	1.096	8.01	7.89	7.94	8.17

Table 6. Root mean square error (*RMSE*) and relative root mean square error (*RRMSE*) of estimation of monthly mean solar radiation by A-P model using the parameters calibrated at all time scales.

Station	RMSE [MJ m^{-2}]				RRMSE [%]			
	TS1	TS2	TS3	TS4	TS1	TS2	TS3	TS4
Mohe	0.753	0.675	0.653	0.662	6.20	5.57	5.38	5.46
Hailaer	1.526	1.526	1.525	1.557	11.52	11.52	11.51	11.76
Heihe	0.685	0.702	0.731	0.760	5.32	5.46	5.68	5.90
Fuyu	0.960	0.960	0.960	0.962	6.82	6.83	6.82	6.84
Suolun	0.783	0.869	0.902	0.929	5.37	5.96	6.19	6.37
Haerbing	0.717	0.668	0.654	0.693	5.69	5.30	5.19	5.50
Jiamushi	0.593	0.614	0.641	0.711	4.72	4.89	5.11	5.66
Tongliao	1.984	1.958	1.942	1.985	13.99	13.80	13.69	13.99
ChangChun	0.717	0.727	0.743	0.780	5.37	5.44	5.57	5.84
Yanji	0.623	0.617	0.637	0.653	4.84	4.79	4.95	5.08
Chaoyang	1.708	1.650	1.642	1.636	12.51	12.09	12.03	11.99
Shengyang	1.183	1.088	1.068	1.052	8.87	8.16	8.01	7.89
Dalian	0.709	0.670	0.664	0.698	5.25	4.96	4.91	5.16
Average	0.995	0.979	0.982	1.006	7.42	7.29	7.31	7.50

The *RMSE* and *RRMSE* for estimation of half-monthly and monthly solar radiation are much lower than those for estimation of daily solar radiation, implying that after the data smoothing by half-monthly or monthly averaging process, most of the instrumental random errors and day-to-day fluctuation of the data are removed. Therefore, if each day within the averaging lag takes the same values of the corresponding time scale mean daily solar radiation, it would not match the day-to-day variation of solar radiation. *Liu et al.* (2009) found that the *RMSE* increased greatly if the monthly mean daily solar radiation estimated at TS3 was directly used as the daily solar radiation approximation. *Gueymard et al.* (1995) stressed the importance of studying the effect of the averaging time (time scale), and believed that the optimum averaging period for smoothing the data remain unanswered. According to our analysis, the optimum averaging period should be less than 15 days, so that most of the instrumental random errors are removed without significant loss of information of the data. It would be significant to investigate further to determine the optimum lag, but it is beyond the objective of this study.

Table 7. Root mean square error (*RMSE*) and relative root mean square error (*RRMSE*) of estimation of seasonal mean solar radiation by A-P model using the parameters calibrated at all time scales.

Station	RMSE [MJ m^{-2}]				RRMSE [%]			
	TS1	TS2	TS3	TS4	TS1	TS2	TS3	TS4
Mohe	0.316	0.254	0.237	0.216	2.47	1.99	1.85	1.69
Hailaer	1.389	1.389	1.388	1.413	10.37	10.37	10.36	10.55
Heihe	0.550	0.556	0.568	0.581	4.23	4.27	4.37	4.47
Fuyu	0.788	0.801	0.801	0.788	5.48	5.57	5.57	5.48
Suolun	0.644	0.753	0.786	0.812	4.32	5.06	5.28	5.45
Haerbing	0.600	0.551	0.529	0.547	4.71	4.32	4.15	4.29
Jiamushi	0.486	0.498	0.516	0.562	3.83	3.92	4.06	4.43
Tongliao	1.861	1.836	1.820	1.863	13.01	12.83	12.72	13.02
ChangChun	0.515	0.520	0.531	0.556	3.82	3.86	3.94	4.13
Yanji	0.516	0.463	0.457	0.457	3.97	3.56	3.52	3.52
Chaoyang	1.605	1.557	1.551	1.545	11.67	11.32	11.28	11.23
Shengyang	1.105	1.039	1.014	0.990	7.95	7.47	7.29	7.12
Dalian	0.566	0.512	0.505	0.544	4.02	3.63	3.58	3.86
Average	0.842	0.825	0.823	0.837	6.14	6.01	6.00	6.09

3.3.3. Estimating seasonal mean solar radiation using the parameters calibrated at all time scales

When estimating seasonal mean daily solar radiation using the parameters calibrated at TS1-TS4, the A-P model retains good performances, with the $RMSE < 1.9$ MJ m^{-2} (averaged 0.833 MJ m^{-2}) and $RRMSE < 13\%$ (averaged 6.07%). The *RMSE* and *RRMSE* are much lower than those at TS1-TS3 due to the data smoothing by seasonal averaging process. Similarly, no significant difference of *RMSE* and *RRMSE* resulted by time scales is found, as it can be seen in *Table 7*, where only the differences for *RMSE* in Shengyang and Suolun are greater than 0.1 MJ m^{-2}, and only that for *RRMSE* in Suolun is greater than 1%. These results indicate that the parameters calibrated at TS1, TS2, and TS3 can replace those at TS4 in the estimation of seasonal solar radiation, again proving that the parameters calibrated at a smaller time scale can be applied to larger time scales.

4. Conclusion

Solar radiation is the principal and fundamental energy for many physical, chemical, and biological processes. Estimation of solar radiation from sunshine duration is common employed when no direct observation of solar radiation is available. Particularly, the *Ångström-Prescott* model is widely used for its simplicity. This paper investigates the effect of time scale on the *Ångström-Prescott* parameters and the estimation accuracy in Northeastern China. The relation between solar radiation and sunshine duration can not be modeled by the *Ångström-Prescott* equation at annual time scale, but less than seasonal time scales. Time scale effects the spatial variation of parameters, it has greater effect on parameter *a* than on *b*, and larger spatial variation are presented at larger time scales. Parameter *a* tends to decrease and *b* increase at larger time scales, and the differences of the parameters caused by time scale are generally large, with 41% of the differences for *a* and 60% for *b* are greater than 10%. Evidently, time scale has greater effect on temporal variation of *b* than that of *a*. However, the large differences of parameters caused by time scale do not result in significant difference of the estimation accuracy, estimation using the parameters from other time scales give the most identical performances with that using the parameters from itself time scale, therefore, parameters at different time scales are interchangeable, the parameters calibrated at larger time scales can be applied to smaller time scales, and vice versa.

Acknowledgments—The work was supported by the Geological Survey program of China Geological Survey (GZH201200503) and Special Fund for Land and Resources Research in the Public Interest (201111023). We thank the National Meteorological Information Center, China Meteorological Administration for providing the long-term data records. Many thanks go to the anonymous reviewers for the comments on the manuscript.

References

Akinoglu, B.G. and *Ecevit, A.*, 1990: Construction of a quadratic model using modified Ångström coefficients to estimate global solar radiation. *Sol. Energy* 45, 85–92.

Allen, R.G., Pereira, L.S., Raes, D., and *Smith, M.*, 1998: Crop evapotranspiration. Guidelines for computing crop water requirements. *FAO Irrigation and Drainage paper 56*. Rome.

Almorox, J. and *Hontoria, C.*, 2004: Global solar radiation estimation using sunshine duration in Spain. *Energ. Convers. Manage 45*, 1529–1535.

Ampratwum, D.B. and *Dorvlo, A.S.S.*, 1999: Estimation of solar radiation from the number of sunshine hours. *Appl. Energ. 62*, 161–167.

Ångström, A., 1924: Solar and terrestrial radiation. *Q. J. Roy. Meteor. Soc. 50*, 121–126.

Ångström, A., 1956: On the computation of global radiation from records of sunshine. *Ark. Geof. 2*, 471–479.

Benson, R.B., Paris, M.V., Sherry, J.E., and *Justus, C.G.*, 1984: Estimation of daily and monthly direct, diffuse and global solar radiation from sunshine duration measurements, *Sol. Energy 32*, 523–535.

Bristow, K.L. and *Campbell, G.S.*, 1984: On the relationship between incoming solar radiation and daily maximum and minimum temperature. *Agr. Forest Meteorol. 31*, 159–166.

Cao, J.C. and *Cao, S.H.*, 2006: Study of forecasting solar irradiance using neural networks with preprocessing sample data by wavelet analysis. *Energy 31*, 3435–3445.

Chen, J.L., Liu, H.B., Wu, W., and *Xie, D.T.*, 2011: Estimation of monthly solar radiation from measured temperatures using support vector machines-A case study, *Renew. Energ. 36*, 413–420.

Chen, R.S., Kang, E.S., Ji, X.B., Yang, J.P., and *Zhang, Z.H.*, 2006: Trends of the global radiation and sunshine hours in 1961–1998 and their relationships in China, *Energ. Convers. Manage 47*, 2859–2866.

Ertekin, C. and *Yaldiz, O.*, 2000: Comparison of some existing models for estimating global solar radiation for Antalya (Turkey), *Energ. Convers. Manage. 41*, 30–31.

Frulla, L.A., Gagliardini, D.A., Grossi G.H., Lopardo, R., and *Tarpley, J.D.*, 1988: Incident solar radiation on Argentina from the geostationary satellite GOES: comparison with ground measurements, *Sol. Energy 41*, 61–69.

Gueymard, C., Jidra, P., and *Eatrada, C.V.*, 1995: A critical look at recent interpretations of the Ångström approach and its future in global solar irradiation prediction, *Sol. Energy 54*, 357–363.

Hansen, J.W., 1999: Stochastic daily solar irradiance for biological modeling applications, *Agr. Forest Meteorol. 94*, 53–63.

Hargreaves, G.H., 1981: Responding to tropical climates. In *The 1980–81 food and climate review, the food and climate forum*. Boulder (Colo): Aspen Institute for Humanistic Studies, 29–32.

Hargreaves, G.L., Hargreaves, G.H., and *Riley, J.P.*, 1985: Irrigation water requirement for Senegal River Basin. *J. Irrig. Drain E-ASCE 111*, 265–275.

Hay, J.E. and *Suckling, P.W.*, 1979: An assessment of the net-works for measuring and modelling solar radiation in British Columbia and adjacent areas of western Canada. *Can. Geogr. 23*, 222–238.

Hunt, L.A., Kuchar, L., and *Swanton, C.J.*, 1998: Estimation of solar radiation for use in crop modelling. *Agr. Forest Meteorol. 91*, 293–300.

Iziomon, M.G. and *Mayer, H.*, 2002: Assessment of some global solar radiation parameterizations. *J. Atmos. Sol.-Terr. Phy. 64*, 1631–1643.

Jiang, Y.G., 2009: Computation of monthly mean daily global solar radiation in China using artificial neural networks and comparison with other empirical models. *Energy 34*, 1276–1283.

Lam, J.C., Wan, K.K.W., and *Yang, L.*, 2008: Solar radiation modeling using ANNs for different climates in China. *Energ. Convers. Manage. 49*, 1080–1090.

Liu, X.Y., Mei, X.R., Li, Y.Z., Zhang, Y.Q., and *Wang, Q.S.*, 2009: Calibration of the Ångström-Prescott coefficients (a, b) under different time scales and their impacts in estimating global solar radiation in the Yellow River basin. *Agr. Forest Meteorol.149*, 697–710.

NCDC (National Climatic Data Center), 1995: *Cooperative summary of the day, dataset TD 3200*. U.S. Department of Commerce, National Oceanographic and Atmospheric Administration, National Climatic Data Center, Asheville, NC.

Newland, F.J., 1988: A study of solar radiation models for the coastal region of South China. *Sol. Energy 31*, 227–235.

Ögelman, H., Ecevit, A., and *Tasdemiroglu, E.*, 1984: A new method for estimating solar radiation from bright sunshine data. *Sol. Energy 33*, 619–625.

Olseth, A. and *Skartveit, A.*, 2001: Solar irradiance, sunshine duration and daylight illuminance derived from METEOSAT data for some European sites. *Theor. Appl. Climatol. 69*, 239–252.

Page, J.K., 1961: The estimation of monthly mean values of daily total short wave radiation on vertical and inclined surface from sunshine records for latitudes 40N–40S. *Proceedings of UN Conference on New Sources of Energy, 4*, 378–390.

Pinker, R.T., Frouin, R., and *Li, Z.*, 1995: A review of satellite methods to derive shortwave irradiance. *Remote Sens. Environ. 51*, 108–124.

Podestá, G.P., Núñez, L., Villanueva, C.A., and *Skansi, M.A.*, 2004: Estimating daily solar radiation in the Argentine Pampas. *Agr. Forest Meteorol. 123*, 41–53.

Prescott, J.A., 1940: Evaporation from a water surface in relation to solar radiation. *T. Roy. Soc. South Aust. 64*, 114–118.

Richardson, C.W., 1981: Stochastic simulation of daily precipitation, temperature, and solar radiation. *Water Resour. Res. 17*, 182–190.

Rivington, M., Matthews, K.B., Bellocchi, G., and *Buchan, K.*, 2006: Evaluating uncertainty introduced to process-based simulation model estimates by alternative sources of meteorological data. *Agr. Syst. 88*, 451–471.

Şenkal, O., 2010: Modeling of solar radiation using remote sensing and artificial neural network in Turkey. *Energy 35*, 4795–4801.

Thorton, P.E. and *Running, S.W.*, 1999: An improved algorithm for estimating daily solar radiation from measurements of temperature, humidity, and precipitation. *Agr. Forest Meteorol.* 93, 211–228.

Trnka, M., Zalud, Z., Eitzinger, J., and *Dubrovský, M.*, 2005: Global solar radiation in Central European lowlands estimated by various empirical formulae, *Agr. Forest Meteorol. 131*, 54–76.

Tymvios, F.S., Jacovides, C.P., Michaelides, S.C., and *Scouteli, C.*, 2005: Comparative study of Ångström's and artificial neural network's methodologies in estimating global solar radiation. *Sol. Energy 78*, 752–762.

Wilks, D.S. and *Wilby, R.L.*, 1999: The weather generation game: a review of stochastic weather models. *Prog. Phys. Geogr. 23*, 329–357.

Yorukoglu, M. and *Celik, A.N.*, 2006: A critical review on the estimation of daily global solar radiation from sunshine duration. *Energ. Convers. Manage. 47*, 2441–2450.

Zhou, J., Wu, Y., and *Yan, G.*, 2005: General formula for estimation of monthly average daily global solar radiation in China. *Energ. Convers. Manage. 46*, 257–268.

IDŐJÁRÁS

Quarterly Journal of the Hungarian Meteorological Service
Vol. 116, No. 2, April–June 2012, pp. 145-169

Influence of carbon-dioxide concentration on human well-being and intensity of mental work

László Kajtár and **Levente Herczeg***

Department of Building Service Engineering and Process Engineering
Budapest University of Technology and Economics
Műegyetem rkp. 3, H-1111, Budapest

*Corresponding author E-mail: herczeg@epgep.bme.hu

(Manuscript received in final form December 19, 2011)

Abstract—In the frame of experiments carried out at the Department of Building Service Engineering and Process Engineering of Budapest University of Technology and Economics BUTE the impact of CO_2 concentration in the air was examined. Subjects' well-being was evaluated by the aid of subjective scales, physiological variables were recorded, and subjects' mental performance was measured by a standard test. Results obtained in the experiments show that subjects evaluated air quality is less acceptable, more unpleasant, and became more exhausted when the CO_2 concentration increased up to 3000 ppm. 3000 ppm CO_2 concentration in the air proved to be less advantageous for mental performance than 600 ppm. Several physiological measures show that a mental task requires a greater effort from the subjects when the CO_2 concentration in the air reaches 3000 ppm. It was shown that human well-being as well as the capacity to concentrate attention are declining when subjects spend 2 to 3 hours in a closed space with 3000 ppm or higher CO_2 concentration in the air.

Standards accurately prescribe the values of fresh air, breathing, and inside air quality assuring the health protection at workplaces.

We examined the level of carbon-dioxide concentration above which the efficiency of mental work and the human well-being significantly declines.

Key-words: air quality, carbon-dioxide, IAQ assessment, measurement technique, mental work

1. Introduction

The comfort in closed spaces is usually understood as thermal, air quality, acoustical, and illumination engineering comfort. The office plays a special role in providing adequate comfort as workers spend a longer time in closed spaces performing intellectual work. In the air-conditioning of comfort spaces, the primary task is to provide a pleasant indoor microclimate for the people staying in the room. In addition to thermal comfort, air quality is also regulated by international requirements and standards. In the occupied zone, a sufficient amount of fresh air of appropriate quality must be provided for the people staying in the room. Hungarian technical regulations do not fully cover these aspects yet, hence the complaints frequently heard from employees working in air-conditioned spaces are the air has an unpleasant 'smell', they experience 'lack of air' or perhaps have headaches. Among pollutants, carbon-dioxide, a by-product of the human metabolism, is regarded as one of the key factors. The carbon-dioxide content of exhaled air is higher than that of the outdoor air, leading to an increase in the carbon-dioxide concentration in the closed space. CO_2 concentration influences human well-being. In closed spaces the allowed CO_2 concentration may be ensured by supplying the adequate amount of fresh air. The exact volume of fresh air varies in Hungarian and international literature, ranging from 20 to 120 m^3/person. This is also a matter of economic efficiency as the volume flow of fresh air has an impact on the energy use of the air conditioning system (*Kajtár et al.*, 2001; *Kajtár* and *Hrustinszky*, 2002, 2003)

The fundamentals of the science of indoor air quality (IAQ) were laid down by Professor *Fanger* at the Danish Technical University. *Max von Pettenkoffer*, who published his research results in a medical journal in Munich in 1858, can be called the pioneer of IAQ. Using the CO_2 concentration in comfort spaces, his research focused on defining the average carbon-dioxide level below which human well-being is still ensured.

Further research conducted in the subject always investigated the joint impact of several factors influencing air quality, therefore the impact of carbon-dioxide on its own could not be determined.

We conducted studies concerning the impact of CO_2 on mental performance and well-being, at the same time determining the necessary fresh air demand.

2. Practical implications

In the present investigation, the influence of CO_2 concentration on human well-being and efficiency of mental work has been evaluated. These issues arise from time to time in connection with office work and the air-conditioning of office

buildings. It is very important to find the optimal balance between the biological requirements of office employees concerning fresh air on the one hand and economic efficiency on the other hand. A reduction in fresh air supply is required according to the arguments for profitability, whereas an increase of fresh air supply is needed when subjects' well-being is taken into consideration.

Table 1 shows the highest allowed CO_2 concentration in closed places provided by Hungarian and international standards and prescriptions.

Table 1. Maximum allowed CO_2 concentration in closed places

No.	Standards and prescriptions	Allowed CO_2 concentration [ppm]
	Comfort spaces	
1.	*MSZ 04.135/1-1982	1400.0
2.	MSZ 21875-2-1991	1066.6
3.	**DIN 1946/2 single office	900.0
4.	DIN 1946/2 landscaped office	733.3
5.	MSZ CR 1752 "A" cat.	860.0
6.	MSZ CR 1752 "B" cat.	1060.0
7.	MSZ CR 1752 "C" cat.	1590.0
	Workplaces	
8.	***TRGS 900	5000.0
9.	MSZ 21461 1-2	4830.0

*MSZ: Hungarian Standard
**DIN: Deutsches Institut für Normung
***TRGS: Technische Regeln für Gefahrstoffe

The above table indicates that the standards and prescriptions have not touched upon a wide range of CO_2 concentration from 1590 ppm to 4830 ppm. The aim of our research was to examine the influence of CO_2 concentration on human well-being and mental effort between 600 and 5000 ppm that was pointed in *Fig. 1.*

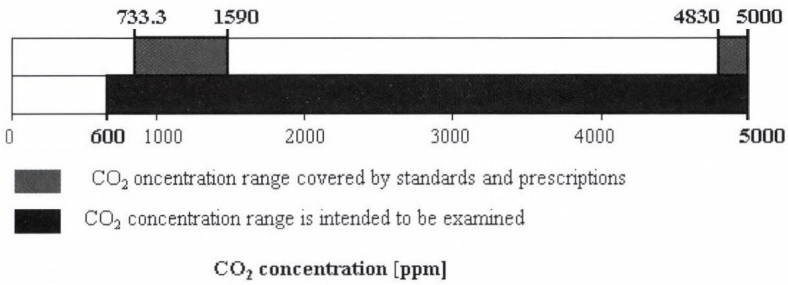

Fig. 1. The aim of our research.

The influence of CO_2 concentration on humans could be specified by means of examination of subjective comfort parameters and such objective parameters which were measured on humans and of performing experiments on subjects. The measuring-room that was built in Indoor Air Quality Laboratory of Department of Building Service Engineering and Process Engineering of BUTE were chosen for carrying out the experiments. Only this room could provide us that other air-polluting material did not influence the results of the measurements and subjects could stay in full thermal and air quality comfort during the measurements.

After finishing and evaluating the measurements, a maximum CO_2 concentration could be determined, under which there could not be any observable change in the human well-being and mental effort.

3. Methods

In the framework of our research, we investigated the impact of carbon-dioxide concentration on well-being and performance in the office. In the laboratory measurements we set the following CO_2 concentrations: 600, 1500, 2500, 3000, 4000, and 5000 ppm. The laboratory measuring room contained two carbon-dioxide sources: two main measuring subjects and carbon-dioxide, suitable for inhaling, fed from a bottle. The circuit diagram for the laboratory measurements is shown in *Fig. 2*.

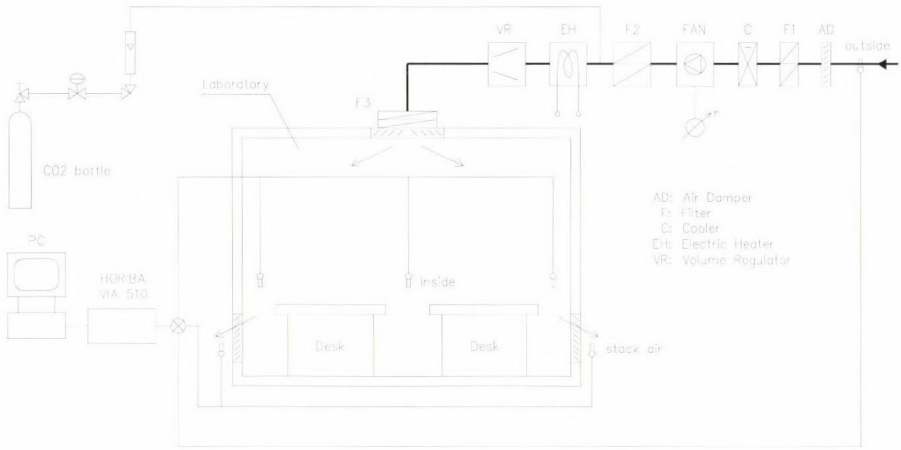

Fig. 2. Circuit diagram of the laboratory measurements.

The carbon-dioxide was fed into the measuring room mixed with 120 m^3/h fresh air. During the measurements, the carbon-dioxide concentration had to be kept at a constant level, therefore, the feeding valve had to be set accordingly. The share of carbon-dioxide sources is contained in *Table 2*. The carbon-dioxide concentration of outdoor air was 360 ppm.

Table 2. Carbon-dioxide sources in the measuring room

Measuring room CO_2 concentration [ppm]	Source of carbon-dioxide		Share human/total [%]
	Total [ppm]	Human [ppm]	
600	240	240	100.0
1500	1140	240	21.0
2500	2140	240	11.2
3000	2640	240	9.1
4000	3640	240	6.6
5000	4640	240	5.2

Carbon-dioxide fed from the bottle, was a gas of 99.995 V% cleanness, suitable for inhaling. Owing to their slight share, other pollutants in the carbon-dioxide gas ($O_2 \leq 25$ vpm, $N_2 \leq 25$ vpm, $HC \leq 1$ vpm, $CO \leq 1$ vpm, $H_2O < 5$ vpm) did not influence the results of the measurements. The pressure reducer and other armatures did not pollute the carbon-dioxide gas as their use is permitted in case of a gas of greater cleanness (99.998 V%).

In the present paper, two series of experiments are presented:

1. series of experiments carried out in 2001,
2. series of experiments carried out in 2002.

Both series of experiments were conducted in a laboratory constructed for the above purposes in the Department of Building Service Engineering and Process Engineering of the Budapest University of Technology and Economics. Inodorous air of appropriate, cleanliness, thermal comfort, as well as appropriate acoustic conditions have to be ensured in the laboratory.

In order to meet the requirements concerning air quality, the laboratory was built using specific low emitting building materials generally used in operating rooms, with practically no emission of contaminant substances.

To produce fresh air supply of the required cleanliness, a two-step filtration has been applied (G4 and F7). Air ducts as well as the filter unit at the second step of filtration were made from rust-proof steel plates.

During the various investigations in the laboratory, a high ventilation rate prevents the indoor air from becoming stale. Overpressure has been induced to prevent the influx of contaminating substances from outside (*Kajtár* and *Hrustinszky*, 2002, 2003).

Main data of the laboratory outlined above:

Floor area:	2.1×3.3 m $= 6.9$ m^2
Inside height:	2.5 m
Volume:	17.3 m^3
Volume flow of supply air:	1 000 m^3/h (maximum)
Ventilation rate:	57.8 l/h (maximum)
Filters:	G3, F7.

During experiments, a HORIBA VIA 510 infrared gas analyzer has been used. Main technical parameters of the instrument:

- Measuring range: 0–1 000 ppm, 0–2 500 ppm, 0–6 000 ppm, 0–10 000 ppm
- Measuring accuracy: ± 1.0%. Measurements were carried out by the aid of two parallel infrared rays. Automatic data collection was carried out by a data-collector developed by us. In this way data were stored and processed by a PC.

To measure comfort parameters, the following instruments were used:

- thermal comfort PMV meter: Thermal Comfort Meter 1212,
- air temperature and humidity meter: TESTO Testotor 175 Logger,
- wall surface temperature meter: TESTO Quicktemp 824-2,
- acoustics meter: ROLINE RO-1350 Sound Level Meter.

Instruments used to record physiological data:

- ISAX instrument,
- blood pressure monitor: wrist model,
- skin surface temperature meter: TESTO T2.

3.2. Subjects and procedures

In the laboratory measurements, a pleasant thermal, acoustic, and illumination technology comfort was provided to ensure that human well-being is only impacted by air quality (carbon-dioxide gas).

A pleasant thermal comfort was ensured for all live subjects by regulating the air temperature and individually selecting the clothing. The sound level in the measuring room was 36.6–37.0 dB(A).

The set carbon-dioxide concentrations were unknown to the subjects.

The number of subjects was defined through an empirical way (*Wyon* and *Bánhidi*, 2003), consequently 10 subjects were enough because significant differences could be found among the results.

3.2.1. First series of experiments

Ten subjects participated in the study (5 males and 5 females, mean age = 22.5 years). Each subject participated in four experimental sessions with different pre-set CO_2 concentrations (600, 1500, 2500, and 5000 ppm). Sessions succeeded each other in the following manner: session 1 (1500 ppm CO_2), session 2 (2500 ppm), session 3 (600 ppm), session 4 (5000 ppm). Each session consisted of 2×70 minutes mental work periods. The mental work involved the reading of a text manipulated for this purpose and the search for typographic errors. Performance of subjects was characterized by the number of rows read by the subjects (quantity aspect), and the percentage of misspelled words found by them (quality aspect). Prior to and following the work periods, questionnaires were to be filled in for evaluating subjective comfort and well-being, as well as physiological tests were carried out and measurements of skin temperature were taken.

3.2.2. Second series of experiments

The same measuring stand was used as in the 1st set of experiments. Ten subjects participated in the study (4 males and 6 females, mean age $= 21.3 \pm 1.5$ years). Each subject participated in 4 experimental sessions with different pre-set CO_2 concentrations (600, 1500, 3000, and 4000 ppm). Sessions succeeded each other in the following manner: session 1 (1500 ppm CO_2), session 2 (3000 ppm), session 3 (600 ppm), session 4 (4000 ppm). Two sessions (with 1500 and 4000 ppm CO_2 concentration) consisted of 2×70 minutes mental work periods. Two sessions (with 3000 and 600 ppm CO_2 concentration) consisted of 3×70 minutes mental work periods. Subjects had to perform a mental work slightly different from the mental work performed in the 1st series of experiments. Prior to and following the work

periods questionnaires were to be filled in for evaluating subjective comfort and well-being, as well as physiological tests were carried out and measures of skin temperature were taken.

The exposure time was longer only for two levels of CO_2 (600 and 3000 ppm). Periods with corresponding exposure time were compared. The measuring stand was the same as in the first session (*Fig. 1*).

3.3. Measurement of objective microclimatic characteristics

The following objective microclimatic parameters were examined:

- Measurements of CO_2 concentration were carried out with the aid of a HORIBA VIA 510 infrared gas analyzer for which the department has developed a data collector to be connected to a computer. Measurements were carried out during the entire experimental session with 30s sampling intervals.
- PMV (predicted mean vote) and PPD (predicted percentage of dissatisfied) values are objective measurements concerning thermal comfort which were conducted with a PMV meter. Data were read every 70 min in a work period.
- Temperature of the supply air, as well as temperature of exhaust air were measured with two temperature data collectors. Temperature and relative humidity in the occupied zone were also measured with the aid of a temperature and humidity data collector. Measurements were carried out during the entire experimental session, with 30s sampling intervals.
- Surface temperature of the four side walls of the floor and the ceiling was measured using a laser surface thermometer. Sampling was done at the start of the session, before the breaks, and at the end of the session.

3.4. Evaluation of subjective comfort

The following parameters were examined in the evaluation of subjective comfort:

- *Fanger scale*: subjects had to report whether they find air quality acceptable or unacceptable by marking +1 (clearly acceptable) and –1 (clearly unacceptable) on a scale (*Fanger* and *Wargocki*, 2002).
- *Hedonic scale*: subjects' comfort was measured in the range of pleasant (5) and unbearable (1) (*Fanger* and *Wargocki*, 2002).
- *Air Quality scale*: analogue scale for evaluation of freshness of the air. The endpoints of the scale were fresh and very unpleasant sensation.
- In the examination of human well-being changes in subjects' freshness, tiredness and concentration were surveyed.

The above measurements were carried out in each session at the beginning, at the end, and in the breaks between the 70 minutes working periods. These way questionnaires were filled in three times during sessions in the first series of experiments. In the second series of experiments, questionnaires were filled in three times during session 1 (1500 ppm CO_2) and session 4 (4000 ppm CO_2) consisting of two working periods, while during sessions consisting of three working periods (session 2 with 3000 ppm CO_2, and session 3 with 600 ppm CO_2), measurements were carried out four times.

The following measurements were carried out at the beginning and end of each session:

- Subjective evaluation of surface temperature of human skin: subjective thermal comfort was recorded with the help of a 7-grade scale (very hot: 3; pleasant: 0; very cold: –3) at 5 different points: forehead, nose, chest, right hand, and left hand.
- Subjective evaluation of general thermal comfort: subjects' thermal comfort was examined using an analogue scale.

3.5. Study of objective physiological parameters for humans

The following physiological and psycho-physiological parameters were measured and computed: systolic blood pressure (SBP), diastolic blood pressure (DBP), pulse rate, skin temperature.

During each session, SBP, DBP, and pulse rate have been taken at the beginning and end of the session, as well as in the pause between 2 reading periods by the aid of a wrist digital sphygmomanometer. The surface temperature of the human skin was measured with a surface thermometer at the beginning and end of the sessions (measured points: forehead, nose, chest, and both hands).

Heart periods (HP) or RR-intervals were collected continuously during sessions (HP is the time elapsed between 2 subsequent R waves of the ECG, this practically means time elapsed between adjacent heart beats). The variation of HP-s is largely determined by a balance between levels of activity of the cardiac sympathetic and parasympathetic nerves. Spectral analysis of heart period variance (HPV) allows the contributions of these autonomic nerves to be isolated providing insight into the actual balance of the activity of autonomic nerves. It has been shown (*Hyndman et al.*, 1971; *Luczak* and *Laurig* 1973; *Mulder* and *van der Meulen*, 1973; *Sayers*, 1971, 1973; *Womack*, 1971; *Akselrod et al.*, 1981, 1985;) that short-term (time-scale of seconds to minutes) fluctuations in heart periods is concentrated in several principal peaks (low-frequency (LF), mid-frequency (MF), and high-frequency (HF) components of HPV). The HF component of HPV is the so called respiratory component of HPV, it reflects the respiratory rate and it is

influenced by the volume of respiration. HF component is mediated solely by the vagus nerve, while MF component of HPV is mediated jointly by sympathetic nerves and n. vagus (*Akselrod*, 1988; *Akselrod et al.*, 1981, 1985; *Lombardi et al.*, 1987; *Pagani et al.*, 1986; *Pomeranz et al.*, 1985; *Weise et al.*, 1987). Thus, the relative power of these spectral components as well as the ratio of MF and HF components can be used to monitor the actual balance of autonomic nerves (*Lombardi et al.*, 1987; *Pagani et al.*, 1986). For more about spectral analysis of HPV see the reviews by *Láng* and *Szilágyi* (1991), *Eckberg et al.* (1997).

A number of studies has shown that increasing mental load causes a decrease in heart rate variance (*Luczak* and *Laurig*, 1973; *Mulder* and *van der Meulen*, 1973). *Sayers* (1971, 1973) found that consistent changes occur in the heart period spectrum especially in the band from 50 to 150 mHz. According to *Mulder et al.* (1973), the mid-frequency band of HPV (70–140 mHz) appeared to be more sensitive to mental workload than total variance or respiratory fluctuations.

It is believed that mental load (when the task requires explicit effort) operates like a defense reaction. The defense reaction is characterized by a decrease in sensitivity of the baroreflex which results in a decrease of HRV, because changes in the blood pressure will be less reflected in changes in HR. Defense reaction involves suppression of the vagal component of the reflex (*Mulder*, 1980).

Spectral analysis of heart period variance (HPV) is extensively used as a mental effort monitor in the field of ergonomics and psychophysiology (*Itoh et al.*, 1989; *Izsó* and *Láng*, 2000; *Izsó*, 2001; *Mulder*, 1980; *Mulder et al.*, 2000).

It was hypothesized that in unfavorable environmental conditions, such as higher concentration of CO_2 in the air, mental task might request more mental effort.

To assess the actual balance of the autonomic nervous system on the basis of spectral analysis of heart period variance (HPV), an integrated system (ISAX) has been developed and validated (*Láng* and *Horváth*, 1994; *Láng et al.*, 1994, 1997).

It consists of:

- a portable , easy to use equipment for 24-hour ambulatory measurement and storage of heart period (HP) beat by beat and, optionally, other bio-signals, plus
- a user-friendly software package for spectral analysis (autoregressive model) of the stored data in a single personal computer, algorithms to evaluate parameters of the significant spectral components of the power spectra of HPV, and plain text table output for further statistical purposes (*Láng et al.*, 1998).

The acquisition module is a small (300g) portable plastic box that can be mounted on the patient by a clip, and connected to the sensors. The ambulatory

recorded data are stored in the built in NVRAM. Two channels serve the purposes of event-marking in order to be able to identify data sequences recorded in special conditions. The recorded data are read and processed by a host computer. Processing of RR-interval series by the ISAX program consists of steps as follows: RR-interval series are interpolated for the sampling procedure (1 Hz). RR-interval time functions are displayed for interactive selection of appropriate analysis frame. A sufficiently long stationary and representative part of the RR-interval function is selected for spectral analysis. The RR-interval function marked for analysis is converted into zero-mean process. An all-pole auto-regressive model is fitted to the data set (*Akaike*, 1969; *Itakura* and *Saito*, 1969) using a modified Burg algorithm (*Gray et al.*, 1980). More compact characteristics of spectral peaks (such as central frequencies and bandwidths) are computed from the numerically determined poles of the synthesis model.

For compatibility with the conventional analysis methods, sub-band powers (low-, mid-, and high-frequency) are calculated by integrating the spectra over sub-band boundaries specified. Using default, the software calculates the spectral power (ms^2) of heart period variability for predetermined frequency ranges [low-frequency range: 10 mHz–70 mHz (LF); mid- frequency range: 70 mHz–150 mHz (MF); high-frequency range:150 mHz–450 mHz (HF)] (*Láng et al.*, 1998). In the recent study the following non-spectral and spectral parameters were computed for further statistical analysis: RR-interval mean (ms) (mean of the analysis frame), MF-power (ms^2), HF-power (ms^2) of the HPV spectrum. Relative powers were expressed in normalized units by dividing each component by the sum of their powers (sum = HF-power + MF-power). Thus, HF-relative = HF-power/sum, MF-relative = MF-power/sum.

One of the problems of spectral analysis is the issue of non-stationarity of the time series to be analyzed. In ISAX program this problem has been attacked by an approach called by *Mulder* (1988) spectral profile method. Spectral computations are carried out on short time segments (20–60 seconds.) By shifting such segments over the time series to be analyzed, and by introducing a certain overlap (90% or more), series of spectral values are obtained. Spectral power of a selected frequency band versus time is the so-called "spectral profile" of this frequency band (*Izsó* and *Láng*, 2000).

3.6. Statistical analysis

Statistical analysis on the above variables was performed using SPSS 10.00 for Windows program package. Differences between sessions, as well as changes appearing during the same session (differences between measurements of the same session) were revealed using analysis of variance with repeated measurements and

appropriate contrasts. Differences were considered significant when $p < 0.05$. More about analysis of variance see in Appendices (*Ferguson*, 1988; *Rosenthal* and *Roskov*, 1987; *SPSS Advanced Statistics 7.0 update*, 1996).

The repeated measures procedure provides analysis of variance when the same measurement is made several times on each subject or case. In repeated measures analysis, all dependent variables represent different measurements of the same variable for different values (or levels) of a within-subjects factor (*SPSS Advanced Statistics 7.0 update*, 1996).

In our case, all dependent variables represent different measurements of the same variable for different levels of CO_2 concentration in the air.

4. Results and discussion

4.1. Results of the first series of experiments

Results of the first series of experiments described in section 3.2. are discussed in this section. Concentrations of CO_2 were set at 600, 1500, 2500, and 5000 ppm.

4.1.1. Results concerning evaluation of subjective comfort

When comparing corresponding measurements of different sessions using the *Fanger scale* the analysis of variance revealed significant differences between sessions with 600 and 5000 ppm CO_2 already at the beginning of the sessions: subjects evaluated air quality less acceptable during the session with 5000 than with 600 ppm CO_2. Between sessions with 5000 and 1500 ppm CO_2 a significant difference appeared only at the end of sessions, that is after 140 minutes: subjects evaluated air quality less acceptable during the session with 5000 than with 1500 ppm CO_2 (*Fig. 3*).

Similar results were found with the *Air Quality scale.*

In the case of *Hedonic scale* subjects evaluated air with 600 and 1500 ppm CO_2 significantly less unpleasant than air with 5000 ppm CO_2.

Concerning *freshness, tiredness* scales difference between the first and the last measurements of the same session was the greatest in the case of session with 5000 ppm CO_2, showing that subjects became the most exhausted in this session. In this respect the difference between session, with 5000 and 600 ppm CO_2 concentration reached the level of significance.

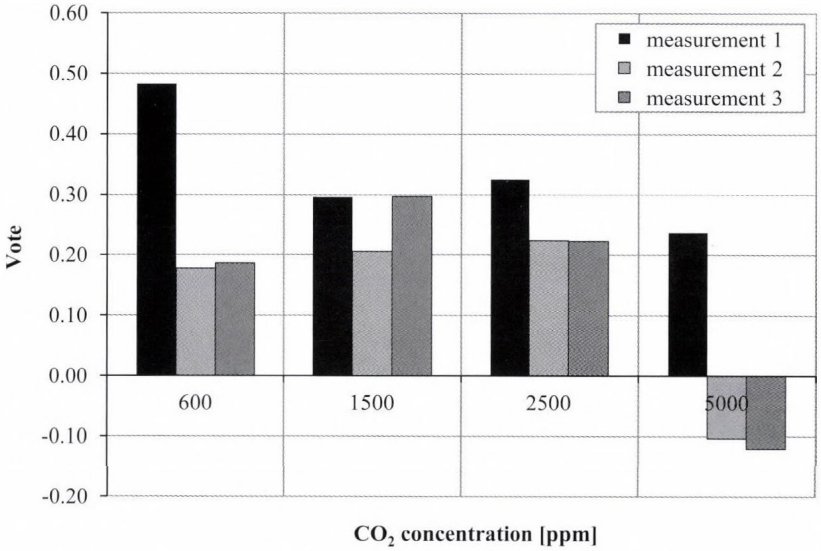

Fig. 3. Results of measurements with *Fanger scale* (acceptable {+1}, unacceptable {-1}). Measurement 1, 2, and 3 were carried out in each sessions at the beginning, before the breaks, and at the end of each session, respectively.

Fig. 4 shows the results of measurement on the tiredness scale.

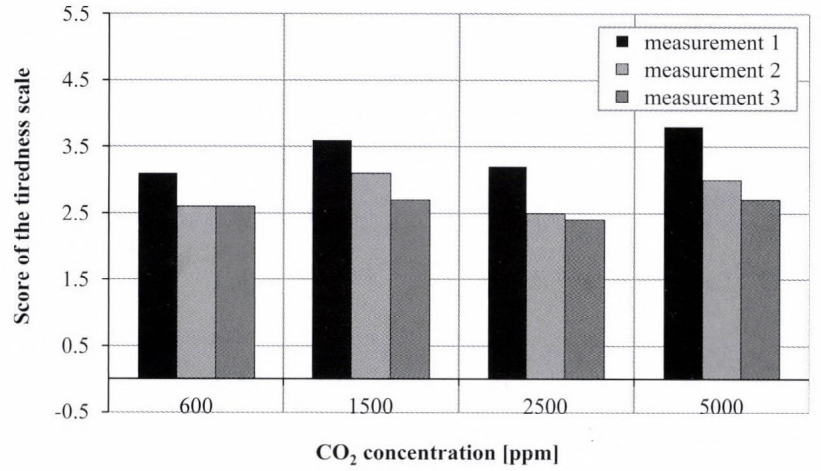

Fig. 4. Results of measurements with tiredness scale. Measurement 1, 2, and 3 were carried out in each sessions at the beginning, before the breaks, and at the end of each session, respectively.

4.1.2. Results concerning mental workload

Subjects' performance characterized by the number of rows read during the session (quantity aspect), as well as the percentage of mistakes found by the subjects (quality aspect of performance) was not significantly impacted by the degree of CO_2 concentration.

4.1.3. Results concerning physiological parameters

Heart rate (pulse rate) showed a decreasing tendency during each session. This is usually the case when subjects are sitting quietly for hours, the mental task does not require a high mental effort, and the temperature of the air does not increase substantially. The degree of this decrease of the heart rate (difference between measurements at the beginning and end of the same session) was significantly less expressed in the case of session with 5000 ppm CO_2 concentration as compared with sessions with lower CO_2 concentration. Changes of the heart rate within sessions (difference between the heart rates observed at the end (measurement 3) and beginning (measurement 1) of the same session) are illustrated by *Fig. 5.*

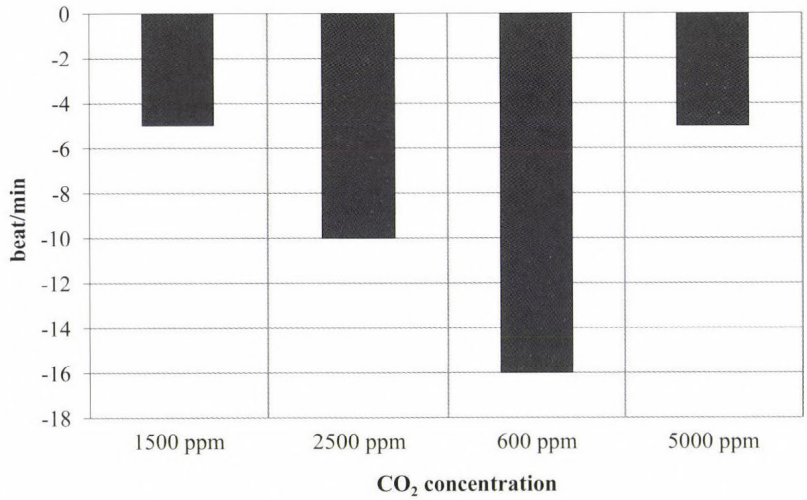

Fig. 5. Changes of the heart rate during the same session.

The analysis of variance revealed a small but significant increase of the *diastolic blood pressure (DBP)* during the session with 5000 ppm CO_2 concentration. Concerning the degree of DBP changes within sessions (difference between measurements at the beginning and end of the same session), sessions with

600 and 5000 ppm CO_2 concentration were significantly different from each other. Increase of DBP usually is caused by the increase of total peripheral resistance due to constriction of blood-vessels (vasoconstriction). It may be supposed that 5000 ppm CO_2 concentration in the air slightly raised the vasoconstrictor tone of subjects.

Fig. 6 illustrates the changes of DBP within sessions (difference between the DBP values observed at the end (measurement 3) and beginning (measurement 1) of the same session).

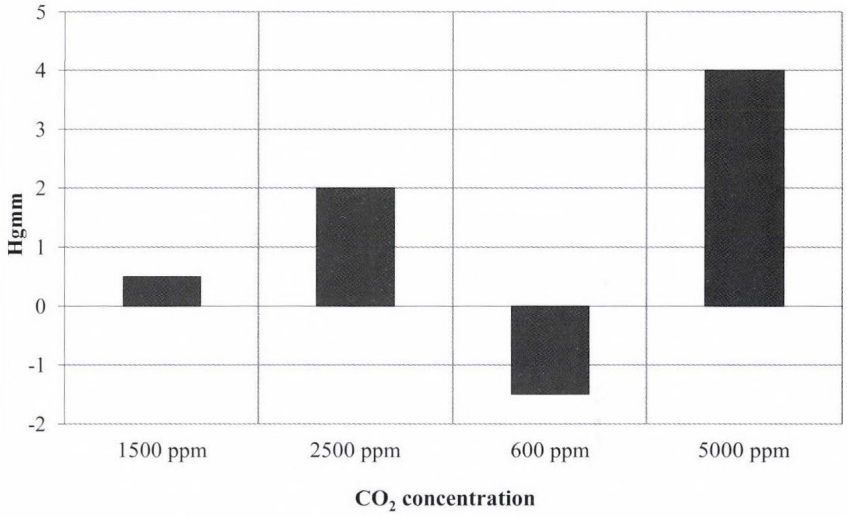

Fig. 6. Changes of DBP within sessions.

By the aid of the ISAX system, it was revealed that the respiratory frequency and the volume of respiration of the majority of subjects were higher in the session with 5000 ppm CO_2 concentration than in the session with 600 ppm. *Fig. 7* shows that the HF component of HPV was significantly higher in the session with 5000 ppm CO_2 concentration than in the session with 600 ppm CO_2 concentration.

In the case of subjects who became very exhausted according to the *freshness, tiredness* scales in the session with 5000 ppm CO_2 concentration but did not show any decrease in mental performance, the HPV analysis revealed a higher mental effort during mental load. As it was mentioned in Section 3 the suppression of MF component of HPV reflects the mental effort invested by the subjects. Thus, it

might be concluded that in the case of the above subjects the mental task might require more mental effort in unfavorable environmental conditions such as higher concentration of CO_2 in the air.

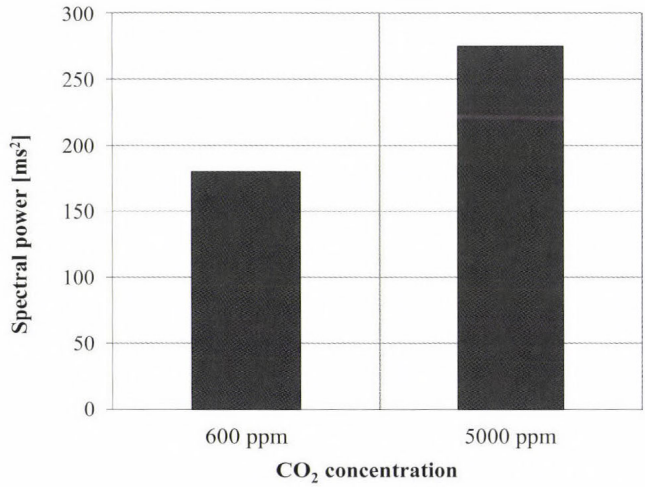

Fig. 7. Spectral power of the HF component (respiratory component) of HPV.

Similary to the measurements of skin temperature and the subjective evaluation of surface temperature and general thermal comfort, the analysis of variance did not reveal significant differences between sessions with different CO_2 concentrations.

4.1.4. Summary of results obtained in the first series of experiments

Significant differences were obtained concerning subjective evaluation of air quality and human well-being between work periods with 600 and 5000 ppm CO_2 concentration, showing a decline of well-being when CO_2 concentration in the air reaches 5000 ppm. At the same time, no significant differences were found concerning mental performance between work periods at different CO_2 concentrations. HPV analysis (MF component) revealed, however, that a mental task required more mental effort under 5000 ppm CO_2 as compared to 600 ppm. Moreover, the respiratory component of HPV reflected an increase in respiratory volume and respiratory frequency at 5000 ppm CO_2 concentration.

4.2. Results of the second series of experiments

Results of the second series of experiments described in Section 3.2. are discussed in this section. Concentrations of CO_2 were set at 600, 1500, 3000, and 4000 ppm.

4.2.1.Results concerning evaluation of subjective comfort

The analysis of variance with repeated measurements using the *Fanger scale* revealed significant differences between measurements of the same session. Subjects evaluated air quality less acceptable at the end than at the beginning of the same session. In the case of session with 600 ppm CO_2, subjects evaluated air quality less acceptable only after the second working period, while subjects' well-being already declined following the first 70-minute working period during other sessions.
Using the *Air Quality scale, s*imilar results were found as in the case of *Fanger scale.* At the same time, there were differences between the sessions. When comparing corresponding measurements of different sessions using the *Fanger scale* the analysis of variance showed that significant differences appeared between sessions only following the second working period, that is after 140 minutes. Subjects evaluated air with 3000 and 4000 ppm CO_2 significantly less acceptable than air with 600 ppm CO_2. Air with 1500 ppm CO_2 concentration was judged as significantly more acceptable than air with 4000 ppm CO_2. In the case of sessions with 600 and 3000 ppm CO_2, three 70-minute working periods were used. After the third working period (210 minutes) air was denoted significantly less acceptable during session with 3000 ppm CO_2 as compared to session with 600 ppm CO_2 (as it was the case already after 140 minutes). *Fig. 8* shows the results of measurements with the *Fanger scale.*

Using *Air Quality scale* similar results were found as in the case of the *Fanger scale*, with the only advantage, that after 140 minutes air with 1500 ppm CO_2 concentration was judged as significantly fresher than air with 3000 ppm. *Fig. 9* shows the results of measurements with the *Air Quality scale.*
The analyses of variance performed on scores on *freshness, tiredness,* and *concentration* scales revealed significant differences between measurements of the same session in the case of sessions with higher CO_2 concentration than 600 ppm, showing that subjects get more tired, became less fresh, and their capability to focus their attention was declining in the course of the session. Concerning scores on *freshness* and *tiredness* scales, when comparing corresponding measurements of different sessions, the analysis of variance showed that significant differences appeared between sessions with 600 and 3000 ppm CO_2 concentration only following the third working period, that is after 210 minutes. Subjects became more exhausted at the end of session with 3000 ppm than at the end of session with 600 ppm CO_2 concentration.

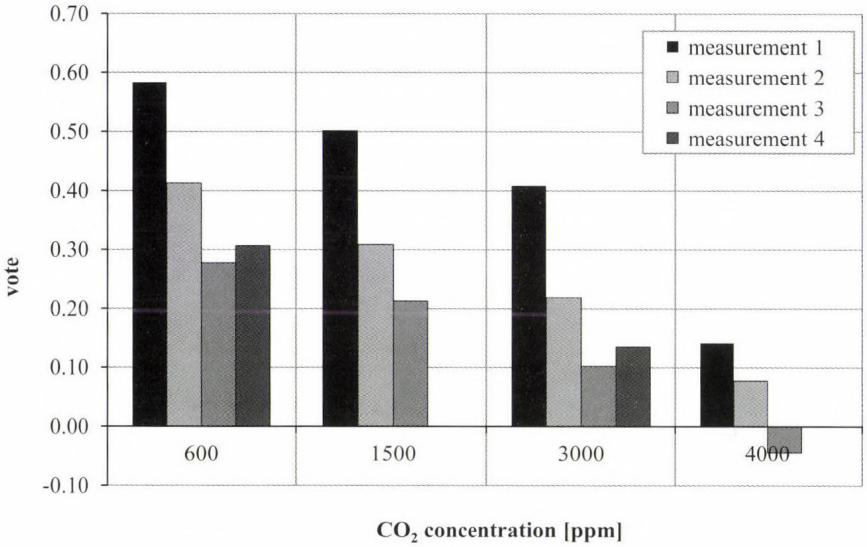

Fig. 8. Results of measurements with Fanger scale (acceptable {+1}, unacceptable {-1}). Measurement 1, 2, 3, and 4 were carried out in each sessions at the beginning, before the breaks, and at the end of each session, respectively.

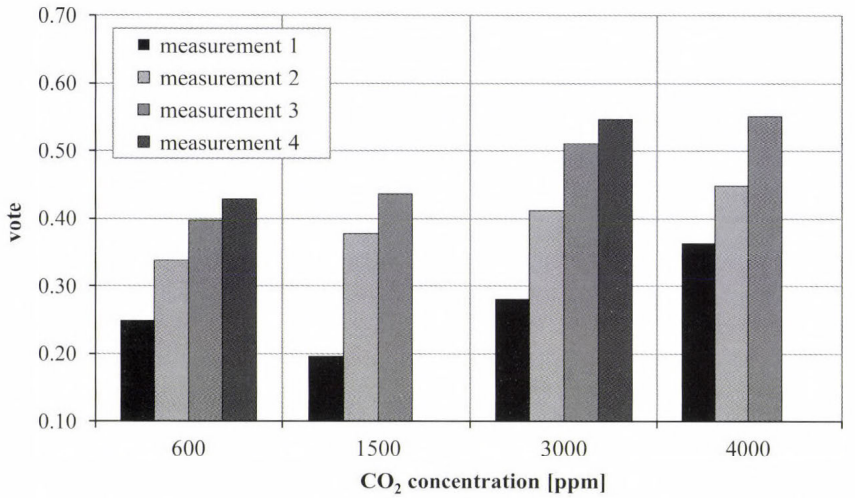

Fig. 9. Results of measurement, with *Air Quality scale* (fresh {0}, very unpleasant sensation {+1}). Measurement 1, 2, 3, and 4 were carried out in each sessions at the beginning, before the breaks, and at the end of each session, respectively.

4.2.2. Results concerning mental workload

As it was mentioned in Section 3, a different text was used in the second series of experiments. In the first series, neither the number of rows read by the subjects, nor the percentage of mistakes found by the subjects were influenced by the degree of CO_2 concentration. Therefore, we decided to use a more difficult text in the second series of experiments.

Subjects' performance characterized by the number of rows read during the session (quantity aspect) was not significantly impacted by the degree of CO_2 concentration. Concerning this variable, the *time effect* (learning) was found: subjects' performance related to the quantity of read rows increased from the first to the last session. The quality aspect of performance (percentage of mistakes found by the subjects), however, proved to be more sensitive to the concentration of CO_2. The analysis of variance revealed that during the second 70-minute working period, the percentage of mistakes found by the subjects was significantly higher in session with 600 ppm CO_2 than in the corresponding working period of session with 4000 ppm CO_2 concentration. Moreover, during the third 70-minute working period of session with 600 ppm CO_2, the percentage of mistakes found by the subjects was almost significantly higher than in the corresponding period of session with 3000 ppm CO_2 concentration. In this case, the number of rows read by the subjects in the session with 600 ppm CO_2 also exceeded the number of rows read in the corresponding period of session with 3000 CO_2 concentration. That means that the third working period with 600 ppm CO_2 proved to be more advantageous for both aspects of mental performance than 3000 ppm CO_2 concentration (*Fig. 10*).

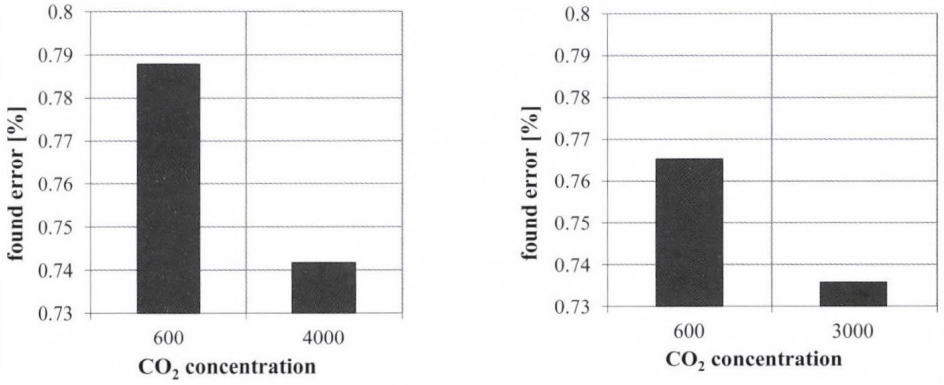

Fig. 10. Influence of CO_2 concentration on percentage of errors found by subjects in the second(left) and third(right) 70-minute working periods.

The quality aspect of mental work expresses the ability to concentrate attention. It seems that human well-being as well as the capacity to concentrate attention decline when CO_2 concentration increases up to 3000 ppm.

4.2.3. Results concerning physiological parameters

The analysis of variance did not reveal any significant effect of CO_2 concentration in air (in the range of 600 to 4000 ppm) on the systolic blood pressure (SBP), and diastolic blood pressure (DBP). In these experiments, these parameters were not sensitive enough to show the impact of CO_2 concentration in air under 4000 ppm. For this reason, in the analysis of physiological parameters we preferred to use the ISAX system, which is based on measuring heart period parameters.

The analysis of variance revealed that heart periods (HP) (time elapsed between two heart beats) increased during each session from the beginning to the end. This means that the pulse rate decreased from the beginning to the end of each session. This is a typical phenomenon when subjects are sitting quietly for hours. Concentration of CO_2 had no impact on the HP. Absolute and relative values of MF (mid-frequency component) of heart period variability (HPV) are used to measure mental effort requested by the task. The less the value of the MF component, the more pronounced the effort invested by the subjects along the mental tasks. As it was mentioned in Section 3., MF component of HPV was proposed to be used as an objective psycho-physiological measure of actual mental effort invested by the subjects (*Mulder*, 1980; *Izsó* and *Láng*, 2000; *Izsó*, 2001).

As a tendency, the lowest values of the MF component could be seen during the session with 4000 ppm CO_2, while the highest values of MF component were obtained in the session with 600 ppm CO_2. Concerning HF component, just the contrary was the case. HF component reflects the frequency of respiration and might reflect the volume of respiration. A significant difference was revealed between sessions with 600 and 4000 ppm CO_2 by the analysis of variance performed on the MF/HF ratio, as well as on relative values of MF and HF components. Increase of HF component indicates increased volume of respiration in sessions with 4000 ppm CO_2 concentration. Decrease of MF component and MF/HF ratio indicates more effort invested by the subject in sessions with 4000 ppm CO_2 concentration. This is in accordance with the declining ability to concentrate attention in sessions with 4000 ppm CO_2 as shown by the scores on *freshness* and *tiredness* scales as well as by the decrease of mental performance.

Figs. 11 and *12* show that the relative value of MF of each subject reaches a higher value in sessions with 600 ppm than in sessions with 4000 ppm CO_2.

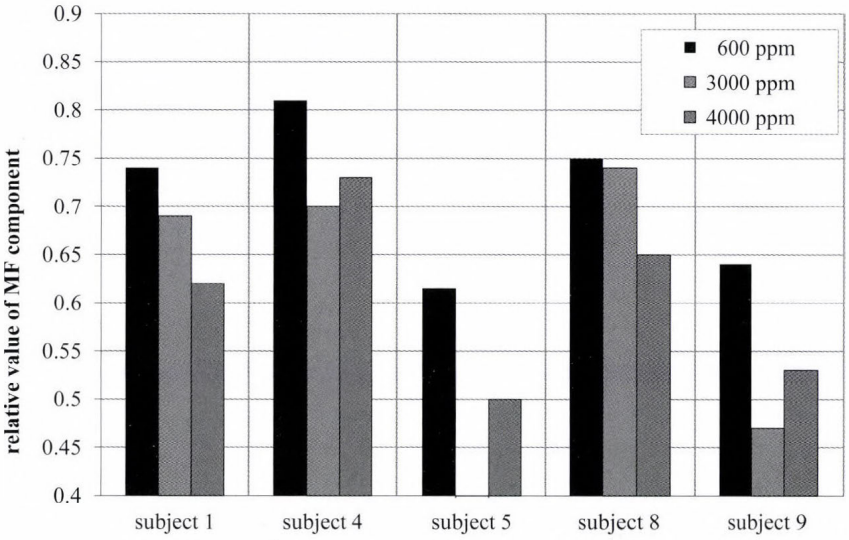

Fig. 11. Impact of CO_2 concentration on the relative value of MF component of HPV in 5 subjects.

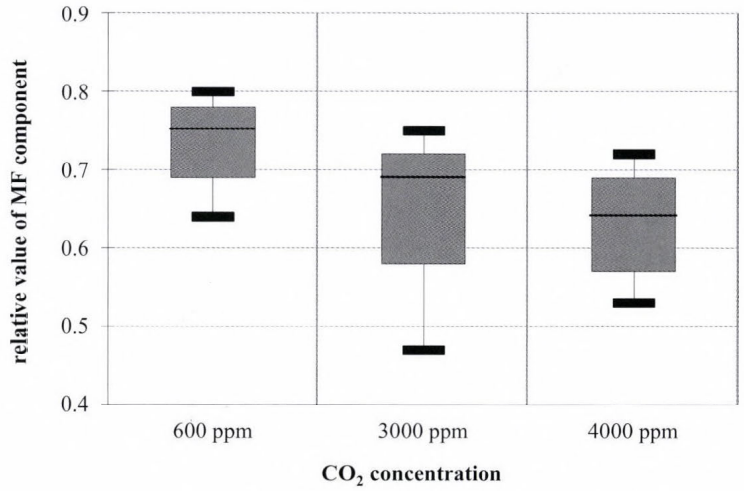

Fig. 12. The relative value of MF component of HPV in sessions with different CO_2 concentration.

Concerning measurements of skin temperature and the subjective evaluation of surface temperature and general thermal comfort, the analysis of variance did not reveal significant differences between sessions with different CO_2 concentration.

4.2.4. Summary of results obtained in the second series of experiments

Significant differences were obtained concerning subjective evaluation of air quality and human well-being between work periods with 600 and 4000 ppm CO_2 concentration after 140 minutes. After 210 minutes, significant differences appeared between work periods with 600 and 3000 ppm CO_2 concentration showing a decline in human well-being in closed spaces with 3000 ppm CO_2 concentration in the air. The same was true for results concerning mental workload: during the second 70-minute working period, the percentage of mistakes found by the subjects was significantly higher in sessions with 600 ppm CO_2 than in the corresponding working period of sessions with 4000 ppm CO_2 concentration. Concerning the third 70-minute working period, sessions with 600 ppm CO_2 proved to be more advantageous for both aspects (quantity and quality aspects) of mental performance than 3000 ppm CO_2 concentration. These results are in accordance with the objective psycho-physiological measurements of actual mental effort derived from HPV spectra.

5. Summary and conclusions

A specific laboratory and measuring stand was constructed to investigate the impact of CO_2 concentration in the air on human well-being and office work intensity, and to determine the necessary fresh air demand. Air of appropriate cleanliness, thermal comfort, as well as appropriate acoustic conditions were ensured in the laboratory.

Objective microclimatic characteristics were measured during experimental sessions. Two series of experiments were conducted with different pre-set CO_2 concentrations in the air.

Various standard scales were used in the evaluation of subjective comfort concerning air quality and human well-being changes indicating the subjects' freshness, tiredness, and concentration. Subjects participating in the investigations were performing a mental task in order to measure their mental effort and efficiency. In addition, objective physiological variables were measured. Data were processed and statistically analyzed. Experience gained from the first series of experiments was taken into consideration when designing the second series of experiments.

It was shown that subjects evaluated air quality less acceptable, more unpleasant, and they became more exhausted when CO_2 concentration increased up to 3000 ppm. 3000 ppm CO_2 concentration in the air proved to be less advantageous for mental performance than 600 ppm. Several physiological measures (spectral components of HPV) show that the mental task required more effort from the subjects when CO_2 concentration in the air reached 3000 ppm.

It was shown that human well-being as well as the capacity to concentrate attention decline when subjects spend 2–3 hours in a closed space with 3000 ppm or higher CO_2 concentration in the air.

Aknowledgements—This study was carried out in the frame of the 'Insurance of indoor air quality in climatized places, required indoor air quality and evaluation method of climate systems' project (T 029451) and received financial support from the Hungarian Scientific Research Fund.

Appendix

The analysis of variance is used to test the significance of the differences between the means of a number of different samples. The null hypothesis is formulated that the samples are drawn from populations having the same mean. Assuming that the treatments applied are having no effect, some variations are expected between means, due to sampling fluctuation. If the variation cannot reasonably attributed to sampling error, we reject the null hypothesis and accept the alternative hypothesis that the treatments applied are having an effect. With only two means, this approach leads to the same result as the obtained from the *t* test for the significance of the difference between means of two samples. If the variation between means is not small and of such magnitude that it could arise in random sampling in less than 1 or 5 per cent of cases, then the evidence is sufficient to warrant rejection of the null hypothesis and acceptance of the alternative hypothesis that the variation differs in yield. The problem of testing the significance of differences between a number of means results from experiments designed to study the variation. For this, the *F* ratio is calculated (S_b^2 / S_w^2) and referred to the table of *F*.

If the probability of obtaining the observed *F* value is small (less than 0.05 or 0.1), the null hypothesis is rejected.

Following the application of an *F* test, a meaningful interpretation of the data may require a comparison of pairs of means. These differences between some pairs may be significant, while other differences may not be. A number of alternative methods exist for making such comparisons (*Ferguson*, 1988).

Contrasts are the significance tests of focused questions. By a focused test (as opposed to an omnibus test), we mean any statistical test that addresses precise questions, as in any 1 *df F* test or *t* test. Omnibus tests, on the other hand, are tests

of significance that address diffuse (or unfocus) questions, as in F test with numerator $df > 1$. Contrasts allow us to answer planned comparisons instead of the overall analysis of variance (*Rosenthal* and *Rosnow*, 1987). In our case series, pairwise comparisons were performed between treatment means.

Contrasts are used to test the differences among the levels of a factor (in our case the factor is the CO_2 concentration in the air). Contrast types used in the study were: simple contrast (compares the mean of each level to the mean of the first or last category of the reference) and repeated contrast, which compares the mean of each level (except the last) to the mean of the subsequent level (*SPSS Advanced Statistics 7.0 update*, 1996).

References

Akaike, H., 1969: Fitting autoregressive models for prediction. *Ann. Inst. Statist. Math. 21*, 243–247.

Akselrod, S., 1988: Spectral analysis of fluctuations in cardiovascular parameters: a quantitative tool for the investigation of autonomic control. *Trends Pharmacol. Sci. 9*, 6–9.

Akselrod, S., Gordon, D., Madwed, J.B., Snidman, N.C., Shannon, D.C., and *Cohen, R.J.*, 1985: Hemodynamic regulation: investigation by spectral analysis. *Am. J. Physiology 249*, H867–H875.

Akselrod, S., Gordon, D., Ubel, F.D., Shannon, D.C., and *Cohen, R.J.*, 1981: Power spectrum analysis of heart rate fluctuations: A quantitative probe of beat-to-beat cardiovascular control. *Science 213*, 220–222.

Eckberg, D.L., Grossman, P., Kaufmann, P.G., Malik, M., Nagaraja, H.N., Porges, S.W., Saul J.P., Stone, P.H. and *van der Molen, M.W.*, 1997: Heart rate variability: Origins, methods, and interpretive caveats. *Psychophysiology 34*, 623–648.

Fanger, P.O. and Wargocki, P., 2002: Increased office productivity through improved indoor air quality. *Proceedings of Fifth International HVAC&R Technology Symposium, Istanbul, 29 April – 1 May (CD-ROM).*

Ferguson, G.A.,1988: Statistical Analysis in Psychology and Education. The Guilford Press, New York.

Gray, A.H., Wong, D.Y., 1980: The Burg Algorithm for LPC Speech Analysis Synthesis. *IEEE Trans. Tr. ASSP. 28*, 609–615.

Hyndman, B.W., Kitney, R.I., and *Sayers, B.McA.*, 1971: Spontaneous rhythms in physiological control systems. *Nature 233*, 339.

Itakura, F., Saito, S., 1969: Speech Analyzis Synthesis Systems based on the Partial Autocorrelation Coefficient. *Acoust. Soc. of Japan Meating.*

Itoh,Y., Hayashi, Y., Tsukui, I., Saito, S., 1989: Heart rate variability and subjective mental workload in flight task. In *Work with Computers: Organizational, Management, Stress and Health aspects* (eds.: *Smith* and *Salvany*). Elsevier Science Publishers B V. Amsterdam.

Izsó, L., 2001: Developing evaluation Methodologies for Human-Computer Interaction. *Delft University Press*, 2600 MG Delft, The Nederlands.

Izsó, L. and *Láng, E.*, 2000: Heart period variability as a mental effort monitor in Human Computer Interaction. *Behav. Inf. Technol. 19*, 297–306.

Kajtár, L., Erdősi, I., and Bakó-Biró, Zs., 2001: Thermal and Air Quality comfort in the Hungarian Office Buildings. *Proceedings of the Second NSF International Conference on Indoor Air Health. Miami Beach, USA, 270–278 p.*

Kajtár, L. and Hrustinszky, T., 2002: Measurements of Indoor Air Quality and Emission of Indoor Materials. *Proceedings of the third conference on mechanical engineering, Budapest, Hungary*, 362–366.

Kajtár, L. and Hrustinszky, T., 2003*:* Investigation of indoor air quality and emission of indoor used materials in Hungary. *7th International Conference Healthy Buildings, Singapore, Proc. 3. 752–757.*

Láng, E. and *Szilágyi, N.,*1991: Significance and assessment of autonomic indices in cardiovascular reactions. *Acta Physiol. Hung. 78*, 241–260.

Láng, E. and *Horváth, Gy.,* 1994: Integrated System for Ambulatory Cardio-respiratory data acquisition and Spectral analysis (ISAX). *User's manual.* Budapest.

Láng, E., Horváth, G., and *Slezsák, I.,*1997: Integrated system for ambulatory cardio-respiratory data acquisition and spectral analysis. *World Congress of Medical Physics and Biomedical Engineering*, Nice 14–19 September, *Medical and Biological Engineering and Computing 5, Suppl.*, 118.

*Láng, E., Bánhidi, L., Antalovits, M., Izsó, L., Mitsányi, A., Zsuffa, A., Magyar, Z., Horváth, Gy., Slezsák, I., Majoros, A., Dombi, I.,*and *Molnár, L.,* 1994: A complex psychophysiological method to assess environmental effects (-temperature, illumination, sound -) on objective and subjective parameters of humans in simulated work setting. *"Healthy Buildings'94". Proceedings of the 3rd International Conference,* Budapest, Hungary, 22–25. August, 799–803.

Láng, E., Caminal, P., Horváth, G., Jané, R., Vallverdu, M., Slezsák, I., and *Bayés de Luna, A.,*1998: Spectral analysis of heart period variance (HPV) - a tool to stratify risk following myocardial infarction. *J. Med. Eng. Technol. 22*, 248–256.

Lombardi, F., Sandrone, G., Pernpruner, S., Sala, R., Garimoldi, M., Cerutti, S., Baselli, G., Pagani, M., and *Malliani, A.*, 1987: Heart rate variability as an index of sympathovagal interaction after acute myocardial infarction. *Am. J. Cardiology 60*, 1239–1245

Luczak, H. and *Laurig, W.,* 1973: Analysis of heart rate variability. *Ergonomics, 16,* 85–97.

Mulder, G., 1980: "The heart of mental effort", Ph.D. Thesis, University of Groningen.

Mulder, L.J.M., 1988: Assessment of cardiovascular reactivity by means of spectral analysis. Ph.D. Thesis, University of Groningen.

Mulder, G. and *Mulder-Hajonides van der Meulen, W.R.E.H.,* 1973: Mental load and the measurement of heart rate variability. *Ergonomics 16*, 69–83.

Mulder, G., Mulder L.J.M., Meijman T.F., Veldman. J.B.P., and *van Roon, A.M.,* 2000: A psychophysiological approach to working conditions. In (Eds.) *Engineering Psychophysiology* (eds.: *R.W. Backs* and *W. Boucsein*) Lawrence Erlbaum Associates, Publishers, Mahwah, 139–159.

Pagani, M., Lombardi, F., Guzzetti, S., Rimoldi, O., Sandrone, G., Malfatto, G., Dell'Orto, S., Piccaluga, E., Turiel, M., Baselli, G., Cerutti, S. and *Malliani, A.,* 1986: Power spectral analysis of heart rate and arterial pressure variabilities as a marker of sympathovagal interaction in man and conscious dog. *Circ. Res., 59*, 178–193.

Pettenkoffer, M. v., 1858: Über den Luftweschel in Wohngebauden. Literarisch-Artistische Anstalt der J.G. Gottaschen Buchhandlung. München.

Pomeranz, B., Macaulay, R.J.B., Caudill, M.A., Kutz, I., Adam, D., Gordon, D., Kilborn, K.M., Barger, A.C., Shannon, D.C., Cohen, R.J. and *Benson, H.,* 1985: Assessment of autonomic functions in humans by heart rate spectral analysis. *Am. J. Physiol. 248;* H151–H153

Rosenthal, R. and Rosnow, R., 1987: Contrast Analysis. Cambridge University Press.Cambridge.

Sayers, B. McA., 1971: The analysis of cardiac interbeat interval sequences and the effect of mental work load. *Proceedings of the Royal Society for Medicine 64*, 707–710.

Sayers, B. McA., 1973: Analysis of heart rate variability. *Ergonomics 16*, 17–32.

SPSS Advanced Statistics 7.0 update, 1996:. Library of Congress Catalog Card Number 95–072794.

Weise, F., Heydenreich, F. and *Runge, U.,* 1987: Contributions of sympathetic and vagal mechanisms to the genesis of heart rate fluctuations during orthostatic load: a spectral analysis. *J. Auton. Nerv. Syst. 21*, 127–134.

Womack, B.F., 1971: The analysis of respiratory sinus arrhythmia using spectral analysis and digital filtering. *IEEE Trans. Biomed. Eng. 18*, 399–409.

Wyon, D.P., and Bánhidi, L., 2003: The Question of Model Size in the Research of the Indoor Environment Effects. *(in Hungarian) Magyar Épületgépészet 52 (12),* 9–10.

BOOK REVIEW

B. Cushman-Roisin and *J.-M. Beckers*: **Introduction to Geophysical Fluid Dynamics - Physical and Numerical Aspects** (second edition). Academic Press, 2011, 828 pages, 22 chapters.

Almost twenty years after the praiseful first edition, Academic Press published the enlarged and updated new edition of the Introduction to Geophysical Fluid Dynamics. B. Cushman-Roisin, the author of the first edition was joined by J.-M. Beckers as coauthor. The aim of the book is to introduce readers, first of all students and scientists in the fields of dynamical meteorology and physical oceanography, to the principles governing air and water flow on large terrestrial scales and to the basic numerical methods and simple models by which these flows can be simulated.

The book is organized into five parts. The introductory part reviews the fundamentals of fluid motion and geophysical flows, as well as diffusion and advection processes. The next two parts are devoted to the effects of rotation and stratification, respectively. Geostrophic flows, vorticity dynamics, Ekman layers, barotropic waves, and barotropic instability are described, turbulence in stratified fluids and internal waves are analyzed. The fourth part is dedicated to the combined effects of rotation and stratification, which play a very important role in the simulation of geophysical fluid processes. The final part is focused on the general circulation of the atmosphere and ocean, equatorial dynamics, and data assimilation. The authors close with a recapitulation of the elements of fluid mechanics, wave kinematics, and a survey of numerical schemes in the appendix.

Extending the content of the first edition with subjects such as turbulence closure techniques and data assimilation, and supplementing it with numerical topics, the text is written easy to understand. Each part is divided into well-organized chapters which conclude with short biographic notes of notable scientists putting science into a historical perspective. The chapters are accompanied by a set of analytical problems and numerical exercises. Useful Matlab codes necessary for some of the numerical exercises are available on the publisher's website related to the book. Unfortunately, the numerical solutions of the analytical problems are not provided. Contrary to the first edition, short descriptions of the suggested laboratory demonstrations are left out. It is very laudable that during the preparation of the book, the actual manuscript was attainable on B. Cushman-Roisin's website.

Outshining the first edition, the authors cover a broad range of topics providing an introduction to the physical principles of geophysical fluid mechanics and computational methods necessary for numerical modeling. This is an excellent textbook, the pearl of GFD literature.

Á. Bordás

INSTRUCTIONS TO AUTHORS OF *IDŐJÁRÁS*

The purpose of the journal is to publish papers in any field of meteorology and atmosphere related scientific areas. These may be

- research papers on new results of scientific investigations,
- critical review articles summarizing the current state of art of a certain topic,
- short contributions dealing with a particular question.

Some issues contain "News" and "Book review", therefore, such contributions are also welcome. The papers must be in American English and should be checked by a native speaker if necessary.

Authors are requested to send their manuscripts to

Editor-in Chief of IDŐJÁRÁS
P.O. Box 38, H-1525 Budapest, Hungary
E-mail: journal.idojaras@met.hu

including all illustrations. MS Word format is preferred in electronic submission. Papers will then be reviewed normally by two independent referees, who remain unidentified for the author(s). The Editor-in-Chief will inform the author(s) whether or not the paper is acceptable for publication, and what modifications, if any, are necessary.

Please, follow the order given below when typing manuscripts.

Title page: should consist of the title, the name(s) of the author(s), their affiliation(s) including full postal and e-mail address(es). In case of more than one author, the corresponding author must be identified.

Abstract: should contain the purpose, the applied data and methods as well as the basic conclusion(s) of the paper.

Key-words: must be included (from 5 to 10) to help to classify the topic.

Text: has to be typed in single spacing on an A4 size paper using 14 pt Times New Roman font if possible. Use of S.I. units are expected, and the use of negative exponent is preferred to fractional sign. Mathematical formulae are expected to be as simple as possible and numbered in parentheses at the right margin.

All publications cited in the text should be presented in the *list of references*, arranged in alphabetical order. For an article: name(s) of author(s) in Italics, year, title of article, name of journal, volume, number (the latter two in Italics) and pages. E.g., *Nathan, K.K.,* 1986: A note on the relationship between photo-synthetically active radiation and cloud amount. *Időjárás 90,* 10-13. For a book: name(s) of author(s), year, title of the book (all in Italics except the year), publisher and place of publication. E.g., *Junge, C.E.,* 1963: *Air Chemistry and Radioactivity.* Academic Press, New York and London. Reference in the text should contain the name(s) of the author(s) in Italics and year of publication. E.g., in the case of one author: *Miller* (1989); in the case of two authors: *Gamov* and *Cleveland* (1973); and if there are more than two authors: *Smith et al.* (1990). If the name of the author cannot be fitted into the text: *(Miller,* 1989); etc. When referring papers published in the same year by the same author, letters a, b, c, etc. should follow the year of publication.

Tables should be marked by Arabic numbers and printed in separate sheets with their numbers and legends given below them. Avoid too lengthy or complicated tables, or tables duplicating results given in other form in the manuscript (e.g., graphs).

Figures should also be marked with Arabic numbers and printed in black and white or color (under special arrangement) in separate sheets with their numbers and captions given below them. JPG, TIF, GIF, BMP or PNG formats should be used for electronic artwork submission.

Reprints: authors receive 30 reprints free of charge. Additional reprints may be ordered at the authors' expense when sending back the proofs to the Editorial Office.

More information for authors is available: journal.idojaras@met.hu

Published by the Hungarian Meteorological Service

Budapest, Hungary

INDEX 26 361

HU ISSN 0324-6329